LINKING BURN SEVERITY TO SOIL INFILTRATION AND RUNOFF IN A MONTANE WATERSHED: BOULDER, COLORADO.

A Thesis

by

ANNA KATHLEEN AHLSTROM

Submitted to the Office of Graduate Studies of
Texas A&M University
in partial fulfillment of the requirements for the degree of

MASTER OF SCIENCE

Approved by:

Chair of Committee,	John. R. Giardino
Committee Members,	John. R. Giardino
	John Vitek
	Vatche Tchakerian
Head of Department,	John R. Giardino

December 2012

Major Subject: Geology

ABSTRACT

Forest fires have an enormous impact on biotic and abiotic variables that control runoff and soil properties in watersheds. Because wildfires do not have a uniform effect on the burned area, significant variability occurs between areas of different burn severity and likely elicits different hydrologic responses within watersheds. Much of the control on this hydrologic response stems from the variability of soil between burned and unburned watersheds. Establishing a linkage between soil infiltration and burn severity may therefore, offer insight into the likelihood of elevated levels of runoff and the likelihood of floods. Although previous studies have sought to establish a quantitative relationship between runoff and burn severity, this relation has not been evaluated with respect to soil moisture and infiltration and varying degrees of burn severity.

The Loretta-Linda Basin presents a unique opportunity to compare areas with different burn severities (with the right fork of the drainage experiencing a much higher burn severity than the left), while eliminating most other variables that may occur with greater spatial variability such as elevation, temperature, precipitation, underlying geology, and soil type. Rainfall, soil moisture, runoff, and infiltration data collected over a two-month period were used to evaluate the relationship between burn severity, runoff, and infiltration for the Loretta-Linda basin as a whole as well as for the individual forks of the basin. The impact of varying burn severity on the two sub drainages was further investigated by creating a dynamic simulation model in TopoFlow®.

Comparative analysis between the two forks did not show a dramatic difference in the runoff and infiltration relationship between the two burn severities. Variability of field

conditions, the presence of parameters affecting runoff not accounted for, and the limitations of point measurements, are reflected by the data analysis and lack of a strong correlation between burn severity, infiltration, and runoff. The use of spatial hydrologic modeling allowed for the investigation of the relative importance of the infiltration parameters as well as the impact of Manning's n on the response of the basin to rainfall. The modeling results indicate a strong correlation between high burn severity, low infiltration capacity, and elevated discharge volumes.

DEDICATION

I would like to dedicate this thesis to my mother and father, Susan and Gary Ahlstrom, who have been a support to me in every way as I've worked on my thesis research. I would not be where I am today without their guidance, encouragement, understanding, and love.

ACKNOWLEDGEMENTS

I would like to thank my committee chair and advisor, Dr. Rick Giardino, and my committee members, Dr. Vatche Tchakerian, and Dr. Jack Vitek for their guidance and support throughout the course of this research. I would especially like to thank Mr. John Moody, my supervisor and mentor at the USGS, without whom this research would have been impossible. John's guidance, enthusiasm, and patience during my internship at the USGS and during the time since, has been invaluable to me for my research and my development as a geologist.

I would also like to thank Deborah Martin and Brian Ebel of the USGS, Scott Peckham of the University of Colorado, and co-worker Melissa Carnicle, for their help in the office and in the field during my time in Colorado, as well as my friends and colleagues in the Geology & Geophysics Department for making my time at Texas A&M University a great experience. I also want to extend my gratitude to Conoco-Phillips for the fellowship that allowed me to focus solely on my research during my last semester as a graduate student.

Finally, thanks to my family and friends back home in North Carolina, whose love and support are always felt and always appreciated, even from many miles away.

TABLE OF CONTENTS

Page

LIST OF FIGURES

Page

LIST OF TABLES

Page

1. INTRODUCTION AND PROBLEM STATEMENT

The Fourmile Canyon fire was ignited northwest of Boulder, Colorado, in September 2010 and burned for eleven days. The fire burned approximately 26 km^2 in the area of Fourmile Creek, a primary tributary of Boulder Creek, before finally being extinguished (Montgomery et al., 2010). With the destruction of 169 homes and over $217 million filed in insurance claims, the Fourmile Canyon fire was the most costly in the history of Colorado.

The landscape-ecosystem short term response to a wildfire affects geomorphic processes mainly through the alteration of soil, vegetation, and hydrology (Swanson, 1979). The effects of these alterations are most pronounced in areas of steep terrain where vegetation regulates physical processes like runoff (Swanson, 1979). Wildfires do not have a uniform effect, however, on the burned area and significant variability occurs between areas of different burn severity and likely different hydrologic responses within watersheds. Although previous studies have sought to establish a quantitative relationship between runoff and burn severity (Moody et al., 2008), this relation has not been evaluated with respect to antecedent soil moisture in a montane watershed such as the Loretta-Linda Basin.

The Front Range climate is semi-arid and summer precipitation is dominated by intense summer convective storms (Moody and Martin, 2001). These intense, short term rainfalls increase the risk of flooding with heightened risk in areas affected by forest fire. The city of Boulder is immediately adjacent to the steep slopes of the Front Range with an ever-growing urban-wilderness interface. This interface contributed to the Fourmile

Canyon fire becoming the most costly in the history of Colorado (Brenkert-Smith and Champ, 2011) and is a contributing factor to risk of elevated levels of runoff and floods. Determining the relationship between burn severity and runoff may, therefore, provide some means of predicting areas at high risk for flooding based on the spatial distribution of burn severities.

Infrared imagery has been used to quantitative burn severity (see Section 2.6) of the watershed as a whole, as well as the burn severity of both sub drainages. Because the burn severity is much higher on the easternmost fork (right fork) than on the westernmost fork (left fork), the Loretta-Linda Basin presents a unique opportunity to compare the effects of different burn severities on runoff while eliminating most other variables that may occur with greater spatial variability. This study focused on linking burn severity to the runoff response and soil infiltration within the Fourmile Canyon burned area by comparing data collected from the adjacent sub drainages of the Loretta-Linda Basin.

1.1 OBJECTIVES

To accomplish the goals outlined in this thesis, the following objectives were established:

1) Characterize soil moisture for each sub-drainage of the Loretta-Linda Basin;
2) Determine properties of each storm cell (duration, intensity, total rainfall);
3) Characterize the infiltration and runoff response of the right and left forks of the Loretta-Linda Basin; and
4) Analyze the impact of varying burn severity on the two sub-drainages by creating a dynamic simulation model.

1.2 HYPOTHESIS

The research for this thesis is driven by the hypothesis:

H_1: The sub drainage with higher burn severity will have less capacity for soil moisture retention, lower rates of infiltration, and greater levels of area-weighted discharge.

H_0: The sub drainage with higher burn severity is not significantly different from the sub drainage with lower burn severity in soil moisture retention, rate of infiltration, or levels of area-weighted discharge.

1.3 STUDY AREA

The Loretta-Linda Basin is a southwest-facing watershed, located approximately three miles west of Boulder within the Front Range of Colorado (see Figure 1). The Front Range rises abruptly from the Colorado Plains and constitutes the major range of the southern Rocky Mountain physiographic province (Peet, 1981). The elevations in the Rocky Mountains range from 1600 ft at the base up to 4350 ft on the highest peaks. With such a range in elevations, great diversity exists geologically and environmentally as you move between low and high regions of the Rockies, with altitude controlling mainly the variables of climate and vegetation.

The distribution and formation of soil results from the impact of climate, vegetation, topographic setting, parent material and time, allowing for the delineation of elevation zones that control soil characteristics (Birkeland et al., 2003). Johnson and Cline (1965) divide the region into four elevation zones that are defined by differences in soil properties. The zones are divided to include the lower montane, upper montane, sub alpine, and alpine zones, each with unique vegetative patterns and soil characteristics. The Loretta-Linda watershed elevation ranges between 2200 and 2500 m, and is, therefore, located primarily in the lower montane zone (Peet, 1981). As seen in Figure 2, the lower montane zone is dominated by Ponderosa Pine (*Pinus ponderosa*) and Douglas Fir trees (*Pseudotsuga menziesii*), with mean annual precipitation of 54.5 cm, and a mean annual temperature of 5.6° C (Birkeland et al., 2003).

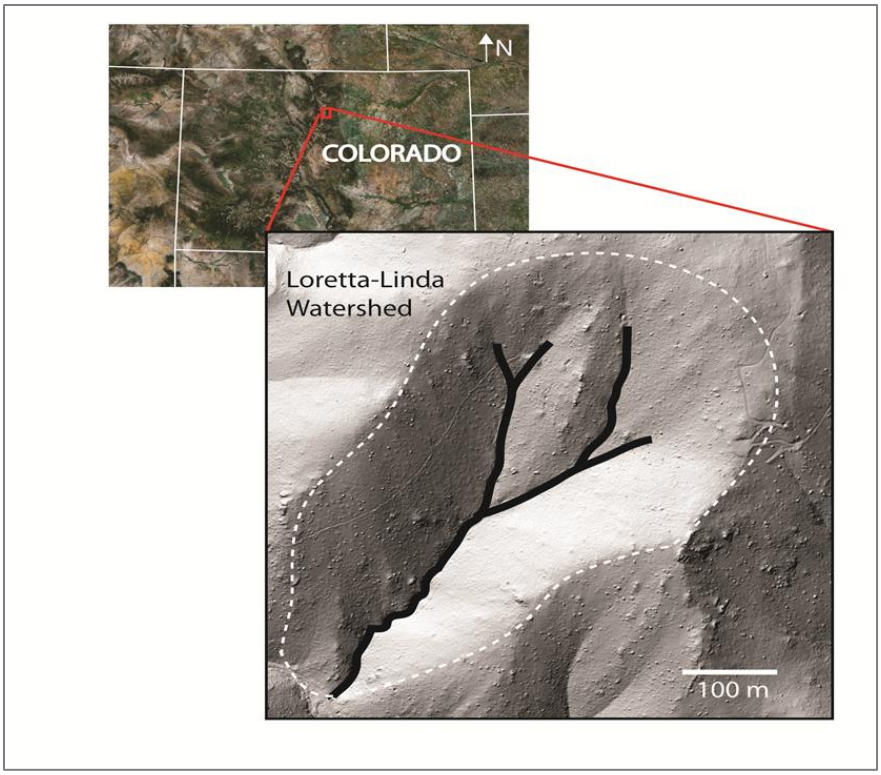

Figure 1- *DEM shaded relief image of the Loretta-Linda watershed with major drainages outlined, with Google Image local map.*

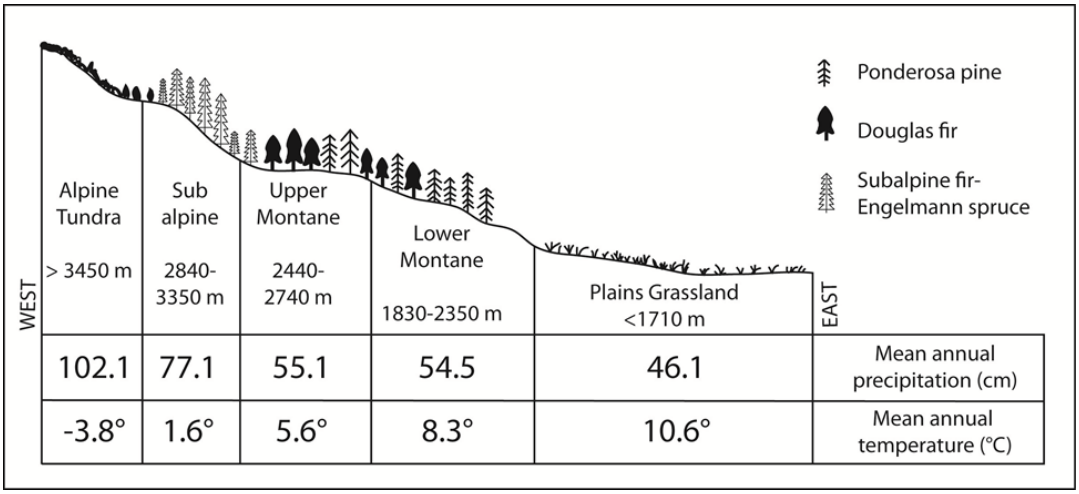

Figure 2- *Vegetation and climate vary with changing elevations on the Colorado Front Range. Gaps in elevation values represent transitional zones (modified from Birkeland et al., 2003).*

Because Loretta-Linda is a relatively small watershed, spanning approximately 300,000 m^2, climate and vegetative changes within the basin are minimal. Although the aspect of the two forks is slightly different, they are both primarily south facing (with the left fork being more southeast facing and the right fork facing southwest). An aerial photograph (Figure 3) taken before the fire shows the pre-fire vegetation of Loretta-Linda and a noticeable difference between sub drainages, the right fork having a much more dense vegetation coverage. The left fork drainage area is 79,800 m^2 and the right fork drainage is 235,000 m^2, and splits into two smaller sub drainages. The underlying bedrock geology of Loretta-Linda is typical of the Front Range, being mostly Lyons sandstone (Permian in age), a tan or pink, fine- to medium-grained, well sorted, well cemented, quartzose sandstone containing large-scale cross stratification (Bilodeaux et al., 1988).

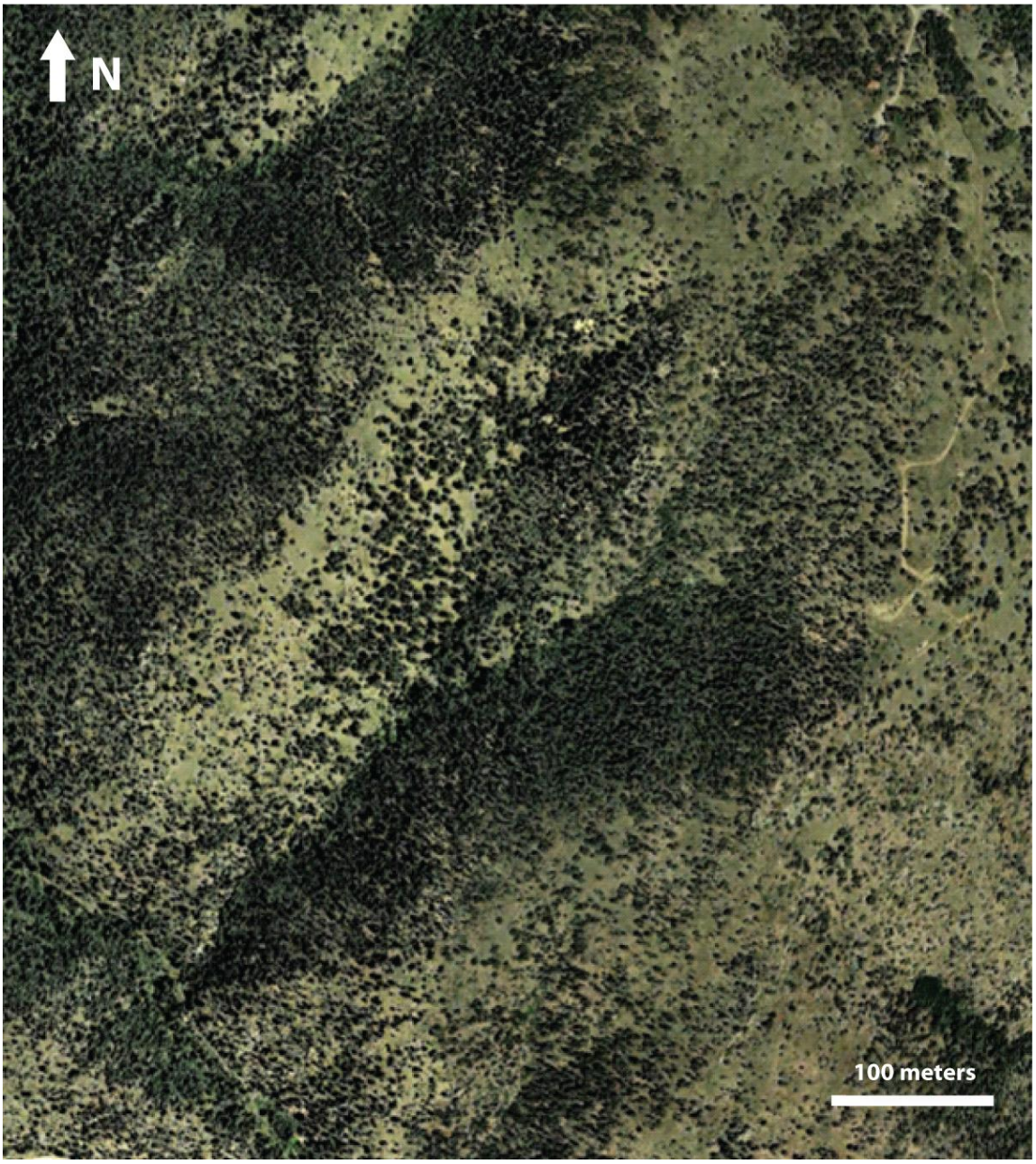

Figure 3*- 2009 Image of the Loretta-Linda basin, showing difference in vegetation between the left and right fork (from GoogleEarth).*

2. LITERATURE REVIEW AND BACKGROUND

2.1 WILDFIRE

In the Rocky Mountains of the western United States, complex topography and landscape patterns, extreme seasonal changes, and steep gradients in temperature and precipitation with changing elevation make hydrologic processes significantly different than lower elevations and more temperate environments (Bales et al., 2006). Hydrologic processes are further complicated by the incidence of wildfires that are common in the region. Previous studies have asserted that wildfires may increase runoff volumes and heighten the risk of downstream flooding, (Ebel et al., 2012; Moody and Martin, 2001; DeBano, 1999; Swanson, 1979; Moody et al., 2007b). The dramatic increase in the size, frequency, and duration of wildfires over the last thirty years has magnified the potential for these hazards, making the investigation of the impact of fire on mountain catchment hydrology timely research (Westerling et al., 2003).

Long-term studies of the impact of fire on the environment are challenging, because post-burn sites are dynamic and constantly changing as they recover from the effects of the fire. Depending on the severity of the burn, the impact of a wildfire may only be significant over a short interval of time immediately following the fire (Moody and Ebel, 2012a). Furthermore, the observation of change between an unburned and burned watershed is often precluded by the lack of pre-burn data collection (with the exception of studies conducted on prescribed fires) (Moody and Ebel, 2012b). The impact of wildfires, however, cannot be underplayed or ignored. Wildfires burn as much as 3.5 million ha every year in the United States (NIFC, 2003). In just the western

United States, the wildland-urban interface increased by 61% between 1990-2000, and over half of these areas are within forested regions characterized by high-severity fires (Schoennagel et al., 2009). Though wildfire has always drawn attention for its capacity for destruction, researchers in the US and specifically western states began to look at wildfires with greater scrutiny following the 1988 burning of over 250,000 ha in Yellowstone National Park and bordering areas (Turner et al., 2003). The trend toward increasing severity and number of wildfires nationwide sparked a debate concerning prevention methods (Turner et al., 2003).

A "let burn" policy was dominant in many fire-prone areas during the 1910s and 1920s (Swetnam, 1988). The 1930s saw a switch to the "hit-em hard and hit-em fast" strategy, advocating total suppression (Swetnam, 1988). By the 1970s and 1980s land management agencies in the western US established a middle ground, using fire for management purposes (Swetnam, 1988). Following the Yellowstone fire, however, a post-burn shock among the public and government officials threatened to push policy in the opposite direction towards a complete fire suppression policy, whereas others argued that this approach leads to extremely large accumulations of fuel between what otherwise would be fires of a manageable scale. Romme and Despain (1989) argued against viewing the 1988 Yellowstone fire as an extraordinary event, pointing out that the large extent of the burn was likely the result of climatic variables (1988 being the driest summer on record in YNP).

The surge of scientific investigation into wildfires was not confined to mitigation but extended into the geomorphologic, hydrologic, biologic, and chemical aspects of fire

impact. Hydrological and geomorphological changes relevant to this study include: changing soil structure and properties, destruction of vegetation, and even the direct weathering of bedrock (fire-induced weathering rates are reported to be one to two magnitudes higher than frost action) (Shakesby and Doerr, 2005). Although the past few decades have seen advances in knowledge of the geomorphic processes associated with wildfire, Shakesby and Doerr (2005) identify a need for a standard fire severity index relevant to soil changes rather than to degree of biomass destruction as well as a greater understanding of the hydrological and geomorphological impact of wildfire in a wider range of fire-prone types of terrain. This study will focus on the hydrologic impact of the 2010 Fourmile Canyon Fire on a montane watershed and how burn severity may control soil infiltration and the response of runoff.

2.2 IMPACT OF WILDFIRE ON SOIL

Soil is a major controlling variable on the hydrology of burned and unburned watersheds. Establishing a linkage between soil infiltration and burn severity is, therefore, an important step in studying burned catchment hydrology and may offer insight into the likelihood of elevated levels of runoff and the likelihood of floods. Post-burn settings and the hydrologic properties, however, are not always straightforward in part because of the pre-burn variability of conditions within any given watershed (Moody et al., 2007a). Inconsistent pre-burn conditions as well as the variability of fire intensity and characteristics make the impact of wildfires extremely varied even over the same watershed (Clark, 2001).

The physical characteristics of soil, affected by the heating process, include color change, loss or reduction of structure, reduction of organic matter, and reduction of porosity. The effects of fire on soil are induced by intense heating, removal of vegetation, litter, and duff, and often by the concentration of plant material substances in the soil (Clark, 2001). Previous studies assert that no irreversible changes occur, but the impact can be severe especially in the time immediately following the fire with issues such as hyper-dry conditions (Moody and Ebel, 2012a), hydrophobicity, and elevated rates of erosion (Certini, 2005; Shakesby and Doerr, 2005; Moody and Martin, 2009). Numerous factors contribute to the degree to which soil is heated during a forest fire, including: fuel loading, fuel moisture content, fuel distribution, rate of combustion, soil texture, soil moisture content, and soil mineral composition (Clark, 2001). Though some studies have noted the benefit of moderate severity fires in promoting renovation of vegetation, high burn severities generally create a negative impact on soil.

In addition to the highest temperature a soil experiences during a fire, the length of exposure time is just as important. In forested areas, the highest temperatures are usually beneath thick fuel accumulations (Clark, 2001). With heavy fuel, temperatures between 500-700°C may be reached on the surface (DeBano, 1999). At a depth of 5 cm, temperatures rarely rise above 150°C and below 20 cm no heating occurs (DeBano, 1999). Fuel accumulations are variable and depth of heating is dependent on soil packing and overall thickness, leaving a mosaic pattern of burn severities across any given burned area (Clark, 2001). Dry soil is a poor conductor of heat (temperatures will rarely exceed 150°C), and pre-burn soil moisture is controlled largely by the presence of

organics (internally and as a protective top layer) (Ice et al., 2004). Therefore, soils in burned areas are largely affected on the surface, or top three centimeters.

Vegetation, litter and duff provide fuel for the fire and the ability of water to conduct heat means that the rate of conductance and temperatures will be higher in moist, organic rich soils. Post-fire, the loss of organic material (termed loss on ignition or LOI) plays a role in the loss of soil moisture immediately following a forest fire, as well as the soils long-term ability to retain moisture. With reduction of soil infiltration, moisture retention, evapotranspiration, and litter and debris interception, levels of runoff are often elevated in burned watersheds (Clark, 2001).

In addition to fueling the fire, the predominant effects of fire on soils results from the combustion of organic matter. Transformation of the organic content in soils leads to a loss of nutrients and often a degradation of structural stability greatly impacting the hydrologic behavior of soils by decreasing porosity and infiltration capacity while increasing erosion and runoff rates (Garcia-Corona et al., 2004). Furthermore, organic material in soil affects the ability of soil to develop a water repellant or hydrophobic layer.

The top layer of mineral soil naturally has a slight hydrophobicity resulting from the aliphatic hydrocarbons that are leached from shallow organic horizons (DeBano, 1999; Deorr et al., 2000; Doerr and Moody, 2004; Certini, 2005). At high temperatures, these aliphatic hydrocarbons are distilled during combustion and are reduced to mostly carbon dioxide and water vapor (Clark, 2001). Drying, volatilization, condensation, charring, and chemical reactions are among the effects of combustion that occur during a

forest fire (Bento-Gongalves et al., 2012). Nutrients in the organic matter will vaporize at different temperatures, two of the most common being Nitrogen (which vaporizes at 200-500°C) and Phosphorous (which vaporizes at 770°C); other nutrients such as Calcium, Magnesium, and Potassium are converted into oxides (Ice et al., 2004). When these organic compounds turn to vapor and subsequently condense on the remaining soil particles and mineral grains, a negatively charged, water repellant layer forms on the surface (Clark, 2001; Ice et al., 2004; Hamlett et al., 2011).

The loss of soil wettability or hydrophobicity has long been a topic of interest in wildfire-affected areas because of its control on runoff. Though decreases in infiltration were initially attributed solely to loss of vegetation, in the 1960s a hypothesis was developed that described the formation of a water repellant layer forming on soils post-fire (DeBano, 1999). Numerous field and laboratory studies confirmed the intensifying of water repellency with increased heating and its control on increased erosion (DeBano and Krammes, 1966). The hydrologic responses to hydrophobicity include but are not limited to infiltration, runoff, rill formation, rain drop splash, and stream flow parameters (DeBano, 1999).

The variability of field conditions, the unpredictability of wildfire (and the subsequent lack of pre-burn data), and the data collecting limitations in large watersheds have discouraged extensive field observations of soil parameters post-wildfire. DeBano (1999) acknowledges that predicting watershed responses by using information gained from conceptual models, laboratory studies and small field plots is difficult because expanding these relationships to a larger scale encompasses more heterogeneous and

highly variable natural systems. Whereas the soil properties are undoubtedly affected by burn severity, hydrophobicity may not be an enduring aspect of wildfire. In a 2004 study of a front range fire in Colorado, MacDonald and Huffman (2004) showed that soil water repellency did interact with burn severity, moisture content, and soil depth but that these effects were not measurable one year after the fire.

Still, the concept of hydrophobicity is important because soil moisture is one of the primary variables studied in the Loretta-Linda Basin. Although LOI and presence of hydrophobicity may be indicative of the varying degrees of burn severity, having pre-burn data for these parameters would be necessary to observe meaningful change in these parameters as a result of the fire. Therefore, in a non-prescribed (wild) fire, such as the Fourmile Canyon fire, it would not be possible to calculate burn severity based on these variables or to truly quantify the change. Rather, soil moisture data are used to better understand the controls on the hydrologic response of the watershed in the two areas of different burn severity, because antecedent soil moisture is an important variable in infiltration and runoff.

2.3 BURN SEVERITY

For many years, no clear definition existed for the term "burn severity," and a distinction was not made between burn severity and terms such as burn intensity (Ice et al., 2004). Fire intensity, burn severity and fire severity, though often used interchangeably refer to very different variables associated with wildfire. Byram (1959) as quoted in Ice (2004), fire intensity has several definitions in the literature to include

the rate of heat energy released per unit time per unit length of fire front (Ice, 2004), the amount of fuel burned per second in kW/m^2 (DeBano et al., 1998), the rate at which fire produces thermal energy (Neary et al., 2005), and the maximum temperature recorded at a certain point and the time that the temperature remains constant in C/s (Ubeda, 1999).

Fire severity as described by Certini (2005), consists of two components: intensity and duration, where intensity is the rate at which a fire produces thermal energy. Duration is cited as the component with the most control on below ground damage. Intense but fast moving fires do not cause heat to penetrate below the top few centimeters of soil (Certini, 2005).

The term burn severity refers less to the properties of the fire itself (though this is a main control on burn severity) and more to the response of ecosystems to fire. Parsons et al. (2010) define burn severity as the effect of the fire on the ground surface characteristics. Surface characteristics include char depth, organic matter loss, soil color and structural changes, and reduced infiltration (Parsons et al., 2010). Degrees of soil burn severity are assigned in post-fire assessments to describe the effect of the fire on flora and fauna, water systems, and the soil (soil burn severity) (Bento-Gongalves et al., 2012; Parsons et al., 2010). DeBano et al. (1998) described the following criteria for burn severity delineations:

> *Low burn severity*: less than 2% of the area is severely burned, less than 15% is moderately and the remainder of the area is burned at a low severity or unburned.
>
> *Moderate burn severity*: less than 10% of the area is severely burned, but more than 15% is moderately burned and the remainder is burned at low severity or unburned.

> *High burn severity*: more than 10% of the area has spots that are burned at high severity, more than 80% is severely or moderately burned and the remainder is burned at low severity.

Many methods exist for measuring and quantifying burn severity, both in using lab experiments and field measurements. Giovanni (1994): studied the consequence of temperature on some chemical soil properties, Dimitrakopoulos et al. (1994) measured the effects of different temperatures on soil samples under laboratory conditions, and Moreno and Oechel (1989) evaluated intensity after wildfire by measuring branch diameter to estimate heat released per unit area (Dimitrakopoulos et al., 1994; Moreno and Oechel, 1989). Remote sensing and the use of infrared imagery are often used when the basin scale makes field methods impractical. The use of near- and mid-infrared imagery of pre-burn and post-burn sites will make it possible to distinguish between low, moderate, and high severities, and also quantify the severity of any given area down to a 1 x 1 m area.

The USDA Forest Service Remote Sensing Applications Center (RSAC) and the USGS Center for Earth Resources Observation and Science (EROS) have provided satellite imagery that can be used to rapidly map the severity of soil burn after a wildfire. Pre- and post-burn satellite images are compared to evaluate landscape change and produce the Burned Area Reflectance Classification (BARC) (Clark and Bobbe 2006). The BARC is derived from an algorithm known as the Normalized Burn Ratio (NBR). The NBR is created with near infrared (NIR) and short-wave infrared (SWIR) bands, collected from the Landsat satellite sensor. NBR is calculated with the algorithm:

eq. 1.1 $$NBR = (NIR - SWIR) / (NIR + SWIR) \times (1000)$$

Near Infrared energy is reflected by green, healthy vegetation, whereas mid infrared energy is reflected by rock and bare soil. Mid-infrared values will, therefore, be higher in areas that have been burned more severely. To determine the effect of the fire on the soil, the pre- and post-burn infrared values must be compared. This value is called the differenced Normalized Burn Ratio (dNBR; Key and Benson, 2004) which is given by:

eq. 1.2 $$dNBR = NBR_{pre\text{-}fire} - NBR_{post\text{-}fire}$$

A BARC layer is created for GIS and mapping programs, though it is not considered a true soil burn severity map until it has been field checked and verified. BARC values range between 0 and 255, with higher numbers representing areas of greater burn severity (Clarke and Bobbe, 2006). A wide range of values for dNBR are represented within large burned areas and even within the same small watershed, as seen in Figures 4 and 5. Figure 4 shows the distribution of burn severities for the entire Fourmile Canyon fire and Figure 5 shows the burn severity within the Loretta-Linda Basin. The difference in overall burn severity between the right and left fork of the watershed is apparent, with the right fork experiencing much greater burn severity.

Although burn severity may be quantified with the infrared remote sensing method, it is also helpful to be familiar with the characteristics of different levels of burn severity and their manifestations on the ground. If broken up, very basically into low,

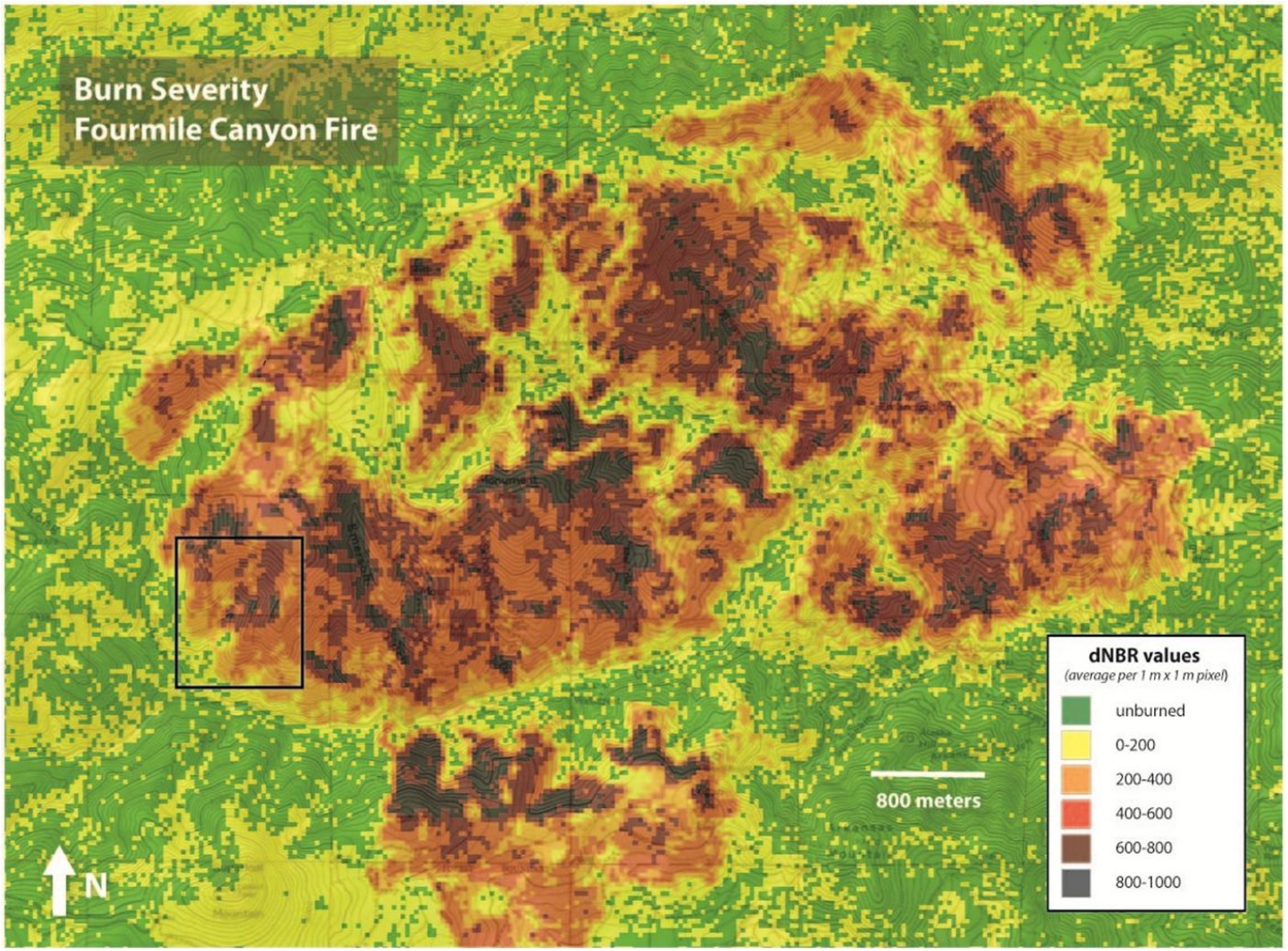

Figure 4- *Burn severity map showing the distribution of dNBR values over the entire burned area.*

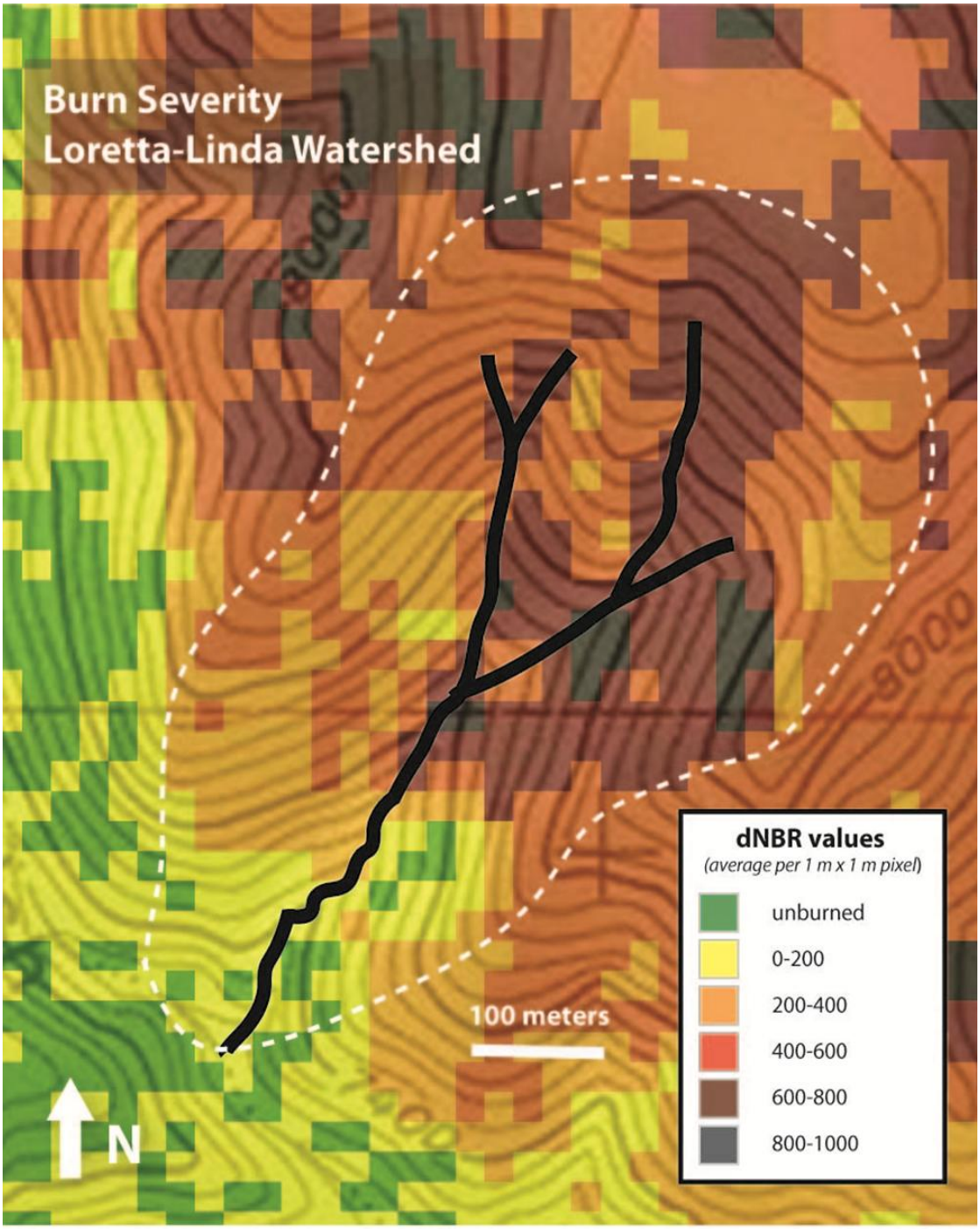

Figure 5*- Burn severity map showing the distribution of dNBR values over the Loretta-Linda watershed. The right fork clearly shows higher average burn severities.*

moderate, and high burn severity classes, the following would be true according to Ice et al. (2004) and Parsons et al. (2010):

> *Low burn severity*: may range from a slight char on finer fuels with no change in soil structure or infiltration, to partial consumption of litter layer and a slight change in structure on the shallow surface only with little to no change in runoff/infiltration;
> *Moderate burn severity*: moderate charring of ground, deeply charred litter and duff layers, roots may have burned in the subsurface, decreased infiltration because of a hydrophobic layer and subsequent elevated runoff levels; and
> *High burn severity*: deep charring of the ground, consumption of litter and duff layer, soil structure is degraded and may undergo color change, infiltration is reduced as hydrophobicity increases, runoff response is, therefore, high.

Ice et al. (2004) asserts that these qualitative assessments of burn severity assume that soil characteristics are the primary control of a watersheds hydrologic response, though antecedent conditions, storm size, and rainfall intensity are important factors to consider as well. Measurements of soil moisture and rainfall duration and intensity were collected in the Loretta-Linda Basin, ensuring that all of these controls on runoff were addressed.

2.4 INFILTRATION

Infiltration, an example of the general phenomenon of water movement in porous media, is one of the most important and complex variables in this study (Philip, 1956). Infiltration is controlled by climate and rainfall properties, geomorphology, soil depth, and soil hydraulic properties (Smith, 2002). The two main forces affecting infiltration

are capillary and gravity. Capillary pressure occurs at the interface of two liquids at the surface of a porous media (Smith, 2002). In the case of watershed hydrology, the water-air threshold is the focus, with water being considered the wetting fluid because it is more strongly attracted to the solid medium (Smith, 2002). The pressure discontinuity at the water-air interface is balanced by a film tension at the surface called capillary tension, the balance of these forces is described with the equation for capillary rise, h:

eq. 2.1

$$h \frac{2\pi \cos\alpha}{Rg(\rho_l - \rho_a)}$$

where a is the angle of wetting, g is the gravitational constant, ρ_l is the liquid density, and ρ_a is the air density. Whereas this equation represents the movement of water into the porous media, flow within the media, whether saturated or unsaturated is described by by Darcy's Law. Darcy's Law describes the proportionality of flow per unit area v, and the gradient of the total potential, H:

eq. 2.2

$$v = -K \frac{dH}{dx}$$

where K is the coefficient of proportionality, x is the measure of distance in the flow direction, and the total potential H is comprised of the capillary pressure potential plus the gravitational potential. K represents hydraulic conductivity of the medium while K_s often refers to saturated hydraulic conductivity (Smith, 2002).

The rate of infiltration is affected heavily by the rate of precipitation or rainfall intensity. This control is magnified further on bare soils like those left after a forest fire. Raindrop impact on bare soils has been shown to destroy surface aggregates and form in

the soil a thin upper layer of lower hydraulic conductivity (Morin and Benyamini, 1977). In a study conducted by Morin and Benyamini (1977), it was found that trends of decreasing rates of infiltration were the same for all rainfall intensities but that it occurs more quickly at higher rainfall intensities. A difference was also observed between soils final rate of infiltration between different rain intensities.

Green and Ampt (1911) (as cited in Smith, 2002) first published a study on infiltration describing the movement of water into soil from a ponded surface. Then in the 1930's Horton, seemingly independent of Green and Ampt sought to describe infiltration with respect to process dynamics, contrary to the way engineering was treating the concept of infiltration. Horton ceased referring to "infiltration capacity" and rather refined this "capacity" to an infiltration rate that declines exponentially over the course of a rainfall event (Smith, 2002). This is the defining difference between Horton's approach and that of Green and Ampt, infiltration from rainfall versus from water ponded on the surface (Smith, 2002).

2.5 RUNOFF

The generation of runoff can be crudely subdivided by two types of soil hydraulic limits: subsurface soil control and surface soil control. Subsurface soil control is important for lower rainfall rates in humid conditions where the soil may be saturated from below, especially if some barrier exists to saturation from the surface (Smith, 2002). Alternatively surface soil control occurs when the rate of rainfall exceeds the rate at which soil can absorb water at the surface, creating saturation excess (Smith, 2002).

During the summer months, the Front Range of Colorado experiences short convective storms (see section 2.6). In the Loretta-Linda watershed, the generation of runoff is a function of surface soil control (the Horton mechanism). In the most simplified terms, the control comes from the interplay of the rate of supply and the limiting rate of intake (Smith, 2002). The short summer convective storms have a major control on the response of runoff in the basin.

2.6 STORM CELLS

In a regional study of wildfires over several years, Westerling et al. (2003) found that in the western United States, wildfire is strongly controlled by seasons. Ninety eight percent of burned area and 94% of fires occur between May and October. This seasonality closely follows the warming trend at this latitude during July and August (Westerling et al., 2003). Along with warming trends are dry springs and early summers that precede Monsoon rains June through August leaving the region susceptible to lightning strikes associated with these storms and heightened potential for anthropogenic influence in the summer seasons.

Whereas dozens of small, localized storms occurred in the Front Range area during the summer of 2011, only eight storms were of a magnitude able to be recorded across the watershed by a minimum of four out of six of the rain gages. A summary of these storm cells is given in Table 1. Whereas many of the smaller storms were recorded by one or two gages in the watershed intermittently throughout the summer, these nine storms represent the measurable precipitation events and will be used to investigate the

infiltration and runoff patterns. The data recorded by instrumentation in the watershed are also the data set used to run and calibrate the spatial hydrologic model created using the program TopoFlow®.

Storm Date	Start Time	Stop Time	Peak rainfall rate (mm/h)	Duration	Total Rainfall (mm)
20 June	23:42:20	5:47:29	30.53	6:05:09	28.845
7 July	18:04:30	21:23:13	30.43	3:18:43	12.433
10 July	19:01:43	22:53:40	8.45	3:51:57	5.471
12 July	21:32:18	22:51:27	7.61	1:19:09	7.460
13 July	18:04:19	23:19:06	21.16	5:14:47	19.396
14 July	12:31:29	14:20:33	6.67	1:49:04	4.725
16 July	13:50:18	19:57:58	10.24	6:07:40	7.957
19 July	17:51:58	18:25:27	8.02	0:33:29	3.730

***Table 1**- Summary table of the largest rainfall events organized into individual storm cells.*

2.7 TOPOFLOW®

Spatial hydrologic modeling is a primary application of geomorphometry, a term used to describe quantitative land surface analysis. TopoFlow® is a spatially-distributed hydrologic model used to model physical processes in a watershed, a linkage based on the relationship between topography, gravity, and the tendency of flow paths to follow the topographic gradient (Peckham, 2009).

Although hydrologic models are not new in the field of geomorphology or hydrology, it has only been with the recent advances in computational ability that large data sets can be analyzed in a practical way. Because spatial hydrologic models analyze each DEM cell separately, each having to conserve mass and momentum as inputs and outputs of water change, a high level processing capability must be available (Peckham, 2009). Each cell in a DEM is subject to the same simple rule that whatever goes in must either come out or be stored in that cells interior.

The DEM is used as the foundation of the model and all tabular data must be converted to grid format so that it can be analyzed spatially. A third dimension of time is added by creating a series of stacked grids, or grid sequence. Physical processes including snowmelt, precipitation, evapotranspiration, infiltration, channel/overland flow, shallow subsurface flow, and flow diversions may all be treated as grid sequences in TopoFlow®. Grids of elevation, slope, aspect, and contributing area are derived from the DEM and serve multiple functions in the model. DEM resolution, in this case 2x2 m pixels is well scaled to resolve the hill slopes of the Loretta-Linda basin (grid size is usually chosen to be smaller than the hillslope and larger than the width of the largest channel) (Peckham, 2009).

Each grid cell has one channel associated with it, allowing for channelized flow to be modeled in a 1D process. Additional channel properties for each grid cell such as sinuosity or channel length, channel bed width, bank angle, and channel roughness parameters, are also stored in each pixel. In steep basins like the Loretta-Linda, it is appropriate to use the simplest means for modeling flow in open channels, the kinematic

wave method (Peckham, 2009). This method uses the same conservation of mass principle while simplifying the momentum conservation by excluding pressure gradient, local acceleration, and convective acceleration, and taking into account only the friction and gravity terms. The "law of the wall" describes this balance of gravity against friction in an equation for depth-averaged flow velocity u:

eq. 2.3 $$u = (g * R_h * S)^{1/2} * \ln\left(a * \frac{d}{z_o}\right) * \kappa^{-1}$$

where g is the gravitational constant, R_h is the hydraulic radius (the wetted cross sectional area/wetted perimeter), S is bed slope, a is an integration constant, d is the flow depth, z_0 is the roughness height, and κ is von Karman's constant (~0.408). Mannings formula is one that may be used in a basin with primarily open channel flow. Manning's formula gives the depth-averaged velocity as:

eq. 2.4 $$u = \frac{R^{2/3} S^{1/2}}{n}$$

where n is the empirical roughness (for other terms definitions refer to equation 2.3). Using the kinematic wave method for the Loretta-Linda requires that the bed slope be computed between each grid cell of the DEM and its neighbor in what is known as a D8 flow grid (Peckham, 2009).

The D8 flow grid, pioneered by O'Callaghan and Mark (1984) is one DEM derivative created in RiverTools® and used in TopoFlow®. D8 gridding is a simple method for specifying flow direction between pixels in a DEM, such that movement can

occur either adjacent or diagonally, in the direction of the steepest slope (named D8 for eight potential flow directions separated by 45°) (Tarboton, 1997). Narrowing flow direction down to one of eight options is a simplification but this method allows for the determination of flow direction based solely on DEMs, thereby determining the path of water, sediment, and contaminant movement, while also calculating the contributing area for each pixel (Tarboton, 1997).

Overland flow is a process that must be treated differently than channelized flow. Even when storm events generate runoff, grid cells with small contributing areas will likely lose these relatively small volumes to infiltration and have little to no surface flux. These cells will also have higher values for relative roughness (average height of roughness elements divided by the water depth), meaning that frictional processes will be more effective at slowing down small flow volumes (Peckham, 2009). Overland flow, or Hortonian flow, tends to flow in a sheet, wetting the entire surface of grid cells. Eagleson (1970) and others have found that Manning's equation may be used to calculate the flow velocity for overland flow but only using a very large "Manning's n" value (around 0.3 or higher), an order of magnitude higher than that used for computing channelized flow velocity (Peckham, 2009).

TopoFlow® models infiltration as a vertical flux in each grid cell. Because infiltration operates in the unsaturated zone between the soil surface and the water table, and represents a combination of capillary and gravitational forces, it is one of the most complicated parameters to model (Peckham, 2009). Most models use a variant of Green-Ampt or Smith-Parlange methods for infiltration which assume a single storm

event, a single soil layer, and no water table. These assumptions may seemingly create uncertainty with over-simplification of the role of infiltration in a watershed; however, by modeling each storm cell experienced in the Loretta-Linda basin separately, each with field-measured values for soil moisture, rainfall, runoff, and infiltration, much of this uncertainty is eliminated. The assumption of a single soil layer also proved to be more appropriate as data from the Decagon soil sensor showed that the short-term response to rainfall was confined to the uppermost soil layers, above the 5 cm depth mark.

Physically based mathematical models have historically had issues with scale. Models developed and tested at plot scale, for instance, may not be appropriate for extrapolation into much larger areas (or will at least be grossly simplified) (Peckham, 2009). The heterogeneity of natural systems also means that models even of the same watershed may vary significantly over large distances. In the 1970s, the first conceptual rainfall-runoff models developed were applied mostly to small and medium sized river basins where discharge measurements were available. (Koren et al., 1999). Despite assumptions of homogeneity, these lumped models yielded reasonable results initially. Scale problems were magnified when these lumped models were applied to un-gauged basins with no adjustment to the various parameters. It was during this time that the International Project on the Representative and Experimental Basins, which collected data on experimental basins throughout the world, declared that a problem with scaling exists in the field hydrologic modeling, and that the modeling results obtained on small

experimental basins could not so easily be transferred to larger watersheds (Koren et al., 1999).

Koren et al. (1999) analyzed several different hydrologic models and found that as the scale increased, the estimation of runoff decreased, indicating that over-scaling a basin may lead to underestimations of runoff. For this study, runoff will be predicted with the modeling tool and field data will be used to check the results after each storm cell run of the model. In addition, challenges represented by heterogeneity in watersheds have been minimized with the thorough collection of field measurements. Wood et al. (1990) suggests that topography, soil, and rainfall are the greatest sources of heterogeneity in watersheds and runoff models (Wood et al., 1990). A DEM with 2 x 2 m resolution, soil moisture data measured consistently throughout the summer, and a network of rain gages throughout the basin, minimize the uncertainty and scaling problems associated with many hydrologic models. As with all hydrologic models, some assumptions must be made where data is either not available or not measurable, however the data set collected in Loretta-Linda means less extrapolation will be needed in the preprocessing steps and subsequent model runs.

3. METHODS

3.1 MEASURING RAINFALL

Determining the temporal intensity and extent of each of the storm cells required organizing the rainfall data into storm cells and extracting statistics about the rainfall. Six tipping bucket rain gages were used in the Loretta-Linda basin for recording rainfall. Data from the five rain gages in the upper reaches of the watershed were used to compute area-weighted rainfall statistics for each sub-basin area, characterizing the storm cells, which can then be linked to the correlating antecedent soil moisture.

Tipping bucket gages consist of a 9-inch diameter opening that funnels rain directly over an interior axle holding the two-sided tipping bucket. Each side of the tipping bucket will hold 2.54 mL of water before tipping and emptying its contents so that the other side may begin to fill. Each rain gage was individually calibrated in the lab before deployment, ensuring that both bucket chambers would hold the correct amount of water before each tip is recorded.

Three gages were placed just below the ridge on the boundaries of the basin, to the east, west, and north (Figures 6 & 7). Gages were also installed at both runoff plots, on the left and right fork of the watershed, and one at the southward mouth of the basin (not shown on instrumentation map). Although tipping bucket rain gages may slightly underestimate the total rainfall (because of the carry-over of partially filled buckets at the end of a rainfall event), unlike standard rain gages, tipping buckets record the intensity of rainfall. Whereas knowing the total volume of rainfall after any event is useful, these data do not necessarily characterize the storm itself (i.e., elapsed time vs.

total rainfall, and changing rate). Because the data logger in each of the rain gages records the time of each bucket tip, each precipitation event is well characterized and statistics (such as rate of rainfall, duration, and intensity) about each storm cell were recorded and extracted (Table 1).

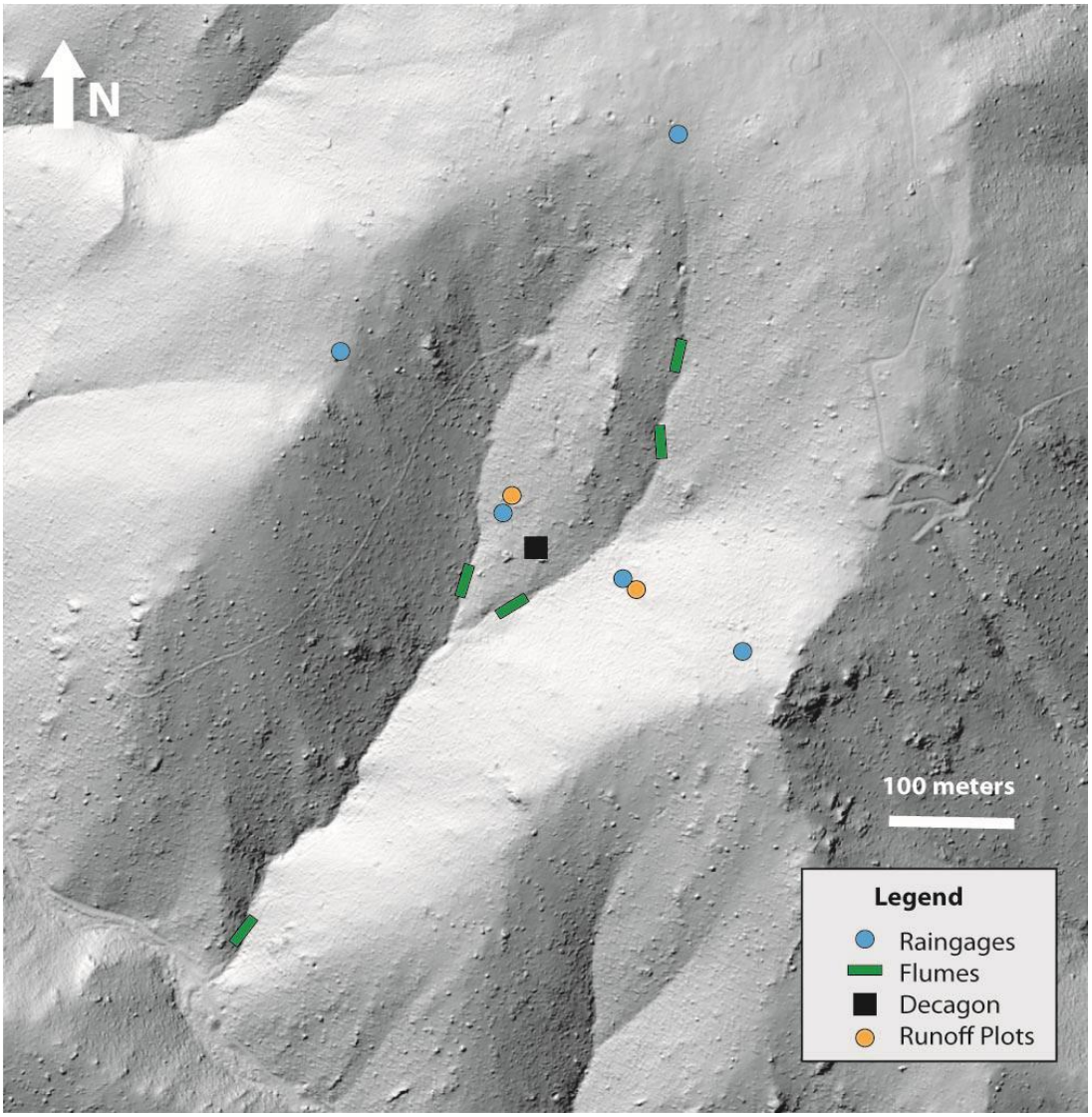

Figure 6*- Map showing the location of instrumentation installed in Loretta-Linda during the summer of 2011*

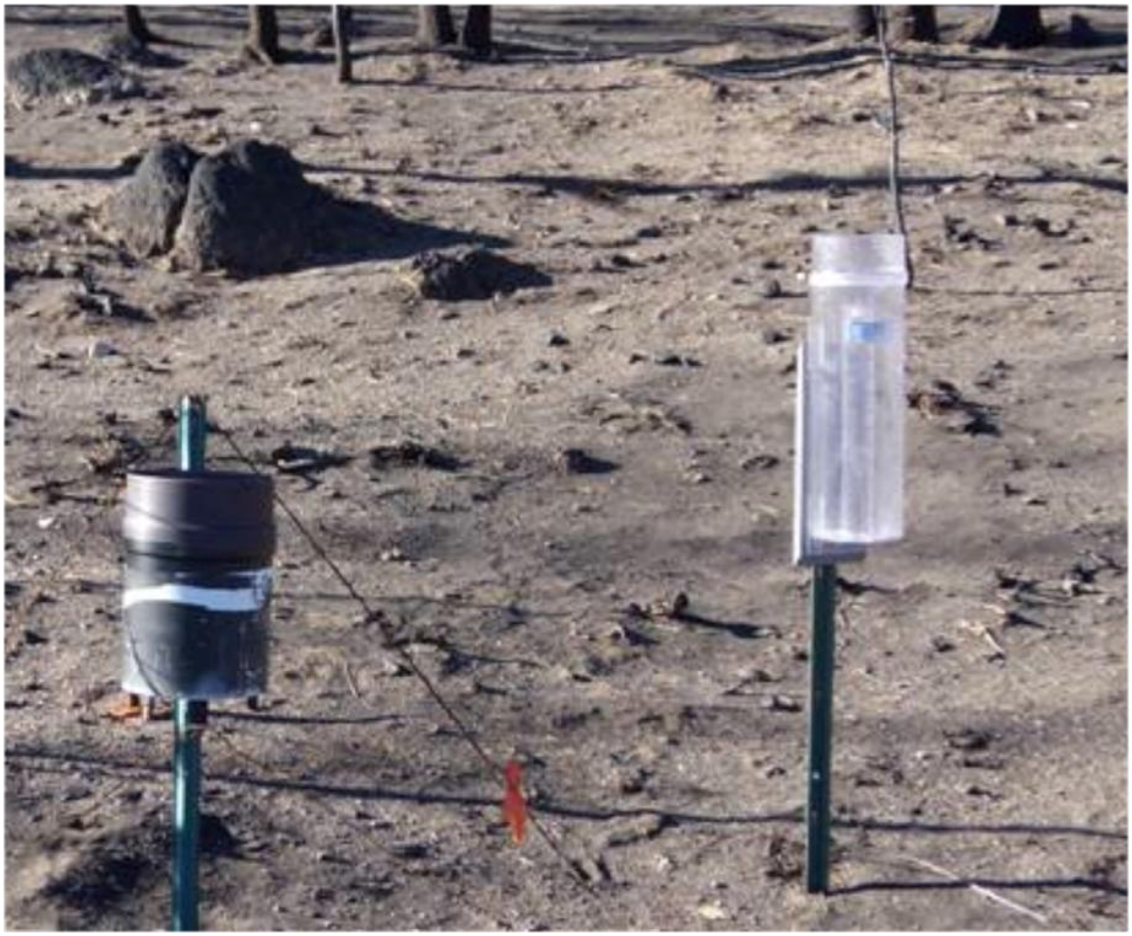

Figure 7*- Photograph of the tipping bucket rain gage (left) with an adjacent visual rain gage (right) (which was used for reference in field work only) (Moody 2011).*

3.2 MEASURING INFILTRATION AND RUNOFF

The runoff response will be determined by processing the runoff plot data to get infiltration as a function of time (Rainfall (t) – Runoff (t)) and by processing the flume data to find water discharge for each sub-drainage. Creating combined plots that show discharge versus time and rainfall versus time will graphically relate the two variables and allow for comparison between areas of different burn severity.

The combination difference infiltrometers offer a unique method for collecting infiltration data. There are many methods for measuring infiltration, however few allow for the measurement of infiltration rates over the course of a rainstorm (as most depend on measuring infiltration from ponded water on the surface). Even fewer methods are capable of measuring infiltration in real time in the field. The combination difference infiltrometers were installed on the left and right fork of the watershed, both on the west facing slop to minimize variability associated with aspect (Figure 8).

Figure 8*- Photograph of a runoff plot with two tipping bucket raingages, one measuring rainfall (right) and one flush with the ground measuring runoff (Moody 2011).*

These plots isolated a circle approximately 1 m in diameter of soil, funneling all surface runoff into a tipping bucket rain gage, placed flush with the ground. With a known confined area, and an adjacent rain gage recording the amount of rain falling on the plot, and another recording how much water runs off the plot, we can calculate the rates of soil infiltration and determine if measurable differences occur in the rate of infiltration in the left and right forks.

3.3 MEASURING DISCHARGE

Five Parshall flumes were installed in the Loretta-Linda basin (Figures 9 & 10) to measure the total discharge as well as discharge within both sub drainages. Several varieties of flumes and weirs can be used to measure fluid flow. The Parshall flume is a variation of the Venturi flume, which is essentially a short stabilized reach of channel designed with a width-contracted section (Kilpatrick 1983). The Venturi flume provides more satisfactory results than a weir with regard to head loss and submergence effect, however, requires the measurement of head in the contracted section and in the upstream reach. The important design change with the evolution of the Parshall flume is the sharp drop in the floor slope through the flume throat (see Figures 11 & 12).

The change in slope causes critical depth to occur there, providing a system that requires only one head measurement for the determination of discharge. Two flumes used overhead sonic sensors to measure distance to the water surface below, sending pulses down that would are reflected by the flow surface (at 20 second intervals),

Figure 9- *Photograph of a modified Parshall Flume installed in the Loretta-Linda basin, using a sonic sensor to measure the distance to the surface of water flow (Moody 2011).*

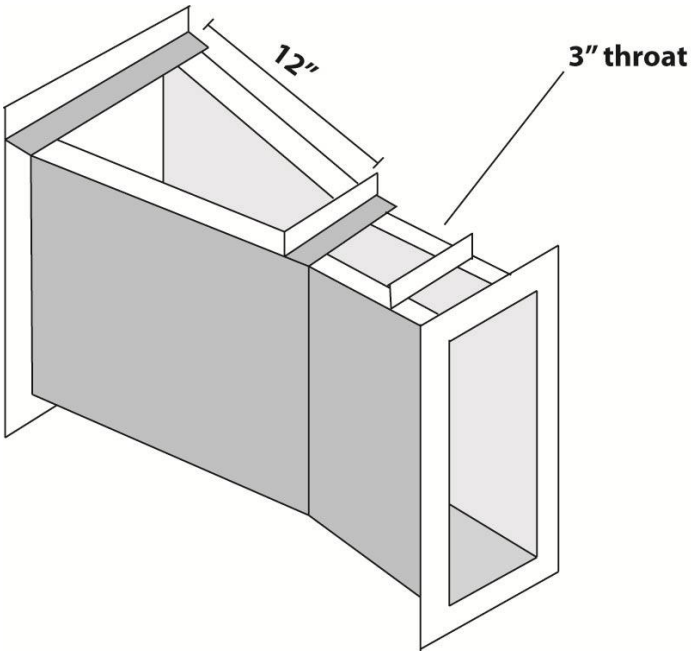

Figure 10- *Oblique view of a modified Parshall Flume with a 3-inch throat. This figure illustrates the dimensions of the four flumes installed in the upper reaches of the watershed.*

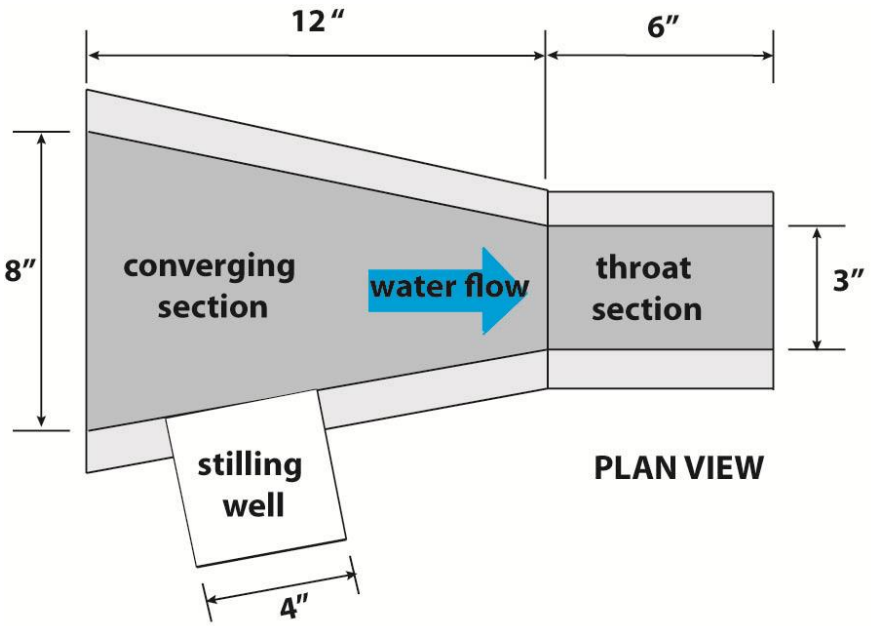

Figure 11- *Plan view of the modified Parshall Flume. The stilling well was located to the side as pictured here in the 9-inch flume while flumes 3-2 and 3-3 had wells inset below the flume (so that the senor was flush with the bottom of the flume)*

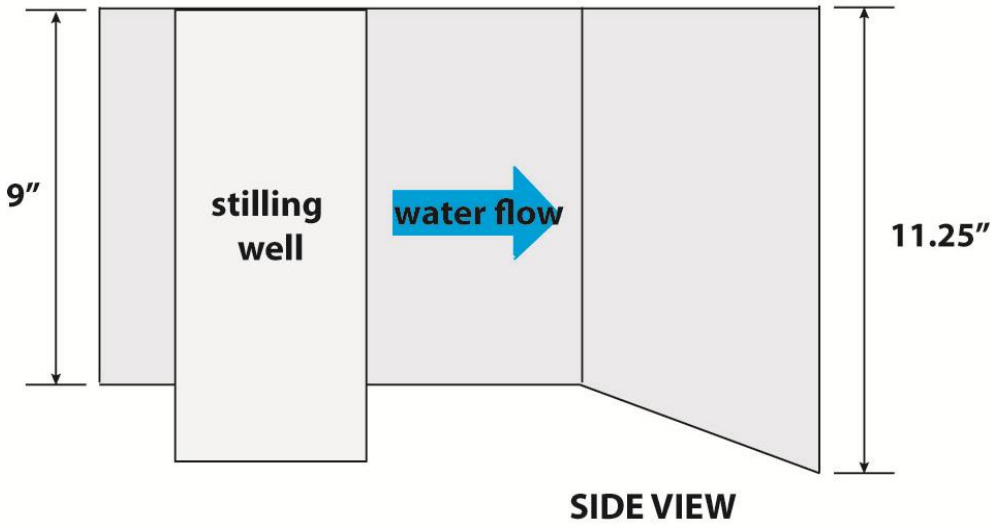

Figure 12- *The side view shows the sharp drop in the floor slope that causes critical depth to occur at this known point. This key design feature of the Parshall Flume allows for the calculation of discharge based on a single depth measurement.*

whereas the other three used Solinst® pressure sensors installed in the base of the flume, recording the overhead pressure and, therefore, the amount of water within the flume (also at 20 second intervals). Because the Solinst® pressure sensors are sensitive enough to pick up slight fluctuations in atmospheric pressure, separate Solinst® sensors were installed above ground, adjacent to each flume. These sensors were used as barometers so that the atmospheric pressure could be subtracted from the values reported by the sensors taking measurements of water pressure.

One 9-inch flume, installed below the main confluence, measured total discharge for Loretta-Linda whereas one 3-inch flume on the left fork, and three 3-inch flumes on the larger right fork recorded localized discharge within the watershed. Boundaries created with GPS points collected in the field as well as observations of topography and the mapping capability of RiverTools® were used to determine the area of each sub drainage. Knowing rates of infiltration for the left and right fork, the character of particular rainfalls, and the discharge for these drainages will be paramount in characterizing the hydrology of this burned watershed and in determining the linkage between these patterns and burn severity. All of these measured parameters provide greater control when creating a simulation of runoff in TopoFlow®. The discharge data collected at these flumes in the field will be used to calibrate the TopoFlow® models that are based on the primary input of rainfall.

3.4 SOIL MOISTURE

Antecedent soil moisture data were collected using two different methods: the Decagon soil moisture probe that measures volumetric water content (VWC) and the collection of soil samples which measure gravimetric water content (GWC, the mass of soil water per unit volume) The 5TE Decagon sensor used in the Loretta-Linda Basin allows for the measurement of temperature, volumetric water content, and electrical conductivity of the soil. Sensors installed at a depth of 5, 10, 15, and 20 cm use capacitance to measure the dielectric permittivity of soils (sensors can record the properties of soils in all directions within a 5cm radius).

Dielectric permittivity (measured in farads per meter) of soil is most indicative of the volume of water in the total volume of soil because the dielectric of water (80 F/m) exceeds that of the components of soil (mineral soil, 4 F/m; organic matter, 4 F/m; air, 1 F/m). Therefore, a change in the amount of water in a soil is clearly picked up with a change in capacitance (Decagon, 2010).

A large soil sample (approximately a 3-gallon bucket full) was collected adjacent to the site of the Decagon installation and was used for an in-lab calibration between values reported by the sensors with soil core sample results (Cobos and Chambers, 2010). A plot created from these values was then used to normalize the Decagon data collected in the field with the Decagon results collected in the lab (Cobos and Chambers, 2010).

Gravimetric soil cores of approximately 3 cm in diameter and 3 centimeters in thickness were taken at the Decagon site and at sites adjacent to both runoff plots. At each sampling site, four cores were taken to obtain values of water content representative of the site and reduce the impact of outlying values. These cores were collected, sealed, and weighed in the lab before and after being heated and dried.

The depth of the Decagon sensors prevents the volumetric water content from being a good indicator of soil water content at the surface. Although the probe at 5 cm depth eventually records surficial moisture from larger rainstorms, soil cores were taken to obtain better measurements of subtle changes in surface moisture. Measurements from the Decagon, and the lack of response even at the sensor installed at 5cm depth indicated that soil moisture fluxes are experienced above 5 cm depth, and largely within 3cm of the surface. The soil cores are, therefore, better indicators of surface moisture that will have a control on runoff.

4. ANALYSIS

4.1 CHARACTERIZING SOIL MOISTURE FOR EACH SUB DRAINAGE OF THE LORETTA-LINDA BASIN

The data obtained by collecting gravimetric soil samples in the field provided the main database for analyzing soil moisture in the basin. The data collected with the Decagon soil sensor, though offering a more complete and continuous dataset (as it collected measurement continuously throughout the summer) is not used in the data analysis. After comparing the soil water content values recorded by the Decagon to the gravimetric soil cores, it was discovered that rain infiltrates primarily into the top 3 cm, and was, therefore, not being measured by the Decagon sensor.

The soil moisture data shown in Table 2 is a compilation of four samples for each of the three sites, collected every three days for a total of 27 days of sampling, and a total of 327 samples. These values were used to create the graph shown in Figure 13, which tracks the fluctuations of soil moisture throughout the summer.

Date (2011)	Soil Water Content (cm^3/ cm^3)		
	Left Fork	**Right Fork**	**Decagon Site**
6 June	-	0.041	0.020
10 June	-	0.055	0.050
13 June	0.028	0.0168	0.023
17 June	0.017	0.0186	0.022
20 June	0.242	0.1613	0.247
22 June	0.139	0.0895	0.091
24 June	0.158	0.1014	0.106
27 June	0.125	0.0501	0.055
29 June	0.097	0.0390	0.026
1 July	0.174	0.0715	0.101
3 July	0.029	0.0318	0.029
5 July	0.035	0.0246	0.028
8 July	0.154	0.2289	0.2110
12 July	0.185	0.156	0.152
14 July	0.183	0.180	0.202
17 July	0.182	0.219	0.265
19 July	0.215	0.087	0.111
21 July	0.182	0.047	0.133
25 July	0.020	0.019	0.037
28 July	0.028	0.035	0.035

Table 2*- Soil water content values calculated from gravimetric soil cores taken at three sites within the basin.*

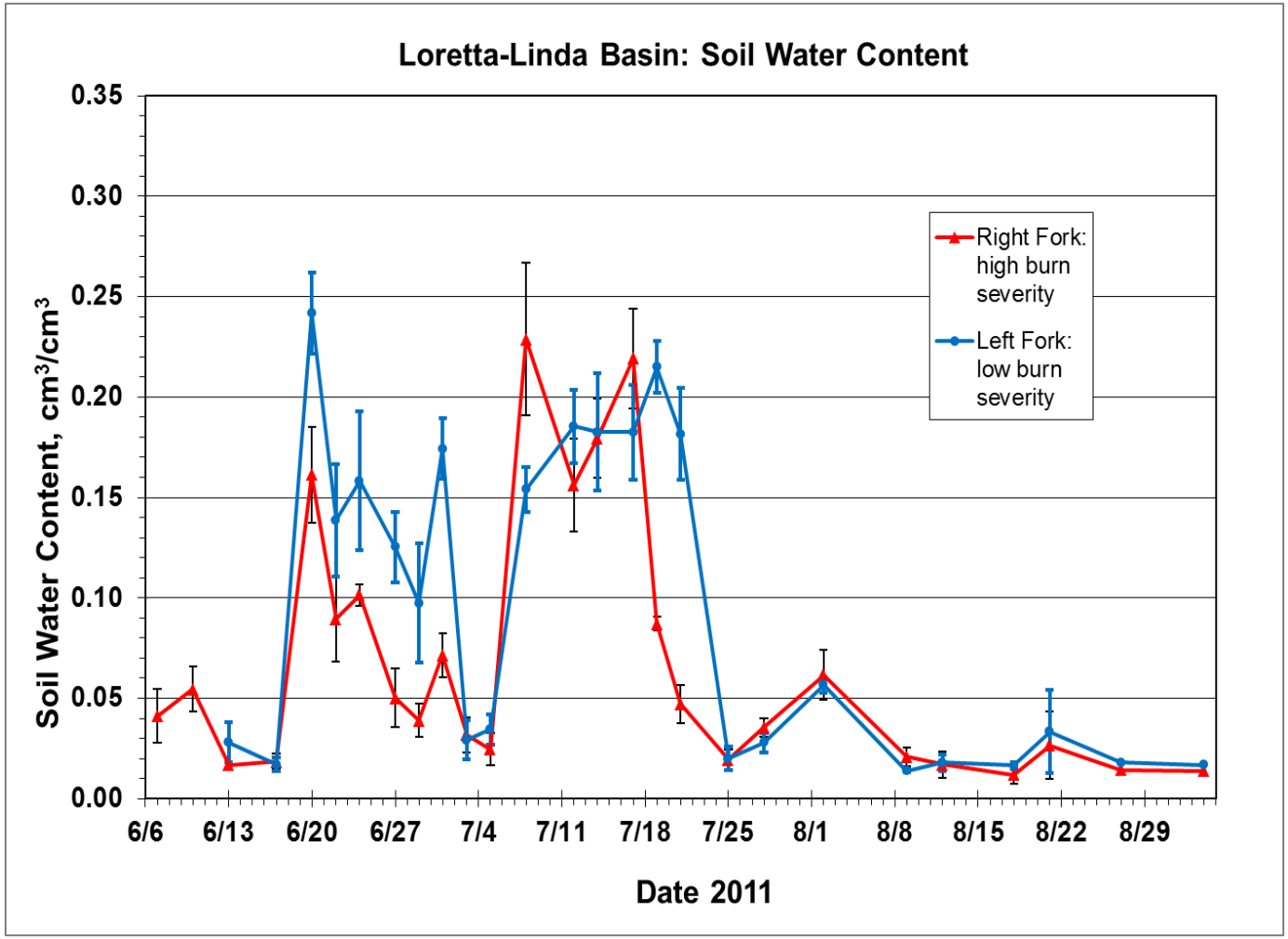

Figure 13*- Plot of the soil water content over the course of the summer. With the exception of two data points collected in July, the right fork (high burn severity) maintained lower values of soil water content.*

4.2 DETERMINING THE PROPERTIES OF EACH STORM CELL

Beyond extracting statistics that describe each rainfall (Table 1), the cumulative rainfall for each rain gage was plotted and organized by storm cell. Figure 14 shows one of the nine storms that were plotted for cumulative rainfall (see Appendix A). The storm on the 14th of July was picked up by all of the six rain gages and shows that although the trends are similar between each of the gages, the timing varies across the basin, as does the total accumulation at the end of precipitation.

To further investigate the spatial patterns of rainfall within the basin, the 1-minute maximum intensities for each rainfall were plotted on a map of the basin. Although most value distributions were too irregular and sparse to create isohyetals, on average the left fork experienced less intense rainfall (see Appendix B). Alternatively, Figure 15 shows the 1-minute rainfall intensity of the 20th of June storm that shows consistent patterns across the basin (for other storm cells see Appendix C).

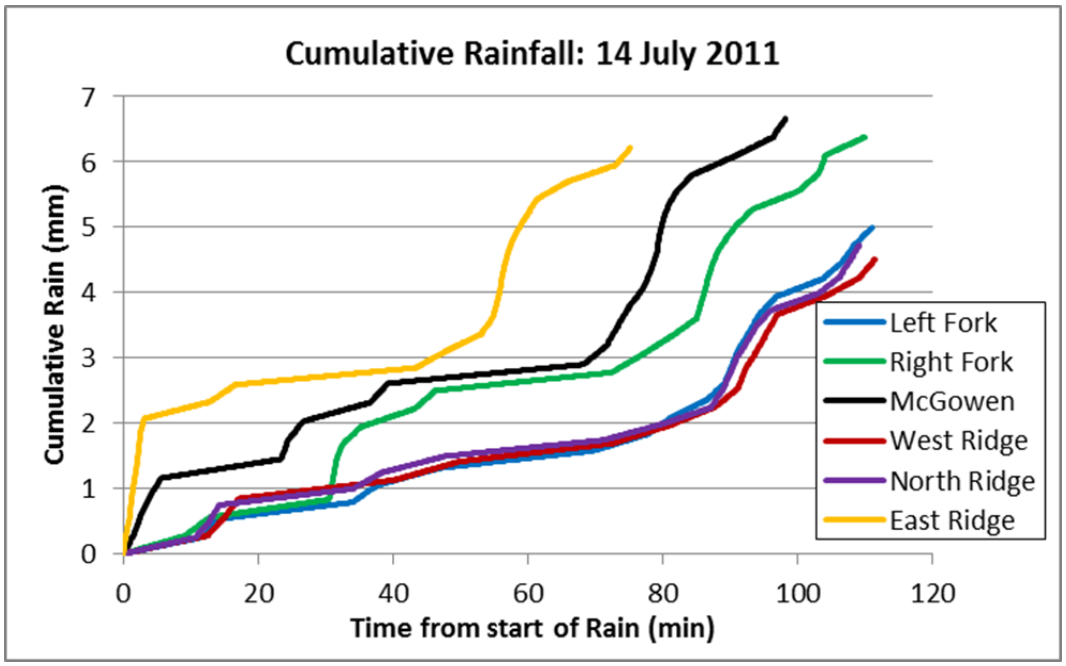

Figure 14*- Plot of cumulative rainfall versus elapsed time from the start of the storm. All of the rain gages show similar trends but with different timing and different accumulation.*

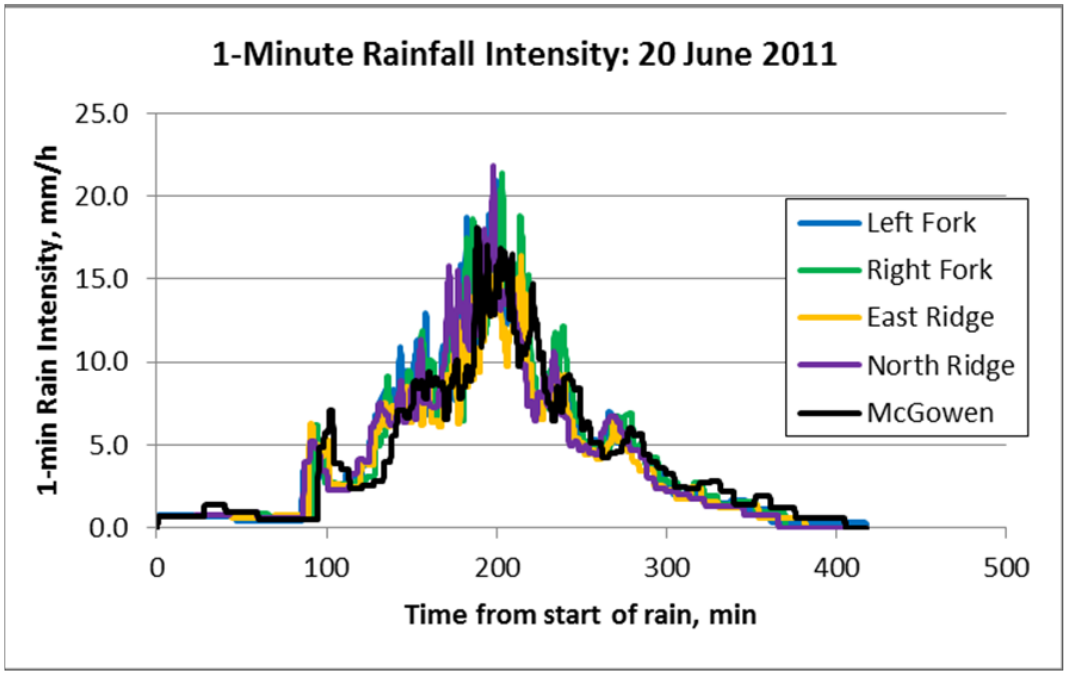

Figure 15*- Plot of rainfall intensity over elapsed time from the start of rainfall. There is a strong correlation between all rain gages in the basin during this storm.*

4.3 CHARACTERIZING THE INFILTRATION AND RUNOFF RESPONSE OF THE LEFT AND RIGHT FORK OF THE BASIN.

The Parshall flumes used in Loretta-Linda to measure discharge were slightly modified from the classic flume design, differing only in the shape of the flow outlet after the constricted channelized section (see Figures 9-11). The slope break and point at which critical flow is reached is the same, so theoretically the conversion from measured depth to discharge should not differ. However, because the flumes were slightly modified, two different methods were used to check the accuracy of the default calibration and conversion factor used with standard Parshall Flumes. Although flow in the upper channel reaches (those where 3-inch flumes were installed) is ephemeral, a measurable flow through the flume was observed on several consecutive data collection field trips. This flow exhibited an opportunity, though limited, to measure the discharge and water depth for the modified flumes on sight. This ephemeral flow, however, only allowed for four tests to be conducted. By collecting and measuring water as it runs through the flume over a known time, and observing the water depth within the flume, a modified Parshall flume specific calibration curve was created. These data points are displayed in Figure 16.

Another calibration test was conducted outside of the Loretta-Linda basin with the modified Parshall Flume in an irrigation channel with consistent flow, where flow meters could be used to measure velocity. The Loretta-Linda site calibration curve is based on only four points (measurements could only be collected when the channel was flowing) and, therefore, does not have strong point control, especially for greater depths.

Comparing the three curves, the irrigation ditch test follows the theoretical curve for a standard Parshall Flume more closely than the field test curve. The lack of data points, the great difference in discharge at greater depths, and the proximity of the theoretical curve to the irrigation curve, led me to select the theoretical curve and the associated equation:

eq. 4.1 $$y = 0.000147983x^{1.550387597}$$

with an R^2 of 1.000. Although this formula is meant for the classic Parshall Flume, the irrigation ditch test, which used the same modified flume as were deployed in Loretta-Linda, yielded numbers that follow the curve closely, making the theoretical calibration curve the best choice for converting the measured water depths to discharge.

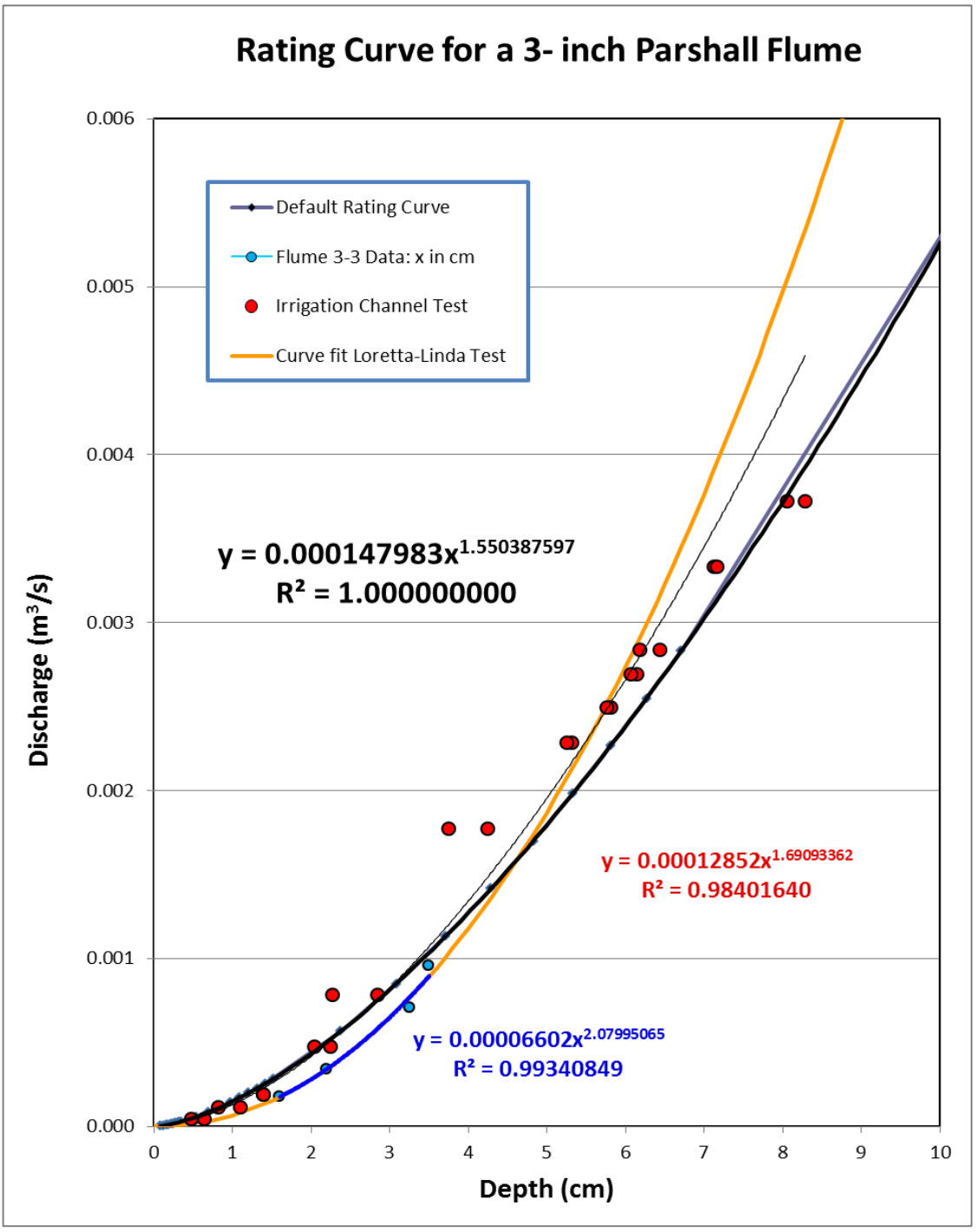

Figure 16*- Values from calibration tests plotted against the standardized calibration curve for Parshall Flumes.*

Using this calibration curve and equation 4.1, the water depths measured by the Solinst® sensors in the three main flumes were converted to discharge in (m^3/s). Because the Solinst® sensors were held in stilling wells below the base of the flume, measuring the pressure exerted by the flow overtop, some error occurred with the introduction of sediment into the flume. Sediment entrained in the flow did not seem to have a significant impact on the measured pressure, however, as flow velocity decreases sediment was often deposited in the bottom of the flume, covering the sensor. This phenomenon is seen in plots of discharge (Figures 17 & 18), where after rain has subsided and a decrease in discharge should follow, a consistent "water depth" appears to be maintained long after the storm has stopped. This is not indicative of a consistent flow but rather of deposition of sediment within the flume. Figure 17 shows a plot of the storm for the 7th of July with both the left and right fork flume data plotted over time.

Although this plot does not show significant difference between the left and right fork peak discharge rate, the evolution of the rate over time is different. There is an initial "spike" in the runoff rate on the right and more severely burned fork that is not seen on the left fork. This initial surge of water may be a result of the presence of small amounts of water and ephemeral flow in the channel on the right fork that was not observed in the left fork. The presence of a hydrophobic layer on the more severely burned soil may also have caused an initial pulse of water that was recorded by the right fork flume. This spike, however, was not observed in the runoff response of subsequent storms (Appendix D).

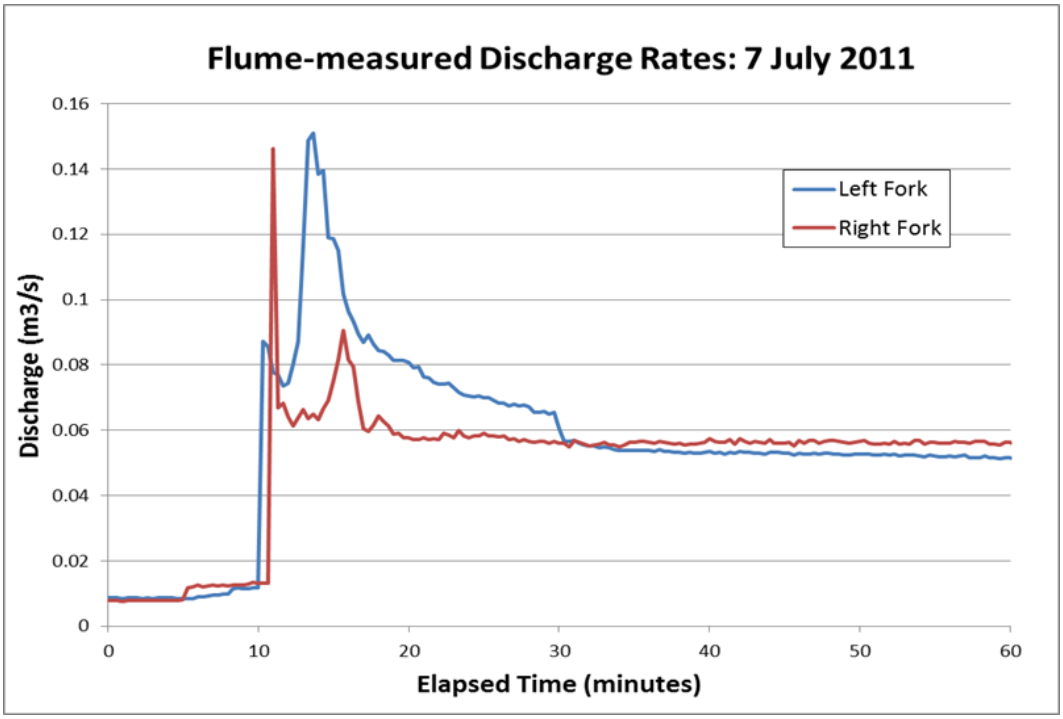

Figure 17*- Plot of the discharge as measured by the left and right flumes for the seventh of July storm.*

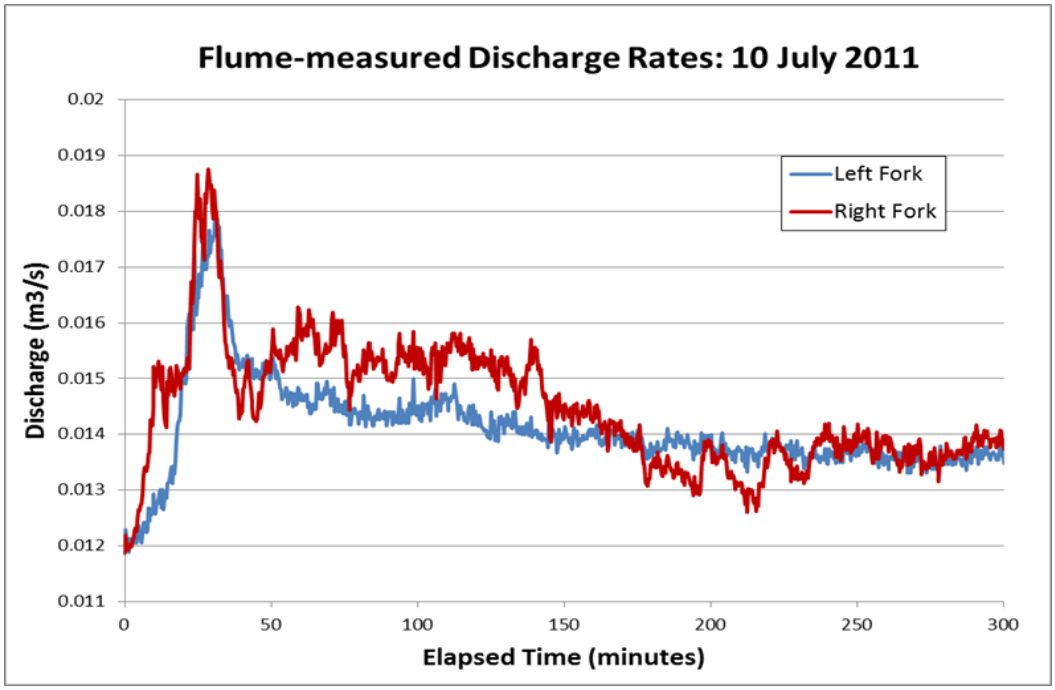

Figure 18*- Plot of the discharge as measured by the left and right fork flumes for the tenth of July storm.*

Figure 18 shows runoff being sustained during a longer storm. As previously discussed, the consistent flow that appears to continue long after the initial runoff spike reflects measurement from the stilling well that has been filled with sediment as flow velocities decrease and entrained particles are deposited. Though the right fork peak discharge is higher in this case, Figure 18 also does not show significant difference between the left and right fork for the runoff response in terms of sustained rate throughout the storm.

Once the field measurements were compiled and calibrated, discharge statistics could be extracted and related to rainfall measurements using the runoff coefficient, a method used for observing the relationship between rainfall and runoff. Two primary methods are currently being applied to flood prediction in burned watersheds (Moody, 2012). Whereas both the USGS regression method and the curve-number method developed by the Natural Resources Conservation Service are vetted methods, they were both developed for unburned watersheds with perennial streams (Moody, 2012). Burned basins like the Loretta-Linda watershed, however, often contain only ephemeral streams. The USGS publication "An Analytical Method for Predicting Postwildfire Peak Discharges" addresses this knowledge gap, the methodology from which was applied in the analysis of discharge data and the calculation for the runoff coefficient in this study (Moody, 2012).

Determining the runoff coefficient is a simple method of linking rainfall and runoff. Often calculated as a dimensionless proportionality constant (or percentage) in

the relation between discharge, rainfall intensity, and contributing area, the runoff coefficient is given as *C* in the rational equation:

eq. 4.2 $$Q=CIA_c$$

where *Q* is equal to discharge in $m^3\ s^{-1}$, *I* is rainfall intensity measured in mm h^{-1}, and A_c is contributing area in m^2 (Chow 1964). This equation was used by Moody et al. (2008) in a study linking the runoff response to burn severity after a wildfire. In a later publication, data pairs of rain intensity and peak discharge were recorded and related in a sampling of burned watersheds across the western United States. Each basin was analyzed separately, though each showed a general decrease in the modified runoff coefficient with greater time after the wildfire. All data sets were combined to create an empirical equation for a modified runoff coefficient that is applicable to a range of rainfall regimes (Moody, 2012):

eq. 4.3 $$Q = C\left(I_1 - I_1^{threshold}\right)A$$

$I^{threshold}$ represents the rainfall threshold intensity, and is calculated by creating a plot of unit peak discharge versus the 1-minute rainfall intensity as shown in Figure 19. In this case, the runoff coefficient represents the rain intensity threshold for a watershed producing runoff.

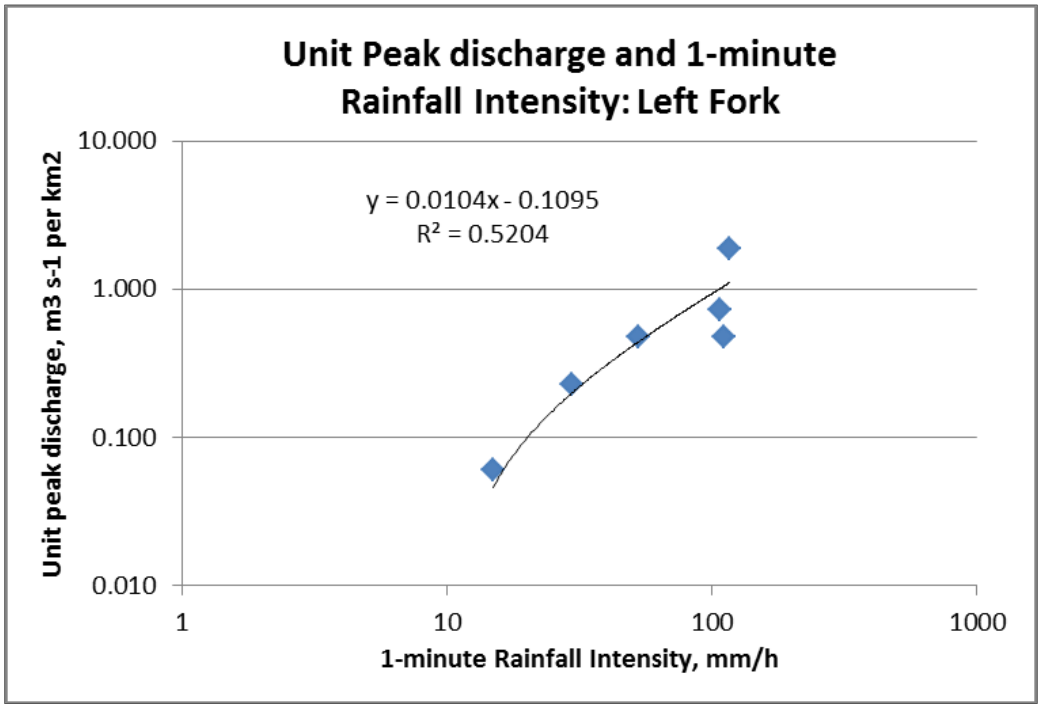

Figure 19- *Plot of unit peak discharge versus the 1-minute rainfall intensities. Each of these points represents a maximum from each of the 6 storms.*

Using the trend line created from these points, the equation for unit peak discharge can be rearranged as:

eq. 4.4 $$Q = 0.0104 * (I_{1min} - 10.55\ mm/h)$$

where, 10.5 mm/h can be interpreted as the approximate rainfall intensity threshold. This value can then be used in equation 4.3 to calculate the modified runoff coefficient. The runoff coefficient is not a constant value throughout a storm, as rainfall and discharge rates and intensities varies through time. The values reported in Table 3 give the calculated modified runoff coefficient values for each storm, based on peak values.

	Modified Runoff Coefficient C’	
Storm Date	Left Fork	Right Fork
20 June	0.0492	-
7 July	0.0638	0.0129
10 July	0.0421	0.0162
12 July	0.0405	0.0155
13 July	0.0266	0.0115
16 July	0.0171	0.0088
Average	0.040	0.0130

Table 3- *Modified runoff coefficients for each storm for the left and right fork.*

Another way to estimate the overall runoff coefficient for a drainage basin (and a method for checking the averages presented in Table 3) is to use a plot of unit peak discharge versus 1-minute rainfall intensities, for the entire elapsed time of the storm. Although the runoff coefficient is not constant, when both variables are converted to the same units, the dimensionless slope of the trend line is a good estimation for the average runoff coefficient. Figure 20 shows the left fork plot of unit peak discharge and 1-minute rainfall intensity whereas Figure 21 shows the same plot for the right fork. The trend-line slope and the estimated average modified runoff coefficient is 0.0374 for the left fork, and 0.012 for the right fork, both of which are comparable to the modified runoff coefficients calculated with peak storm values given in Table 4, respectively.

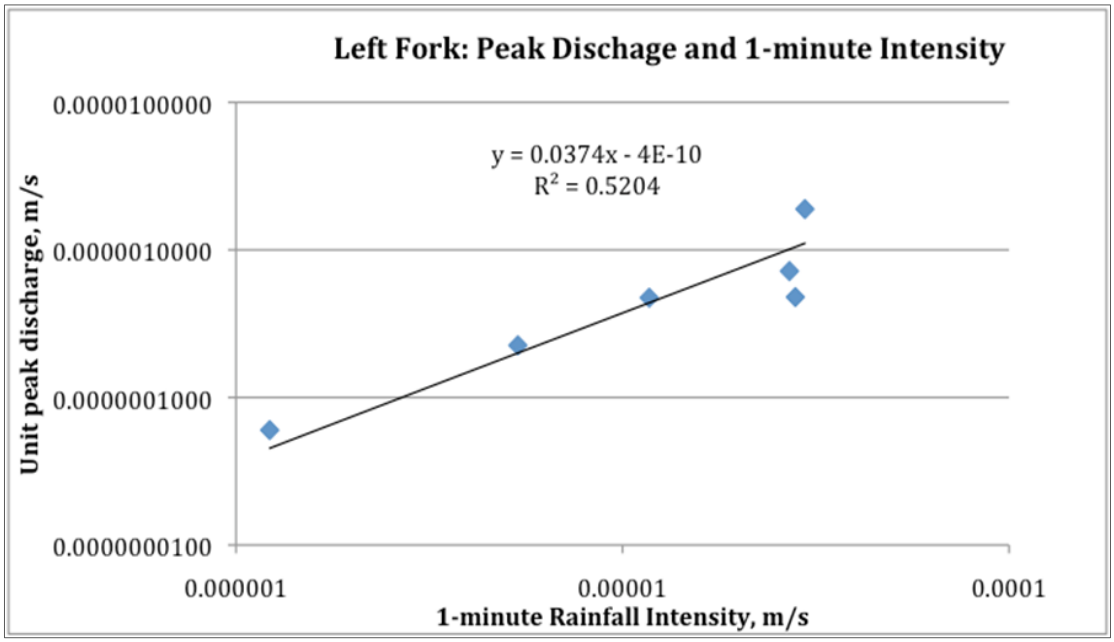

Figure 20*- A plot created of unit peak discharge versus rainfall intensity. The slope of the trend line for these points is an estimated average modified runoff coefficient for the left fork.*

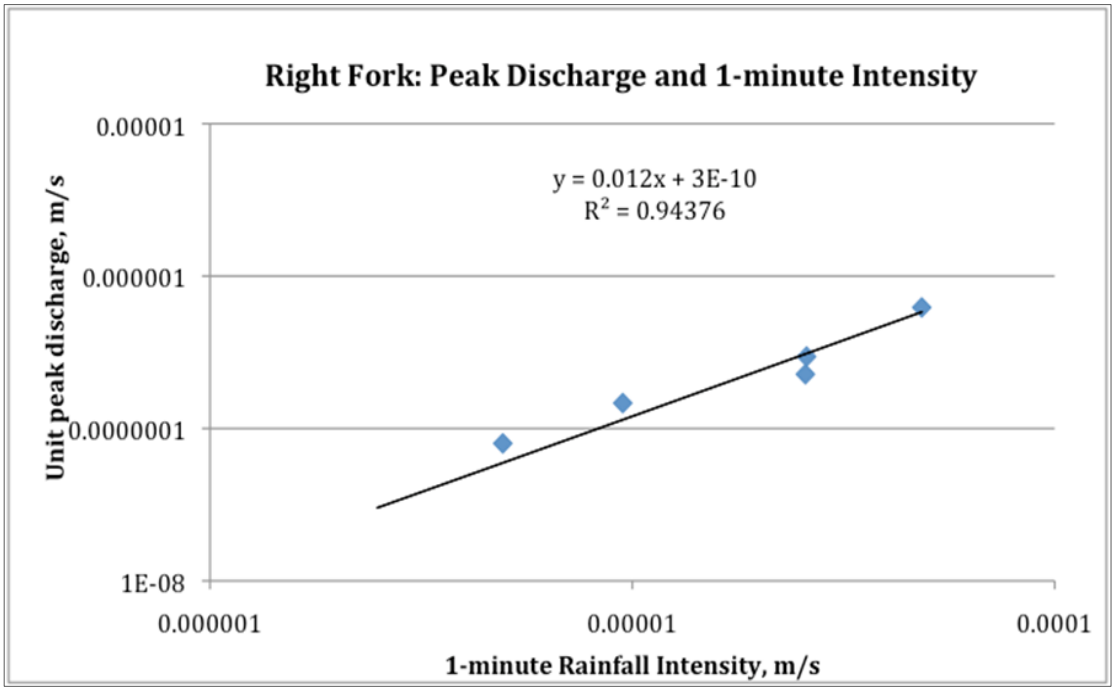

Figure 21*- A plot created of unit peak discharge versus rainfall intensity. The slope of the trend line for these points is an estimated average modified runoff coefficient for the right fork.*

The relation between rainfall and runoff was also investigated through the use of infiltration plots installed on each fork. Though the paired tipping bucket rain gage method is an effective way to measure rainfall, and would seemingly also be effective in measuring runoff from the isolated plots, the presence of debris and sediment in the runoff presented a problem for several of the storm cells recorded. Of the data collected throughout the summer, only three of the storms were recorded by both the left and right fork infiltration plots without severe interference from either sediment in the rain gage or debris clogging the drain pipe. Figures 22 and 23 show the rain, runoff, and infiltration rates measured on the left and right fork plots for the seventh of July storm (see Appendix E for other precipitation events).

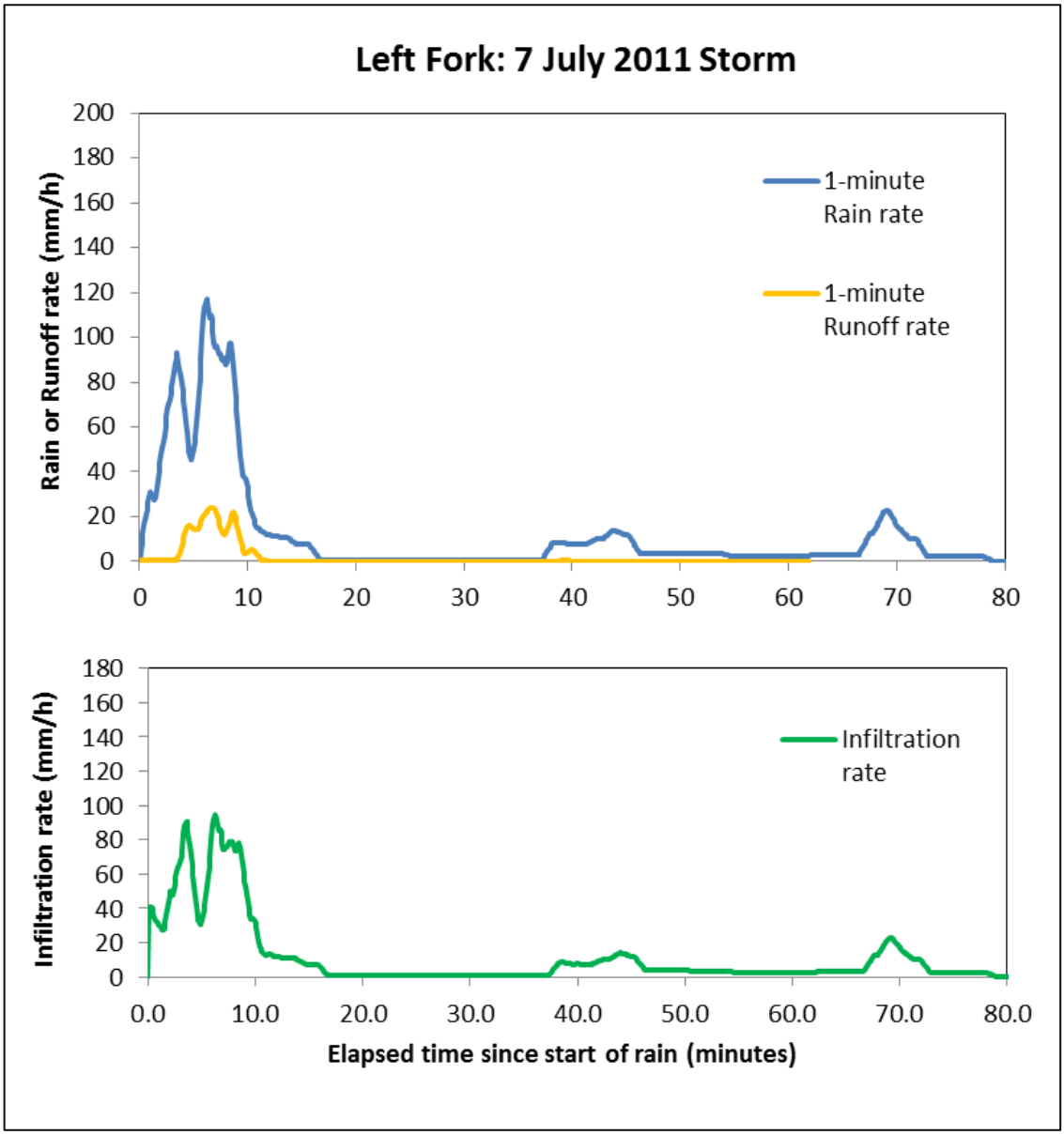

Figure 22- *Rain, runoff, and infiltration rates as measured by the left fork infiltration plot on the seventh of July.*

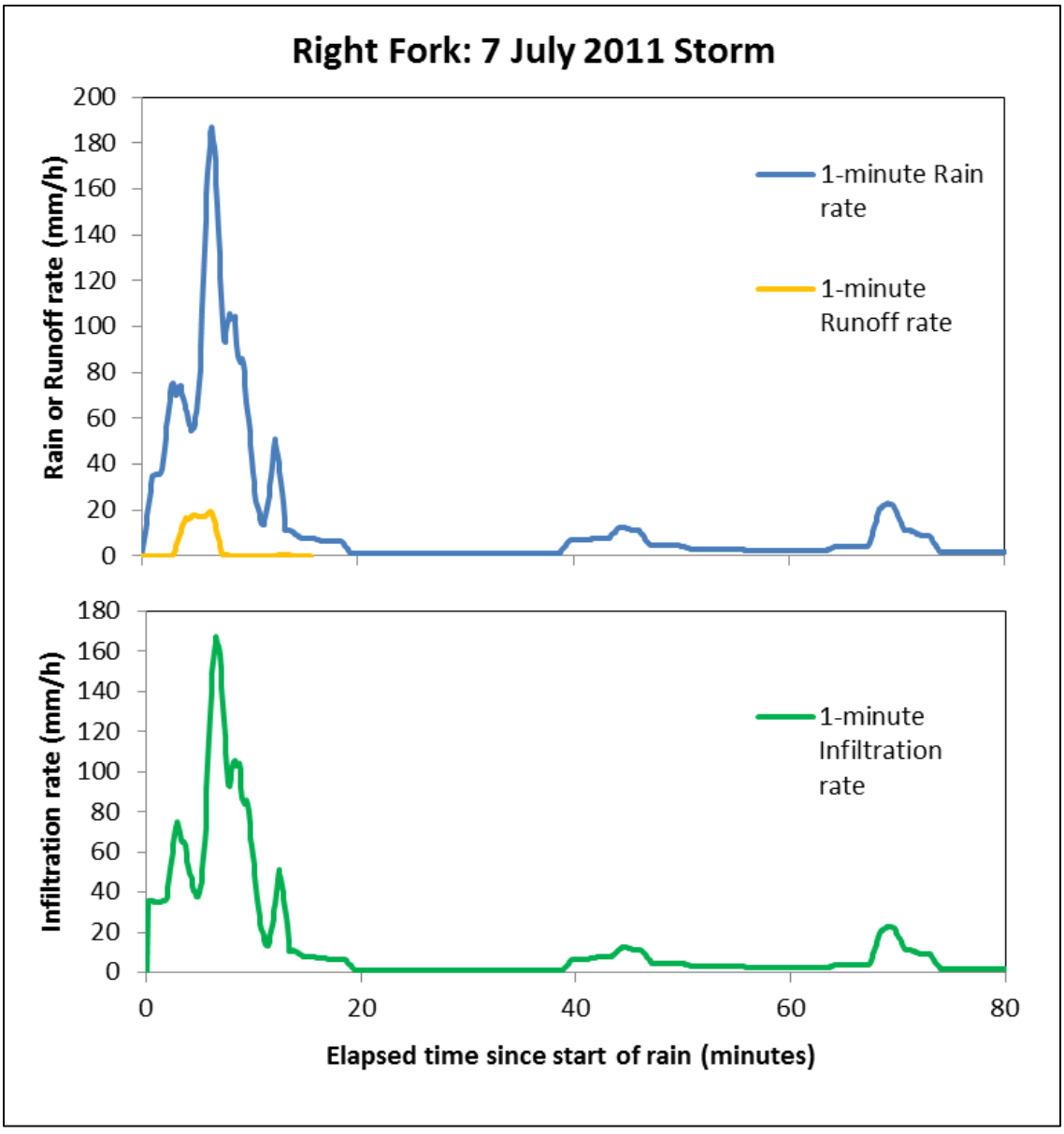

Figure 23*- Rain, runoff, and infiltration rates as measured by the right fork infiltration plot on the seventh of July.*

4.4 ANALYZING THE IMPACT OF BURN SEVERITY ON THE TWO SUB DRAINAGES BY CREATING A MODEL IN TOPOFLOW®, SPATIAL HYDROLOGIC MODELING SOFTWARE.

To run data through a spatial hydrologic model, such as TopoFlow® that is based on a DEM and associated grids, several pre-processing steps must be taken to convert point data into a grid format. First, a profile smoothed DEM must be generated. The original pixel elevations of a watersheds main channel are read from the file as Flint's Law (S=c *Ap) is applied to find the best fit elevations and areas for these pixels (where S is slope, and A is contributing area). These new parameters are used in combination with contributing area grids to produce a new DEM that assigns floating point elevations to every pixel in the original DEM. The elevations will be similar to the original pixel values, but the stair stepping fabric, where slopes were either measured as zero or were beyond pixel resolution, will be eliminated.

The extraction of a flow direction grid, a slope grid, and a contributing area from the foundational DEM grid is only the beginning of the data processing and preprocessing necessary for TopoFlow®. Initial conditions such as the depth of water in channels and the antecedent soil moisture may be adjusted, as well as dimensions of the channels such as length, width, slope, roughness, height, and bank angle (Peckham, 2009).

These parameters along with the original DEM are used in creating a channel geometry grid. This grid is created with data on the roughness for the three zones of overland, transitional, and channel flow. To calculate roughness and create the channel

geometry grid, an estimation of Manning's n was taken at several places within the Loretta-Linda basin. Three cross-sections for each channel were used to compute an average slope and wetted perimeter based on high-water marks, these values were then used to compute the hydraulic radius. Using the calculated hydraulic radius and measured slope and assuming a Froude number =1 for critical flow (which is valid in steep channels), velocity can be calculated as:

eq 4.5 $$v = (gR)^{1/2}$$

and

eq 4.6 $$v = \frac{R^{2/3}S^{1/2}}{n}$$

where g is the gravitational constant, and R is the hydraulic radius in meters. This critical flow assumption then allows for a modified version of Manning's equation to solve n:

eq. 4.7 $$n = R^{1/6}(S/g)^{1/2}$$

where S is the energy gradient and n is the roughness coefficient or resistance to flow (Marcus et al., 1992). As discussed in section 2.7, roughness is accounted for with Manning's n in the basic Manning's equation for estimating stream velocity. The cross sections, however, can only estimate Manning's n values for channel flow and do not address the overland/hillslope flow.

Manning's Equation was developed for channel flow, and it is, therefore, more difficult to apply to hillslopes, with very little information available for shallow overland

flow on natural surfaces (Engman, 1986). Overland flow on a smooth slope is often assumed to behave as "Hortonian" or sheet flow, however in the Loretta-Linda basin, slopes are not smooth and hillslope flow occurs predominantly within small rills on the slopes. Flow velocities within these rills were measured for a south-facing basin also burned during the Fourmile Canyon, approximately 2 km south of Loretta-Linda on Sugarloaf Mountain. The site at which these measurements were taken was severely burned, and therefore is comparable to the right fork hillslope, where most vegetation has been removed. The Sugarloaf study calculated a Manning's n of 0.21 for the severely burned hillslope (Ebel et al., 2012).

Because no analog data were available for the left fork, values were estimated with respect to a version of the Soil and Water Assessment Tool (SWAT), a well-established distributed eco-hydrologic model, that has recently been updated to characterize low mountain ranges (Eckhardt et al., 2001). In a 2001 study, Eckhardt et al., showed that the modified model (SWAT-G) yields far better results in catchments with steep slopes and shallow soil where base flow is low (Eckhardt et al., 2001). The model calculated a lower bound and upper bound for several parameters in watershed hydrology, including range from 0.20 to 0.50 for Manning's n for overland flow (see Appendix F for full table). These bounds were used as parameters for selecting a Manning's n of 0.35 for overland flow on the less severely burned left fork. Table 5 gives the total width, cross-sectional area, mean depth, wetted perimeter, hydraulic

		Left Fork (above Flume 3-2)	Right Fork (above Flume 3-3)
Channel	Width (m)	1.57	2.97
	Contributing Area (km^2)	0.0798	0.138
	Manning's n	0.114	0.106
Overland (hillslope)	Width (m)	0.00	0.00
	Contributing Area (km^2)	0.00	0.00
	Manning's n	0.35	0.21

Table 4- *Parameters used to create channel geometry grids for the left and right fork.*

radius, mean slope and the Manning's n value for both the right and left forks. The preprocessing function of TopoFlow® uses these value pairs of contributing area and a Manning's n estimation to create a power law that will be applied to the entire basin.

Another preprocessing step is to convert the forcing variables in station format (rainfall, runoff, etc.) into spatially gridded data. "Forcing variable" refers mostly to weather-related parameters such as precipitation, temperature, humidity, cloudiness, wind speed etc. (Peckham, 2009). Because each of these variables cannot be measured for each individual grid cell, the data must be interpolated between points of measurement (Peckham, 2009). In Loretta-Linda, the rainfall data are collected as a time series at six different rain gage locations in the basin. Each rain gage station was recorded as an "x,y,z, triple" and, therefore, must be converted into coordinates

associated with individual grid cells of the DEM. The data collected at any given time are then assigned to this pixel, whereas time is added as a third dimension by stacking the grids that have been created, a new grid for each time step.

5. DISCUSSION

The impact of burn severity on the measured values of discharge, infiltration, and soil moisture in this study was not dramatic. The discharge rate based on flume data show very little difference between the left and right fork, whereas the peak discharges and area weighted runoff coefficients did not reflect the anticipated response of the two different burn severities. There are likely several factors at work in the basin that we were not able to account for in the collection of data in the field. Although the selection of two primarily south facing watersheds attempted to minimize variability associated with aspect, the aerial image of the pre-burn vegetation shows that there was a significant difference in vegetation and therefore an increased potential for different soil properties between the left and right fork.

Another potential explanation of similar discharge rates and the converging trends of SWC, is the elapsed time since the wildfire. Although wildfires have been proven to negatively impact a soils infiltration capacity by creating a hydrophobic layer and reducing porosity, previous studies have shown that these effects were not measurable one year after the fire (MacDonald and Huffman, 2004). Beginning nine months after the Fourmile Canyon fire, the measurements collected only spanned two months but during the summer season with regular rainfall and a temperate climate, the recovery of vegetation is rapid and may have minimized the discrepancy of soil moistures between the two burn severities as time passed.

Although soil water content trends over the course of the summer do not appear to show a strong pattern of one fork with higher water contents than the other (with the

occasional cross-over of the left and right fork trend lines), upon closer examination, only two values of SWC for the right fork are higher than that of the left fork of all of the values collected throughout the summer. Initially the correlation between the left and right is clear, with the left fork maintaining a consistently higher SWC value than the right fork during June. However with the inclusion of the anomalously high values the trend does not continue through July. These two atypical values seem to indicate that the difference between the soils on the two forks is not significant or that the elapsed time since the fire has minimized measurable difference between the two sites. However, examining the spatial distribution of rainfall for the 7th of July storm immediately preceding the soil sample collection (Figure 24), shows that there was a significant difference in the rain intensity during the storm immediately before the samples were collected, with much higher rain intensities occurring on the right fork.

The comparative data analysis shows that hydrologic parameters such as soil moisture, and channel/hillslope roughness, are significantly different between burn severities, whereas infiltration runoff rates show minimal differences. Infiltration and runoff measurements collected with infiltration plots and flumes were impacted by sediment transport, potentially skewing the results. Also, the presence of ephemeral flow in the right fork drainage was not accounted for in the comparative analysis but is likely very important in the generation of runoff.

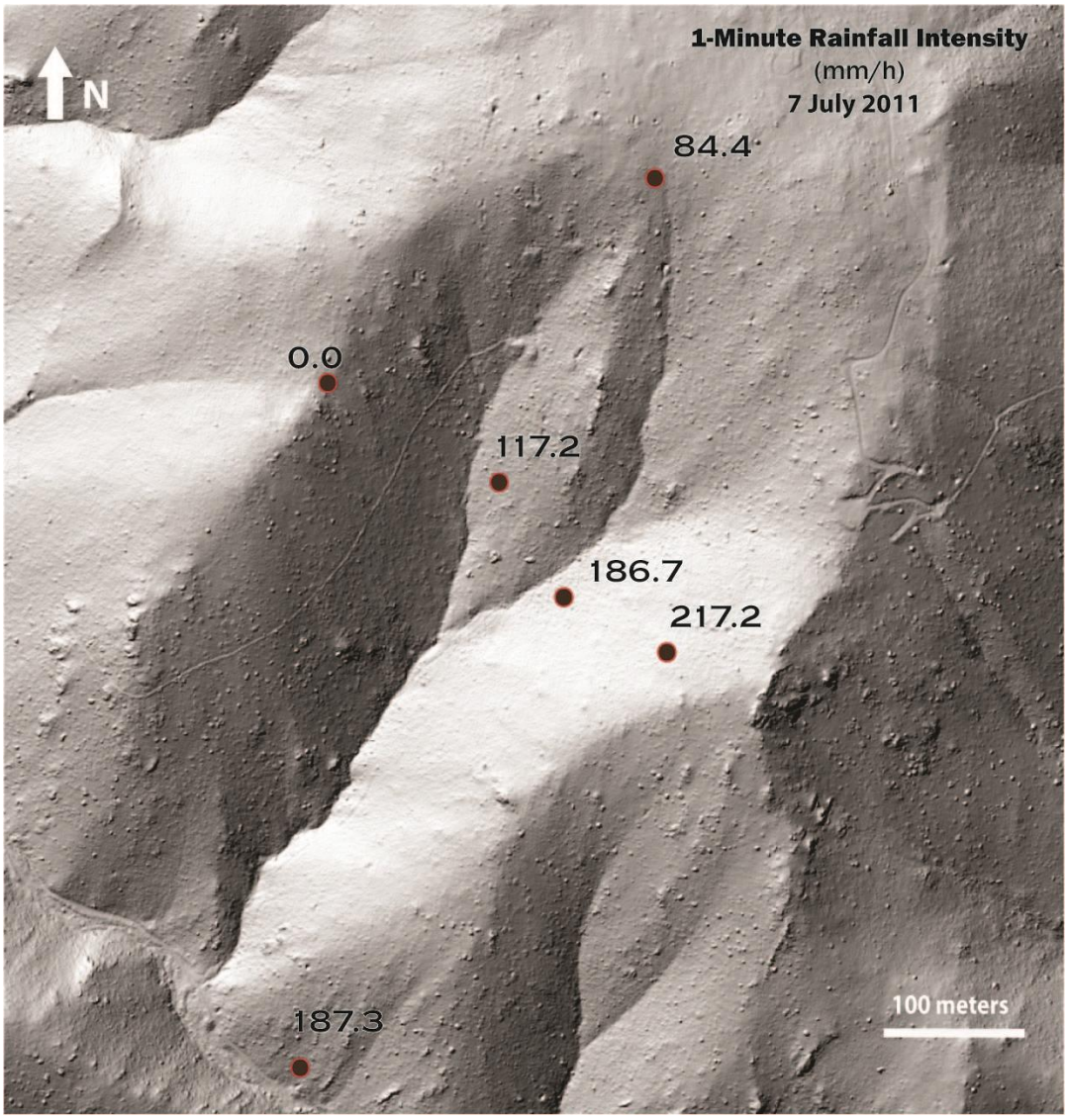

Figure 24- *1-minute rainfall intensities recorded by each rain gage for the seventh of July storm. The left fork shows much lower precipitation values than the right fork.*

Although each of the parameters analyzed did show some variation (even if not the anticipated direction) not all variables necessarily have a significant impact on changing runoff volumes. To investigate these parameters and determine which of those measured here are truly controlling the changing runoff volumes seen between different

burn severities, a sensitivity analysis was conducted using spatial hydrologic modeling software, TopoFlow®.

By selecting one storm and using the data gathered on rainfall, runoff, and soil moisture, several iterations of the model were run, changing parameters each time to investigate the runoff response. The runoff values given by the model can also be compared to those collected in the field. Several questions were posed to guide the direction of these model runs:

1) How does the change in channel and hillslope roughness affect the runoff response?
2) Does a difference in antecedent soil moisture have a significant impact on the infiltration capability?
3) Do the parameters of infiltration such as soil moisture, hydraulic conductivity, and capillary length that vary with burn severity significantly affect runoff rates?

Initial data interpretation of the measurements collected in the field was based on a paired analysis of runoff and rainfall measurements collected on each of the two forks of the Loretta-Linda Basin. In the case of each variable, it was a simple method for comparing the two drainage basins for each of the storms recorded over the summer. However, with such large datasets, it was difficult to decipher which variables were truly controlling runoff volumes.

The use of a spatial hydrologic model, however, allows for these large data sets to be adjusted and tweaked; in this case by producing several model iterations with varying infiltration rates, soil water contents, and channel geometry patterns. A dynamic process model such as this allows for more realistic simulations of drainage in a basin that has been affected by wildfire and as a result exhibits even greater heterogeneity than unburned watersheds.

TopoFlow® is not designed specifically to observe or quantify the effects of burn severity. There is no "burn severity" input in the model framework. However, as we have observed in the course of this study, burn severity is expressed through the variables that are affected by fire such as soil moisture, infiltration capacity, and hillslope/channel roughness. It is, therefore, through the adjustment of these parameters that we are able to investigate the two levels of burn severity. The storm on the 7th of July, 2011, was selected to complete the model iterations discussed in this section because it shows a clear beginning and end of rainfall and runoff and is representative of short summer convective storms of the summer season.

Although TopoFlow® is set up to model the discharge of an entire basin, the two subdrainages are the focus of this research and were, therefore, analyzed independently. In addition to focusing in on the sub drainages, data from the 3-inch flumes at the base of the left and right fork were used preferentially to data from the 9-inch flume because they were more sensitive to smaller amounts of runoff. The 9-inch flume was located well below the confluence of the left and right fork and had consistent flow throughout the summer, and as a result had a greater influx of sediment that obscured the depth

measurements collected by the Solinst sensor. Also, because the rain gages were focused on measuring precipitation for the two sub drainages, the estimations produced in a model of the entire basin would likely underestimate rainfall for the downstream reaches and contributing drainage areas. The consistency of flow through the 9-inch flume also suggests that flow was being sustained by a subsurface source. Therefore, the 9-inch flume was not able to collect meaningful discharge values for the basin and was not used to calibrate the model runs in TopoFlow®.

As discussed in section 4.4, TopoFlow® utilizes data on the channel and hillslope roughness. Manning's n, quantifying roughness, has been observed as varying systematically over watersheds: as contributing area increases (downstream sections), roughness values decrease. This concept can be seen in watersheds at any scale, as boulders and larger roughness elements are concentrated at headwaters, whereas downstream sections with lower flow energies have finer grained material and therefore fewer obstructions to flow. Field observations confirmed this concept, and did not show extreme variability in channel roughness between the two forks. On both forks, channels were mostly clear of vegetation, meaning that frictional loss because of vegetation consumption during a wildfire would be mostly confined to the hillslopes.

To investigate the degree to which changes in channel roughness versus hillslope roughness would impact the changing runoff levels, several channel geometry grids were created. For the channels, using the known contributing area above each flume site, and the cross sections taken at those locations (see section 4.4), two variations of the power law $N = c\,(A + b)^p$ were created. Though the two power laws derived represent the grid

that will be applied to the entire watershed, they account only for the effect that loss of vegetative litter and debris has on channels. These functions operate under the assumption that contributing area and roughness are inversely related:

eq 5.1 Left Fork: $N = 0.1415 (A + 536.96)^{0.0124}$

eq 5.2 Right Fork: $N = 0.2805 (A + 0.205)^{0.5676}$

Adjusting the Manning's n, coefficient and nothing else (having nothing differ except the channel geometry grid) yielded the hydrograph in Figure 25 for the 7th of July storm. The difference between the two forks demonstrates that a change in channel roughness as a result of fire creates measurable but not dramatic impact on the basins discharge. With no infiltration parameter being used in this scenario, all rain was eventually expressed as runoff for both iterations, causing the unrealistically high values for discharge. Peak discharge for the left fork reaches 3.47 m^3/s while the right fork peak discharge was 3.67 m^3/s. With more vegetation and therefore more roughness elements and flow energy loss, the grid created for lower burn severity (left fork) has a slightly lower discharge rate.

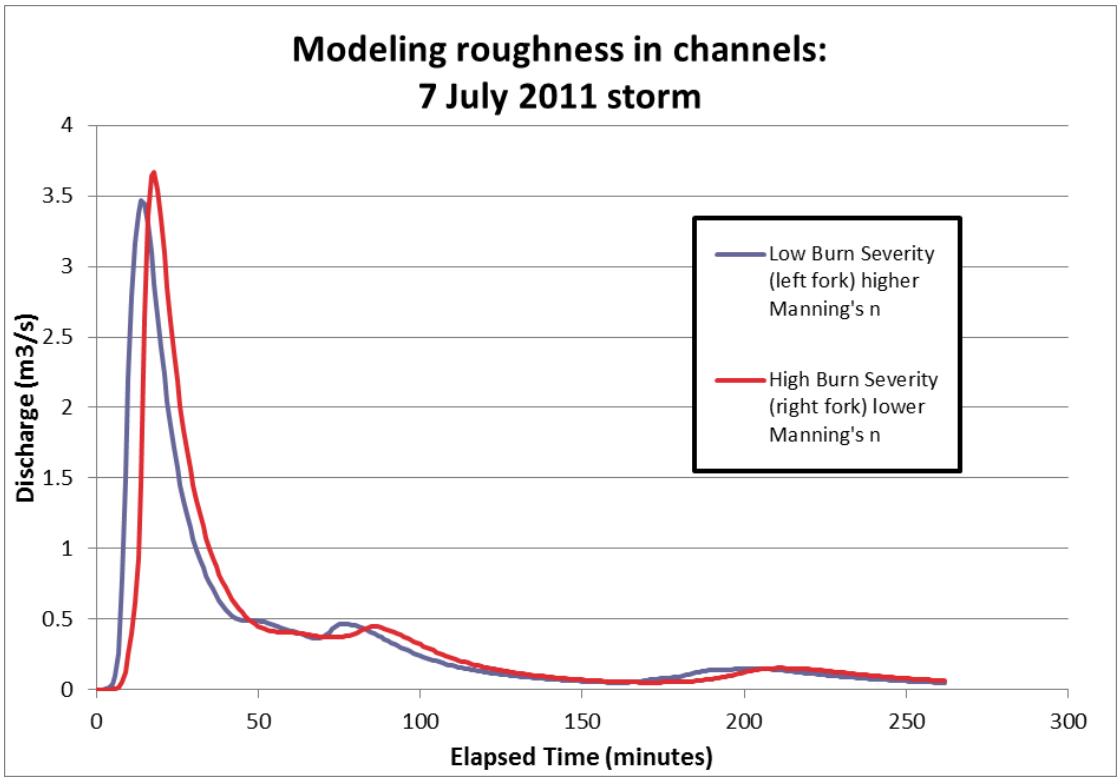

Figure 25*- TopoFlow(R) runoff output, modeling only the difference in channel roughness between the left and right fork.*

The same methods for creating a channel geometry grid were used to create grids that also account for the change in hillslope roughness. The values given in section 4.4 based on Sugarloaf analogs were used to create another set of power laws, this time accounting for the impact of fire on the channel and the hillslope roughness

eq 5.3 Left Fork: $N = 0.4790\ (A + 0.4973)^{1.2477}$

eq 5.4 Right Fork: $N = 0.1568\ (A + 0.3482)^{0.2659}$

Figure 26 displays the hydrograph for the same storm, this time accounting for not only channel roughness but also hillslope roughness. The difference between the left and right fork is much more dramatic with this model iteration, showing that the adjustment of hillslope roughness significantly affects the runoff response. In the field this is evident when observing channels and hillslopes. Steep-sloped channels such as these are mostly bare rock and are not as sensitive to fire, while the heavily vegetated slopes show significant changes from unburned to burned hillslope roughness.

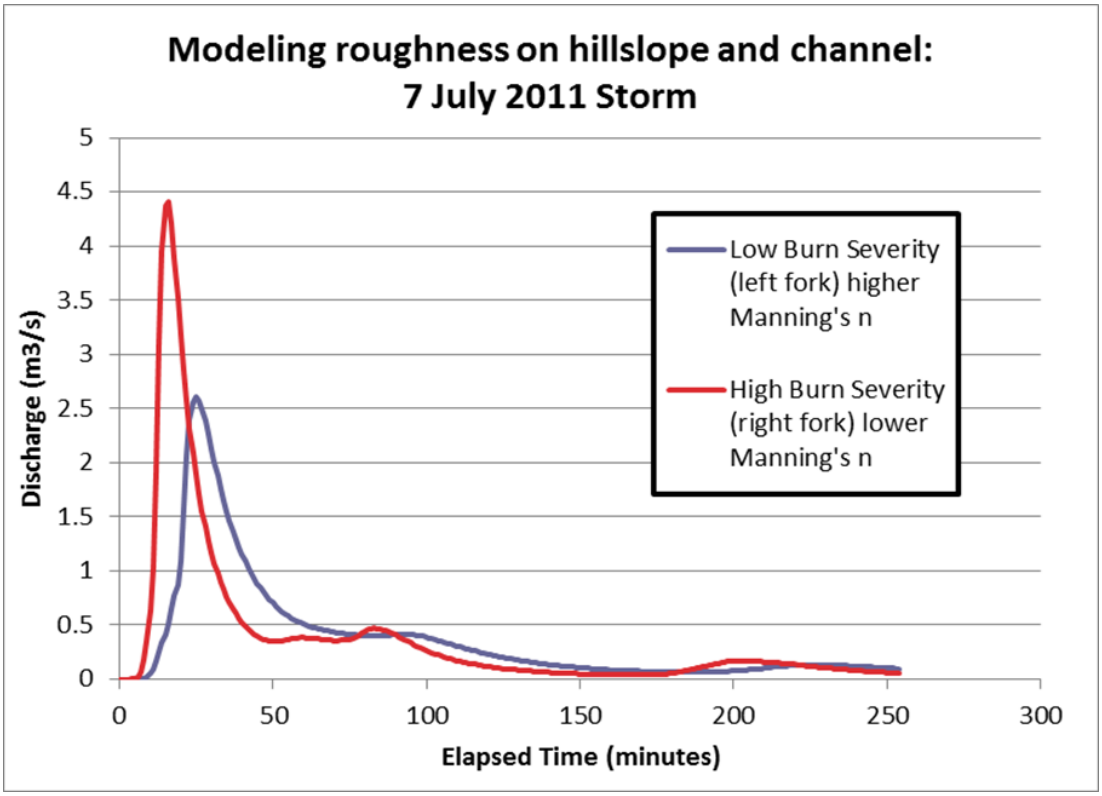

Figure 26- *TopoFlow® runoff output, showing the impact of changing channel and hillslope roughness with two separate channel geometry grids.*

In addition to adjusting the channel geometry grids, TopoFlow® offers several methods for calculating infiltration in the basin being modeled. The Smith and Parlange equation was used to model infiltration for the Loretta-Linda basin (Smith and Parlange, 1978). This method allows the user to either select the closest soil type from sand, loamy sand, sandy loam, silt loam, loam, sandy clay loam, loam, sandy clay loam, silty clay loam, clay loam, sandy clay, silty clay, or clay. Based on which soil type is selected the parameters listed in Table 6 (from Dingman, 2002) and 7 (from Smith, 2002) are given the corresponding default inputs.

Soil Texture	Porosity, φ	K_{sat} (cm/s)	K_{sat} (hm/h)	ψ_B	b	λ=1/b
Sand	0.395 (0.056)	1.76 e-2	634	-12.1 (14.3)	4.05 (1.78)	0.247
Loamy sand	0.410 (0.068)	1.56 e-2	562	-9.0 (12.4)	4.38 (1.47)	0.228
Silty sand	-	-	-	-	-	-
Sandy loam	0.435 (0.086)	3.47 e-3	125	-21.8 (31.0)	4.90 (1.75)	0.204
Loam	0.451 (0.078)	6.95 e-4	25.0	-47.8 (51.2)	5.39 (1.87)	0.186
Silt	-	-	-	-	-	-
Loamy silt	-	-	-	-	-	-
Silty loam	0.485 (0.056)	7.20 e-4	25.9	-78.6 (51.2)	5.30 (1.96)	0.189
Sandy clay loam	0.420 (0.059)	6.30 e-4	22.7	-29.9 (37.8)	7.12 (2.43)	-
Clay loam	0.476 (0.053)	2.45 e-4	8.82	-63.0 (51.0)	8.52 (3.44)	0.117
Silty clay loam	0.477 (0.057)	1.70 e-4	6.12	-35.6 (37.8)	7.75 (2.77)	0.129
Sandy clay	0.426 (0.057)	2.17 e-4	7.82	-15.3 (17.3)	10.4 (4.45)	0.096
Silty clay	0.492 (0.064)	1.03 e-4	3.71	-49.0(62.1)	10.4 (4.45)	0.096
Clay	0.482 (0.050)	1.28 e-4	4.61	-40.5 (39.7)	11.4 (3.70)	0.088

Table 5- *TopoFlow® default parameters associated with each soil type (from Dingman 2002).*

Soil Texture	Typical K_{sat} (mm/h)	G (mm)	Dry soil S (mm/h^0.5)	Time scale, tc (h)
Sand	30.0	82	38	0.08
Loamy sand	15.0	97	29	2.0
Silty sand	-	-	-	-
Sandy loam	4.4	165	21	11.0
Loam	10.0	385	48	12.0
Silt	2.5	914	37	109
Loamy silt	-	-	-	-
Silty loam	4.5	724	44	48
Sandy clay loam	13.0	240	43	5.5
Clay loam	2.6	804	35	92
Silty clay loam	0.7	1590	26	680
Sandy clay	1.2	589	21	73
Silty clay	0.4	3570	29	2600
Clay	4.0	2230	73	167

Table 6*- Default parameters associated with each soil type (from Smith 2002).*

The soil in Loretta-Linda did not fall into any of the soil types given as options in TopoFlow®, as it was observed in the field to be gravelly sand. Using the Sugarloaf site as an analog for soil properties in the Loretta-Linda basin a particle size analysis for the top 3 centimeters of soil found:

19% gravel (2-32 mm)
67% sand (0.063-2 mm)
15% silt and clay (<0.063 mm) (Ebel et al. 2012)

Despite the obvious difference between the hydrologic behavior of a sand and a sandy gravel, two model iterations (one for the left fork and one for the right fork grid) were completed using the TopoFlow® values for a sand (the closest option available in the default values), to test the behavior of the model when infiltration was added. The earlier model runs, where Manning's n was the only variable affecting the rain between the precipitation input and the discharge output, the model runs could be relatively short,

approximately the same temporal duration as the rainfall event. This was not the case when infiltration was included in the model runs, which have a larger temporal extent. Figure 27 shows that the right and left fork grids behave very differently once infiltration is incorporated. The reported discharges are also orders of magnitude less than those when infiltration was ignored altogether. The difference seen between the two forks in this model iteration compared to what was observed in the field is also unrealistic and suggests that other variables are affecting the different infiltration behavior between the two forks.

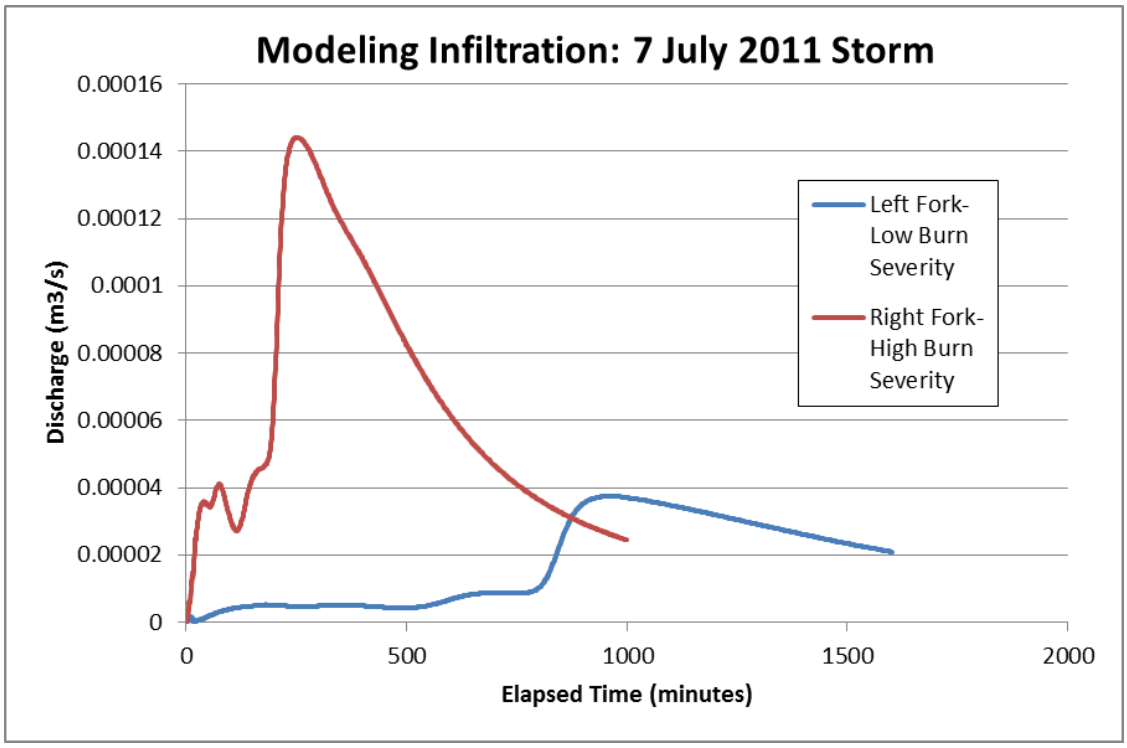

Figure 27*- TopoFlow® runoff output, modeling infiltration in a sandy soil, with channel and hillslope grids for each fork.*

Two more model iterations of the model were completed, for the left and right fork, using the respective channel geometry grids in addition to the Smith and Parlange (1978) variables specific to each burn severity. The Smith and Parlange (1978) method for calculating infiltration in TopoFlow® uses several equations (Appendix G) and requires input values for the variables of: saturated hydraulic conductivity (K_{sat}), initial hydraulic conductivity (K_i), saturated soil water content (Θ_s), initial soil water content (Θ_s), capillary length (G), and the Smith-Parlange parameter (γ). Soil moisture data was available for Loretta-Linda, but hydraulic conductivity and capillary length (a function of sorpitivity) calculations were not available. The Sugarloaf study site was once again used as an analog for Loretta-Linda. Infiltration experiments conducted on the Sugarloaf site provided the data in Table 8 (Ebel et al., 2012). These values were used to create linear models that provide a rough estimate for sorpitivity S and saturated hydraulic conductivity for varying burn severities (Figure 28 & 29).

dNBR	**Sorpitivity, S**				**Saturated Hydraulic Conductivity (K_{sat})**		
	Mini-disk Mean value (mm $s^{-0.5}$)	StDev (mm $s^{-0.5}$)	Mini-disk (mm $h^{-0.5}$)	StDev (mm $s^{-0.5}$)	Mini-disk mean value	Mini-disk StDev (mm h^{-1})	Inverse Modeling
0	0.39	0.17	23.4	10.2	82	47	82
834	0.0056	0.025	0.336	1.5	10	28	1

Table 7*- Data collected at Sugarloaf Mountain study site, (from Ebel et. al., 2012).*

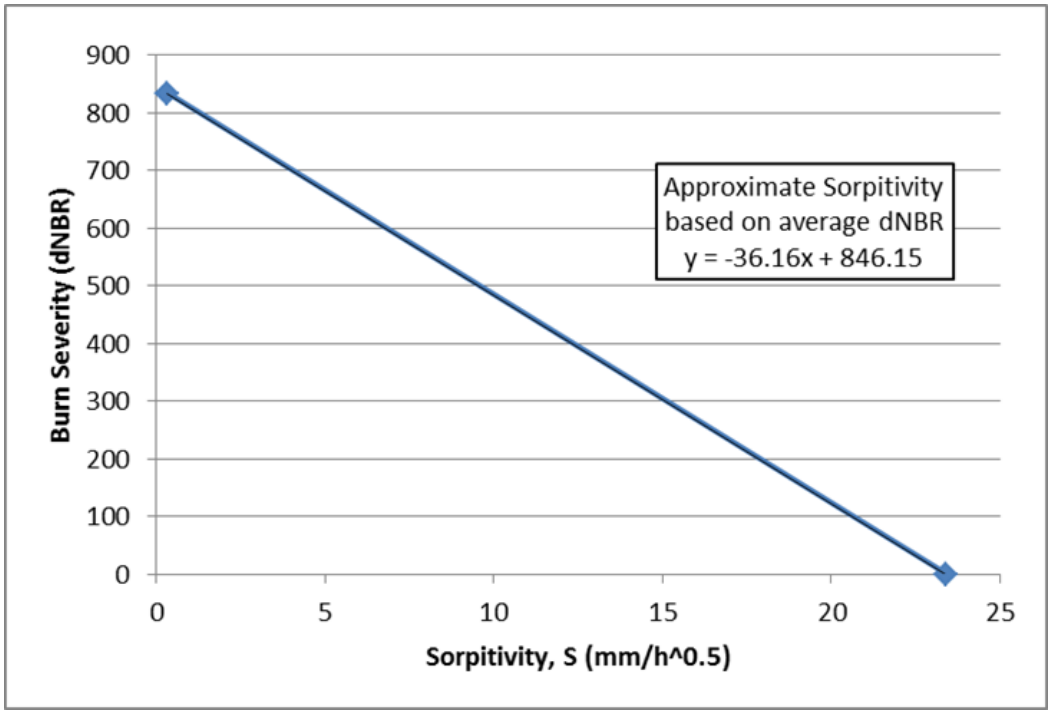

Figure 28- *Linear plot estimating sorpitivity values based on burn severity.*

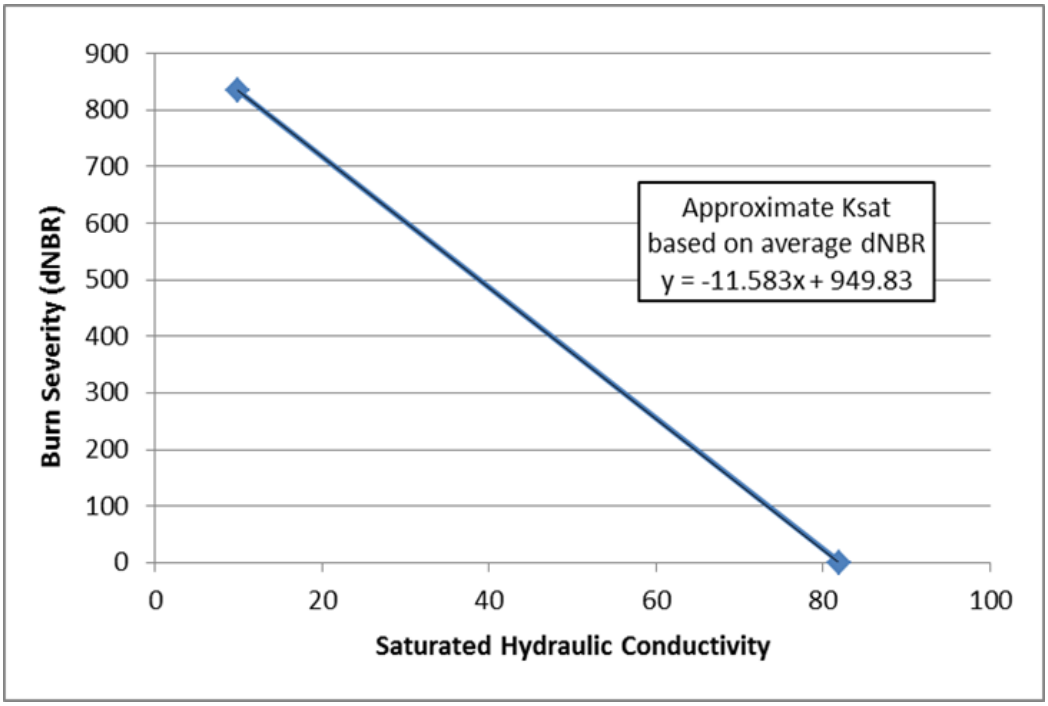

Figure 29- *Linear plot of saturated hydraulic conductivity trends with increasing burn severity.*

Because these graphs represent approximations based on limited data, and because Ebel et al. (2012) state that the variability in measurements of saturated hydraulic conductivity made it difficult to make generalizations about the difference between burned and unburned soils, the values obtained using Figure 28 and Figure 29, were cross-checked with the values given in Tables 6 and 7, to verify that they were reasonable when compared to default values provided in TopoFlow® (though we expect values to differ from the tables which are for use in unburned watersheds).

Based on the Sugarloaf analog data and the soil moisture data collected in the field, the values compiled in Table 9 were used in a model iteration using the Smith and Parlange (1978) infiltration method. Figure 30 displays the model iteration completed using these variables.

Variable	Default values	Left Fork values dNBR 520	Right Fork values dNBR 613
K_s (m/s)	0.000176 6	0.000010308	0.00902
K_i(m/s)	1.71157 e -8	1.03 e -8	9.02 e -6
Θ_s (unitless)	0.3950	0.30	0.21
Θ_i (unitless)	0.18547754	0.10	0.15
G (m)	0.082	0.061	0.059
gamma (unitless)	0.82	0.61	0.59

Table 8*- Values used for input variables in the Smith Parlange infiltration method in TopoFlow®.*

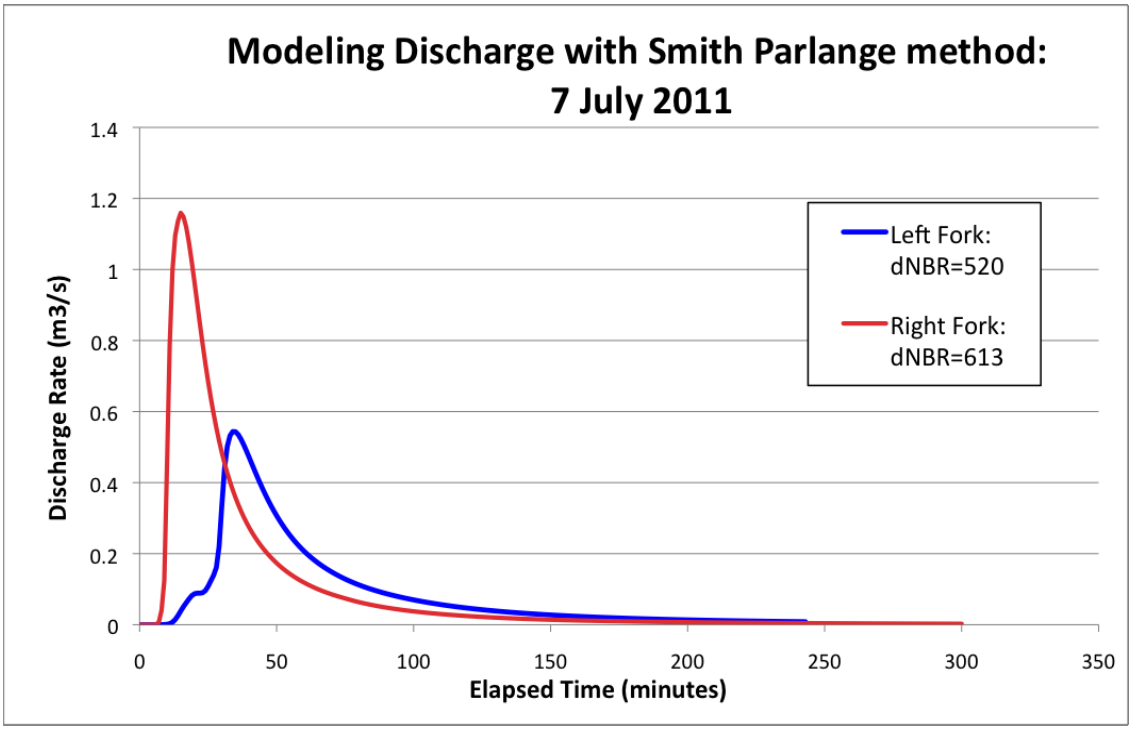

Figure 30*- TopoFlow® discharge output, modeling the response to a rainfall event using unique channel geometry grids and infiltration parameters.*

The inclusion of infiltration in the model iteration made a significant difference between Figure 26 and Figure 27, which only used the default parameters provided by TopoFlow®. However, the adjustment of infiltration parameters specific to burned watersheds and specific to Loretta-Linda, showed just as significant a change between the two infiltration plots (Figure 27 and 30). Because TopoFlow® operates under idealized conditions, with only rainfall, flow pattern, roughness, and infiltration accounted for, these model iterations do not show the same fluctuations throughout the course of the storm as were measured in the field. However, the Smith and Parlange method used to produce Figure 30, did create the closest approximation of the evolving

runoff trends as were observed in the field measurements. The "shape" of the curves, though smoothed out in the model run, are closely representative of those measured by the flumes (Figure 17). The initial and narrow spike of the right fork is captured as is the slight step up trend of the left fork flume discharge. The magnitudes of discharge values are significantly greater in the model hydrograph. This is likely a result of variables that were not accounted for in the model iterations such as evaporation, evapotranspiration, and subsurface flow and storage.

6. CONCLUSIONS

The question posed for this research was: What is the correlation between burn severity, soil infiltration and runoff in a watershed affected by wildfire? From that question, four objectives were established:

1) Characterize soil moisture for each sub-drainage of the Loretta-Linda watershed;
2) Determine properties of each storm cell (duration, intensity, total rainfall);
3) Characterize the infiltration and runoff response of the right and left forks of the Loretta-Linda Basin; and
4) Analyze the impact of varying burn severity on the two sub-drainages by creating a dynamic simulation model.

The research was driven by the hypothesis:

H_1: The sub drainage with higher burn severity will have less capacity for soil moisture retention, lower rates of infiltration, and greater levels of area-weighted discharge.

H_0: The sub drainage with higher burn severity is not significantly different from the sub drainage with lower burn severity in soil moisture retention, rate of infiltration, or levels of area-weighted discharge.

The impact of burn severity is expressed most dramatically in the destruction of vegetation, the alteration of soil properties, and the subsequent hydrologic changes that occur as a result of this alteration. This research sought to investigate these variables and determine how each is affected by wildfire in a watershed such as Loretta-Linda, while specifically asking whether varying degrees of burn severity showed measurable difference in how these variables impact the hydrologic response of the basin. Whereas most studies have compared burned to unburned sites, this analysis sought to answer the question of whether these parameters were in fact significantly impacted by the degree burn severity. Although comparative data analysis was unable to distinguish a consistent or dramatic difference between the two severities studied here, the use of a spatial hydrologic modeling allowed for the investigation of individual parameters on the hydrologic behavior of a watershed.

The impact of infiltration and the affect that soil moisture has on this response proved to be significant, as did the difference in hillslope roughness observed between the two forks. Accounting for hydraulic conductivity, sorpitivity, channel and hillslope roughness, and antecedent soil moisture, yielded the closest approximation of discharge rates of any other method tested. The differences between burn severities observed in the field and in analog basins, shows that the impact of burn severity on these parameters is significant for the production of runoff, as seen in Figure 28. The lack of a regular trend over the course of the summer in the discharge data collected in the field does not disprove this hypothesis but rather suggests that other variables are at work in the basin that could not be accounted for by simply observing the flume-measured discharge.

This study concluded that the degree of burn severity is an important factor in determining the hydrologic response of a watershed. While the methods used in the field were not able to record a consistent trend of high levels of discharge for the more severely burned sub drainage, measurements of soil moisture, channel and hillslope roughness that were used in the TopoFlow®, illustrated how basins with different burn severities would respond if all other factors were consistent. This lack of homogeneity in the field and the limitations of the instrumentation installed prevented the field measurements of discharge from reflecting this trend. The data collected here and the use of the TopoFlow® model to predict runoff, however, represents a unique approach to predicting elevated runoff levels and potential flood hazards.

The ever-growing urban-wildland interface is especially evident in the Fourmile Canyon area. The presence of this interface, the frequency of fires on the Front Range, and Fourmile Creek serving as a tributary for Boulder Creek, all increase the likelihood of post-fire flood hazards and demand continuing research on this subject. The modeling approach used in this study would be easily applied to basins in any area where data is available. This study is, however, most important in its contribution to the body of knowledge and understanding of the soil properties and hydrologic response post-wildfire. An ever-growing database of information on burned soil properties, and an increasing availability of research for analog basins will allow for more comprehensive studies and development of more accurate flood-prediction methods.

As research continues on burned areas of the Front Range and Fourmile Canyon specifically, the data collected in Loretta-Linda may continue to be applied. Research

in Loretta-Linda could be supplemented with a similar method of data collection and comparative analysis on an adjacent unburned basin (with similar slope aspect). With no time constraints on data collection, instrumentation in the Loretta-Linda basin would have been installed and monitored immediately after the Fourmile Canyon fire and continually throughout the year following the fire. This would afford the opportunity to observe not only the different hydrologic response between burn severities as time progresses but also the recovery and rebound of the burned watershed as a whole. The most ideal scenario would have pre-burn data available on the burned watershed, however, the unpredictability of wildfires makes the availability of such datasets rare.

There is still much research to be done in burned watershed hydrology. The expansion of this body of knowledge and continued investigation of the infiltration capabilities of a range of soil burn severities will be invaluable in not only academic and research pursuits in this field but more importantly, the ability to better predict flood-hazards associated with elevated runoff.

REFERENCES

Bales, R. C., Molotch, N. P., Painter, T. H., Dettinger, M. D., Rice, R., Dozier, J., 2006. Mountain hydrology of the western United States: Water Resources, Vol. 42, No. 10.1029: 1-41.

Bento-Gongalves, A., Vieira, A., Ubeda, X., Martin, D., 2012. Fire and soils: Key concepts and recent advantages: Geoderma, Vol. 191, No. 10.1016.: 1-11.

Bilodeaux, S. W., Van Buskirk, D., Bilodeau, W. L., 1988. Geology of Boulder, Colorado, United States of America: Bulletin of the Association of Engineering Geologists, Vol. 24, No. 3: 289-332.

Birkeland, P. W., Shroba, R. R., Burns, S. F., Price, A. B., Tonkin, P. J., 2003. Integrating soils and geomorphology in mountains-an example from the Front Range of Colorado: Geomorphology, Vol. 55: 329-344.

Brenkert-Smith, H., Champ, P. A., 2011. Fourmile Canyon: Living with wildfire in Boulder County, Colorado: Rocky Mountain Research Station, Vol. 71, No. 2: 33-39.

Certini, G., 2005. Effects of fire on properties of forest soils: A review: Oceologia, Vol. 143: 1-10.

Chow, V. T., 1964. *Runoff: Handbook of Applied Hydrology*, McGraw-Hill: New York, N.Y.: 680 p.

Clark, B., 2001, Fire Effects Guide, soils, water and watersheds: National Wildfire Coordinating Group: U.S. Fish and Wildlife Service, NFES 2394.

Clark, J., Bobbe, T., 2006. Using remote sensing to map and monitor fire damage in forest ecosystems: *Understanding Forest Disturbance and Spatial Pattern: Remote Sensing and GIS approaches*, Wulder, M. A., Franklin, S., E., (Editors). Taylor and Francis Group: Boca Raton, Florida: 113–131.

Cobos, D. R., Chambers, C., 2010. Calibrating ECH_20 Soil Moisture Sensors: Decagon Devices, Inc.

DeBano, L. F., Krammes, J. S., 1966. Water repellent soils and their relation to wildfire temperatures: International Bulletin of the Association of Hydrological Sciences, Vol. 2: 14–19.

DeBano, L. F., Neary, D. G., Folliott P. F., 1998. *Fire's effects on ecosystems*. John Wiley & Sons: Hoboken, New Jersey: 335 p.

DeBano, L. F., 1999. The role of fire and soil heating on water repellency in wildland environments: A review: Journal of Hydrology, Vol. 231: 195-232.

Dimitrakopoulos, A. P., Martin, R. E., Papamichos, N. T., 1994. A simulation model of soil heating during wildland fires: *Soil erosion as consequence of forest fires*, Sala, M., Rubio, J., L., (Editors). Geoforma Ediciones: Barcelona, Valencia: 207–216.

Dingman, S. L., 2002. *Physical Hydrology*, 2nd ed., Prentice-Hall Inc.: Upper Saddle River, New Jersey: 299 p.

Doerr, S. H., Shakesby, R. A., Walsh, R. P. D., 2000. Soil water repellence: Its causes, characteristics and hydro-geomorphological significance: Earth Science Reviews, Vol. 51: 33-56.

Doerr, S. H., Moody, J., 2004. Hydrological impacts of soil water repellency: On spatial and temporal uncertainties: Hydrological Processes, Vol. 18: 820-832.

Eagleson, P. S., 1970. *Dynamic Hydrology,* McGraw-Hill: New York, New York: 462 p.

Ebel, B. A., Moody, J. A., Martin, D. A., 2012. Hydrologic conditions controlling runoff generation immediately after wildfire: Water Resources Research, Vol. 48: 1-13.

Eckhardt, K., Haverkamp, S., Fohrer, N., Frede, H. G., 2001. SWAT-G, a version of SWAT99.2 modified for application to low mountain range catchments: Physics and Chemistry of the Earth, Vol. 27: 641-642.

Engman, E. T., Asce, M., 1986. Roughness coefficient for routing surface runoff: Journal of Irrigation and Drainage Engineering, Vol. 112, No. 1: 39-53.

García-Corona, E., Benito de Blas, E., Varela, M. E., 2004. Effects of heating on some soil physical properties related to its hydrological behavior in two north-western Spanish soils: International Journal of Wildland Fire, Vol. 13: 195-199.

Giovanni, G., 1994. The effect of fire on soil quality: *Soil erosion as a consequence of forest fires*, Sala, M., Rubio, J. L., (Editors). Geoforma Ediciones: Barcelona, Valencia: 15-27.

Grayson, R. B., Moore, I. D., McMahon, T. A., 1992. Physically based hydrologic modeling: A terrain-based model for investigative purposes: Water Resources Research, Vol. 28, No. 10: 2639-2658.

Hamlett, C. A. E., Shirtcliffe, N. J., McHale, G., Arhn, S., Bryant, R., Doerr, S. H., Newton, M. I., 2011. Effect of particle size on droplet infiltration into hydrophobic porous media as a model of water repellent soil: Environmental Science Technology, Vol. 45, No. 22: 9666-9670.

Ice, G. G., Neary, D. G., Adams, P. W., 2004. Effects of wildfire on soils and watershed processes: Journal of Forestry, Vol. 102: 16–20.

Johnson, D. D., Cline, A. J., 1965. Colorado mountain soils: Advanced Agriculture, Vol. 17: 233-281.

Key, C. H., Benson, N. C., 2004. Ground measure of severity, the composite burn index.: Fire effects monitoring and inventory system, General Technical Report: U.S. Department of Agriculture, Forest Service, Rocky Mountain Research Station: 28 p.

Kilpatrick, F. A., Schneider, V. R., 1983. Use of flumes in measuring discharge: U.S. Geological Survey Techniques of Water-Resources Investigations, Vol. 3, No. 14: 1-46.

Koren, V. I., Finnerty, B. D., Schaake, J. C., Smith, M. B., Seo, D. J. Duan, Q.Y., 1999. Scale dependencies of hydrologic models to spatial variability of precipitation: Journal of Hydrology, Vol. 217: 285–302.

MacDonald L., Huffman, E. L., 2004. Post-fire soil repellency: persistence and soil moisture thresholds: Soil Science Society of America Journal, Vol. 68: 1729–1734.

Marcus, W. A., Roberts, K., Harvey, L., Tackman, G., 1992. An evaluation of methods for estimating Manning's n in small mountain streams: Mountain Research and Development, Vol. 12, No. 3: 227-239.

Montgomery, D., McClain, T., Love, E., Erlenbach, B., Casella, A., Bogdanova, T., 2010. *Results of the Four Mile Canyon fire on Chemical Water Quality of Fourmile Creek, a thesis*: Metropolitan State College of Denver: 40 p.

Moody, J. A., 2012. An analytical method for predicting postwildfire peak discharges: U.S. Geological Survey Scientific Investigations Report No. 2011–5236: 36 p.

Moody, J. A., Martin, D. A., 2001. Initial hydrologic and geomorphic response following a wildfire in the Colorado Front Range: Earth Processes and Landforms, Vol. 26: 1049-1070.

Moody, J. A., Martin, D. A., Oakley, T. M., Blanken, P. D., 2007a. Temporal and spatial variability of soil temperature and soil moisture after a wildfire: U.S. Geological Survey, Scientific Investigations Report No. 2007-5015: 89 p.

Moody, J. A., Martin, D. A., Haire, S. L., Kinner, D. A., 2007b. Linking runoff response to burn severity after a wildfire: Hydrological Processes, Vol. 22: 2063-2074.

Moody J. A., Martin, D. A., Cannon, S. H., 2008. Post-wildfire erosion response in two geologic terrains in the western USA: Geomorphology, Vol. 95: 103-118.

Moody, J. A., Martin, D. A., 2009. *Forest Fire Effects on Geomorphic Processes: Fire Effects on Soils and Restoration Strategies,* Science Publishers: Enfield, New Hampshire: 80 p.

Moody J. A., Ebel, B. A. 2012a. Hyper-dry conditions provide new insights into the cause of extreme floods after wildfire: Catena, Vol. 93: 58–63.

Moody, J. A, Ebel, B. A., 2012b. Difference infiltrometer: a method to measure temporally variable infiltration rates during rainstorms: Hydrological Processes, Vol. 26: 3312-3318.

Moreno, J. M., Oechel, W. C., 1989. A simple method for estimating fire intensity after a burn in California Chaparral: Acta Oecologica, Vol. 10: 57–68.

Morin, J., Benyamini, Y., 1977. Rainfall infiltration into bare soils: Water Resources Reseach, Vol. 13, No. 5: 813-817.

National Interagency Fire Center (NIFC). 2003. Wildland fire statistics. NIFC, from www.nifc.gov/stats/wildlandfirestats.html.

Neary, D. G., Ryan, K. C., DeBano, L. F., 2005. Wildland fire in ecosystems: Effects of fire on soil and water: General Technical Report RMRS-GTR-42: U.S. Department of Agriculture, Forest Service, Rocky Mountain Research Station, Vol. 4: 250 p.

Parsons, A., Robichaud, P. R., Lewis, S. A., Napper, C., and Clark, J., 2010. Field guide for mapping post-fire soil burn severity, Rocky Mountain Research Station, Forest Service, U.S. Dep. of Agriculture, Fort Collins, Colorado: 30 p.

Peckham, S. D., 2009, Geomorphometry and spatial hydrologic modeling: Developments in Soil Science, Vol. 33: 579-602.

Peet, R. K., 1981. Forest vegetation of the Colorado Front Range: Vegetatio, Vol. 45: 3-75.

Philip, J. R., 1956, The theory of infiltration: The infiltration equation and its solution: Soil Science, Vol. 83, No. 5: 345-358.

Romme, W. H., Despain, D. G., 1989. Historical perspective on the Yellowstone fires of 1988: American Institute of Biological Science, Vol. 39, No. 10: 696-699.

Rosenfield, C. L., 1994. The geomorphological dimensions of natural disasters: Geomorphology, Vol. 10: 27-36.

Schoennagel, T., Nelson, C. R., Theobald, D. M., Carnwath, G. C., Chapman, T. B., 2009. Implementation of national fire plan treatments near the wildland-urban interface in the western United States: Proceedings of the National Academy of Sciences of the United States of America, Vol. 106, No. 26: 10706-10711.

Shakesby, R. A., Doer, S. H., 2005. Wildfire as a hydrological and geomorphological agent: Earth-Science Reviews, Vol. 74: 269-307.

Smith, R. E., Parlange, J. Y., 1978. A parameter-efficient hydrologic infiltration model: Water Resources Research, Vol. 333: 1355-1361.

Smith, R. E., 2002. Infiltration theory for hydrologic applications: American Geophysical Union, Water Resources Monograph, Vol. 15: 1-212.

Strahler, A. N., 1957. Quantitative analysis of watershed geomorphology: Transactions, American Geophysical Union, Vol. 38, No. 6: 913-920.

Swanson, F. J., 1979. Fire and geomorphic processes: U.S. Department of Agriculture, Forest Service, Pacific Northwest Forest and Range Experiment Station: Proceedings: Fire regimes and ecosystems conference.

Swetnam, T. W., 1988. Fire history and climate in the southwestern United States: Panel paper presented at conference: Effects of fire in management of southwestern natural resources, Tucson AZ, November 14-17.

Tarboton, D. G., 1997. A new method for the determination of flow directions and upslope areas in grid digital elevation models: Water Resources Research, Vol. 33, No. 2: 309-319.

Turner, M. G., Romme, W. H., Tinker, D. B., 2003. Surprises and lessons from the 1988 Yellowstone fires: Frontiers in Ecology, Vol. 1, No. 7: 351-358.

Úbeda, X., 1999. Structural changes on soils after forest fires: Extended abstracts of 6th international meeting of soils with Mediterranean type of climate. Universitat de Barcelona, Barcelona, Spain, 1999: 793–796.

Westerling, A. L., Gershunov, A., Brown, T. J., Cayan, D. R., Dettinger, M. D., 2003, Climate and wildfire in the western United States: Bulletin of the American Meteorological Society, Vol. 84, No. 5: 595- 604.

Wood, E. F., Sivapalan, M., and Beven, K. J. 1990. Similarity and scale in catchment storm response: Reviews Geophysics, Vol. 28: 1-18.

APPENDIX A- CUMULATIVE RAINFALL

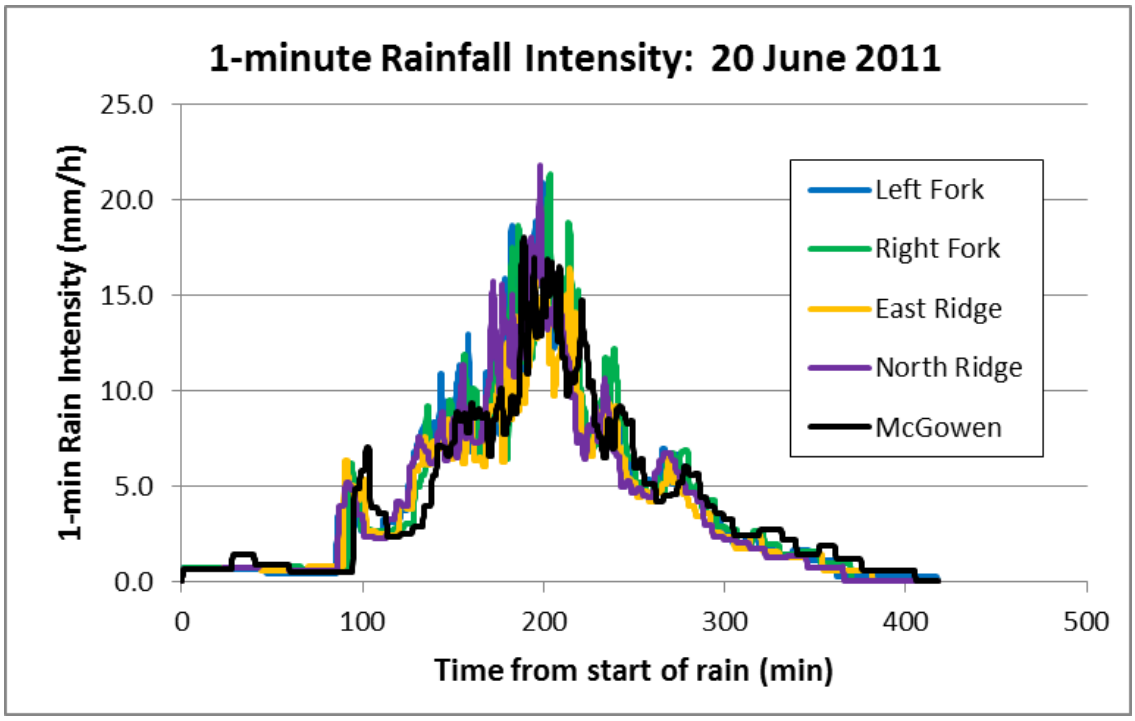

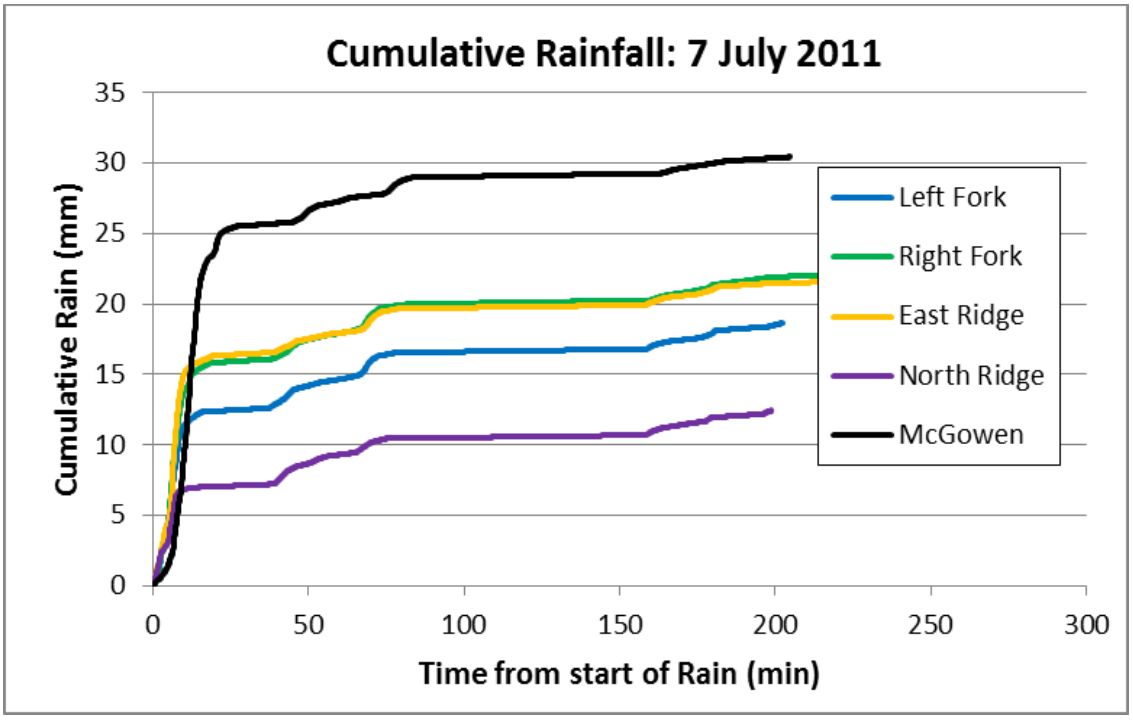

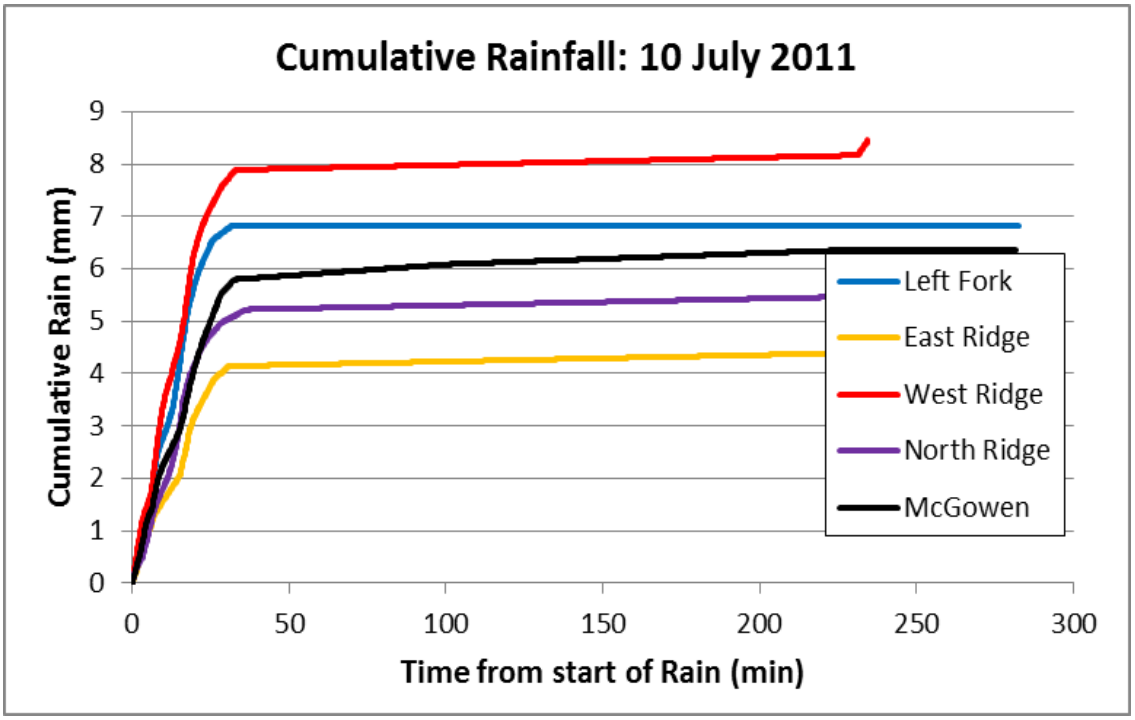
Cumulative Rainfall: 10 July 2011
Cumulative Rain (mm)
0
1
2
3
4
5
6
7
8
9
0
50
100
150
200
250
300
Time from start of Rain (min)
Left Fork
East Ridge
West Ridge
North Ridge
McGowen

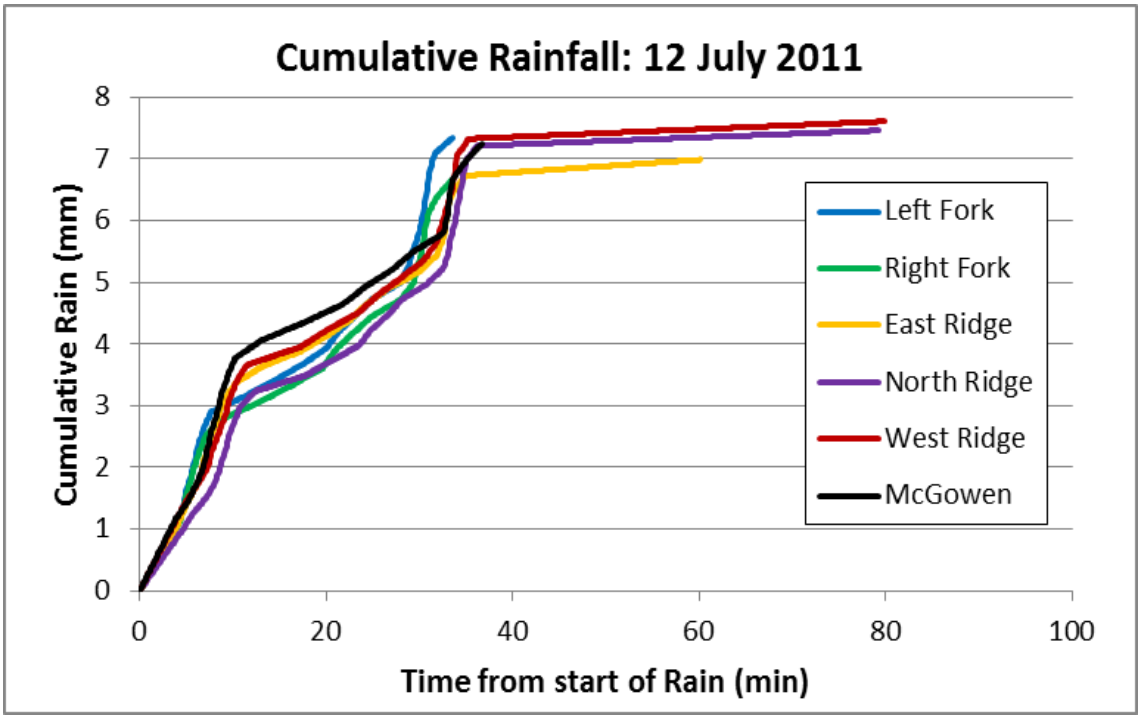
Cumulative Rainfall: 12 July 2011
Cumulative Rain (mm)
0
1
2
3
4
5
6
7
8
0
20
40
60
80
100
Time from start of Rain (min)
Left Fork
Right Fork
East Ridge
North Ridge
West Ridge
McGowen

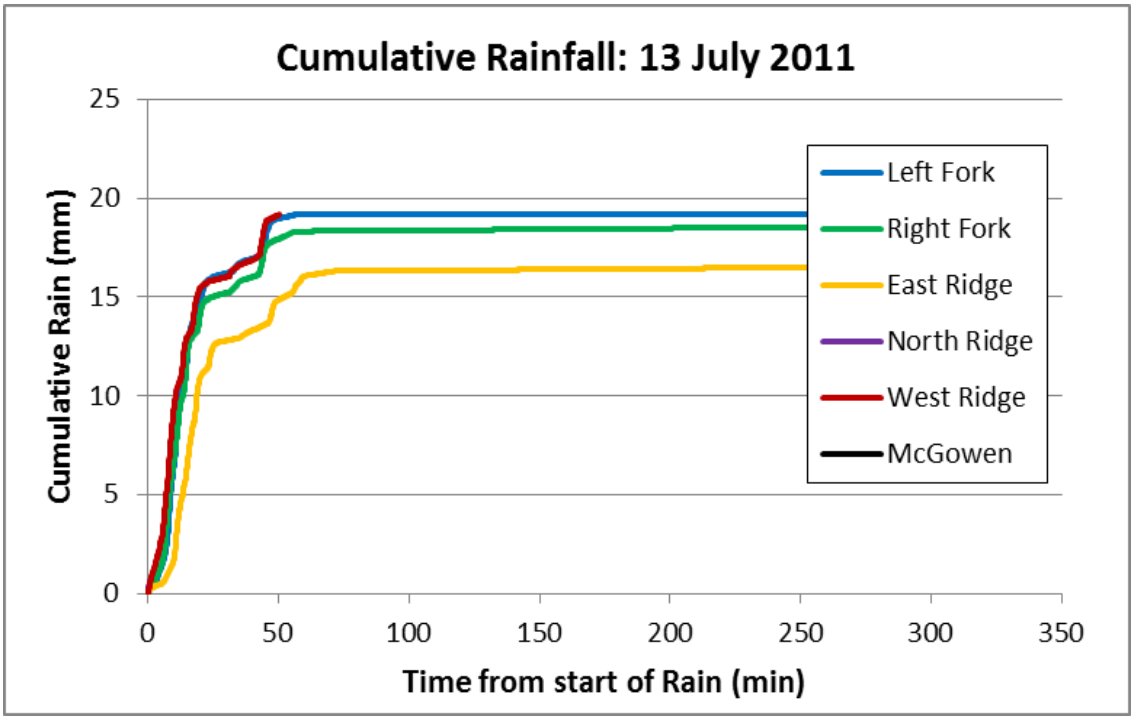
Cumulative Rainfall: 13 July 2011
Cumulative Rain (mm)
25
20
15
10
5
0
0
50
100
150
200
250
300
350
Time from start of Rain (min)
Left Fork
Right Fork
East Ridge
North Ridge
West Ridge
McGowen

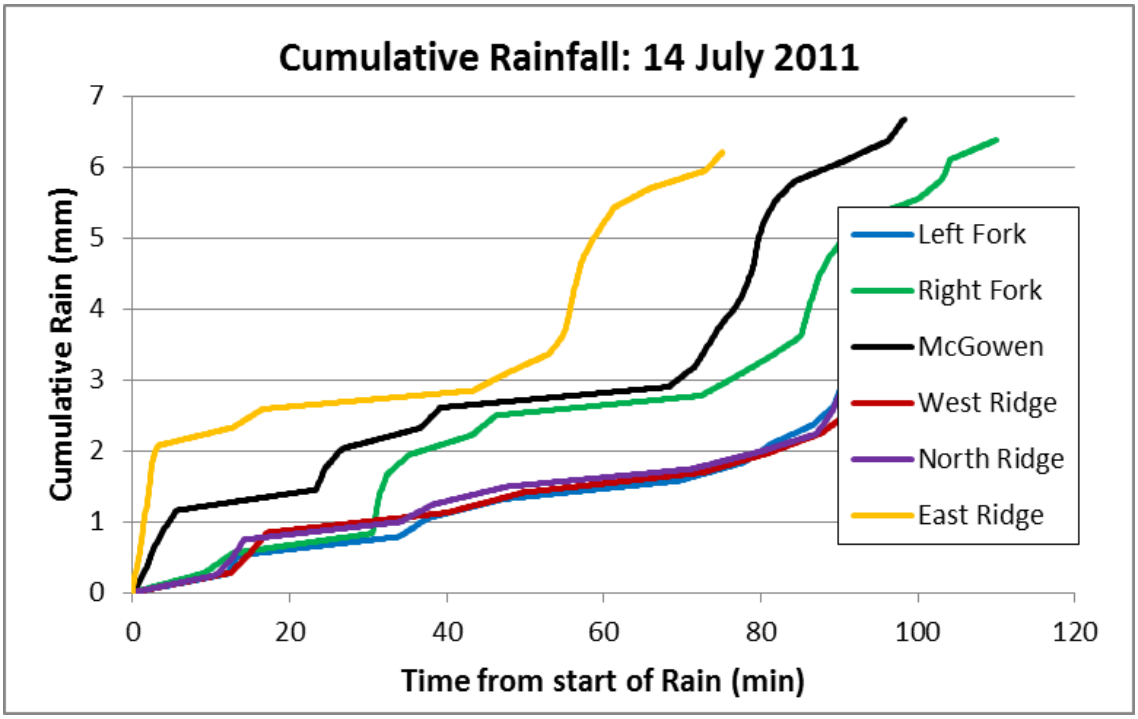
Cumulative Rainfall: 14 July 2011
Cumulative Rain (mm)
7
6
5
4
3
2
1
0
0
20
40
60
80
100
120
Time from start of Rain (min)
Left Fork
Right Fork
McGowen
West Ridge
North Ridge
East Ridge

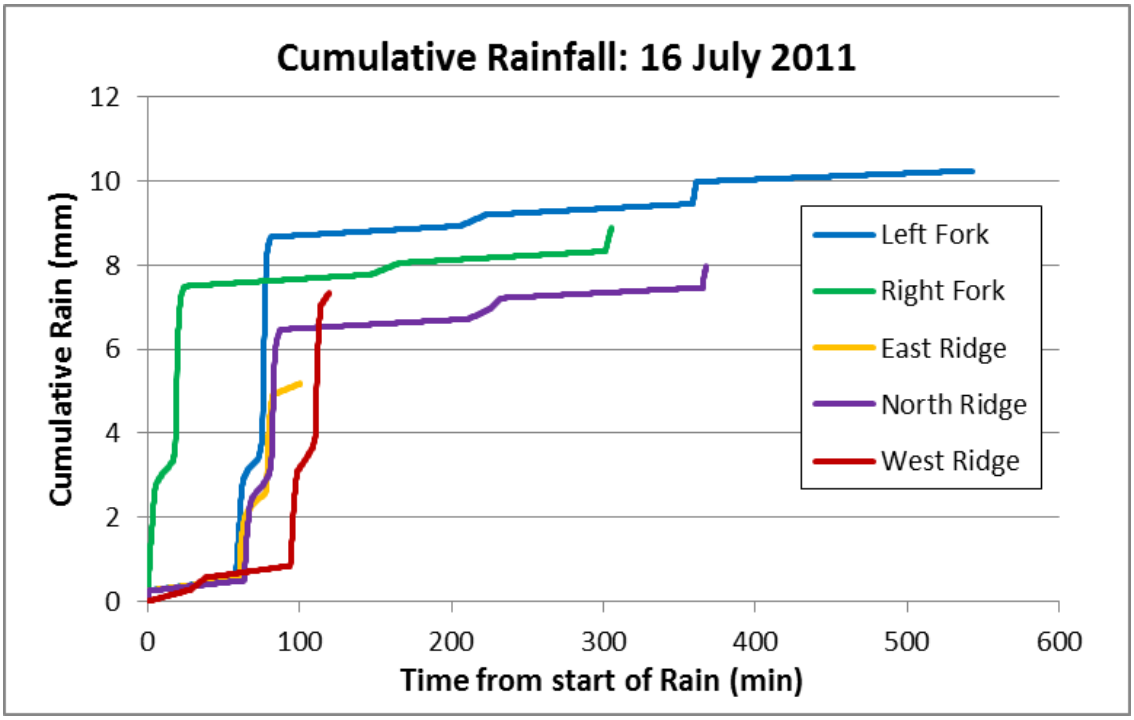
Cumulative Rainfall: 16 July 2011
Cumulative Rain (mm)
0
2
4
6
8
10
12
0
100
200
300
400
500
600
Time from start of Rain (min)
Left Fork
Right Fork
East Ridge
North Ridge
West Ridge

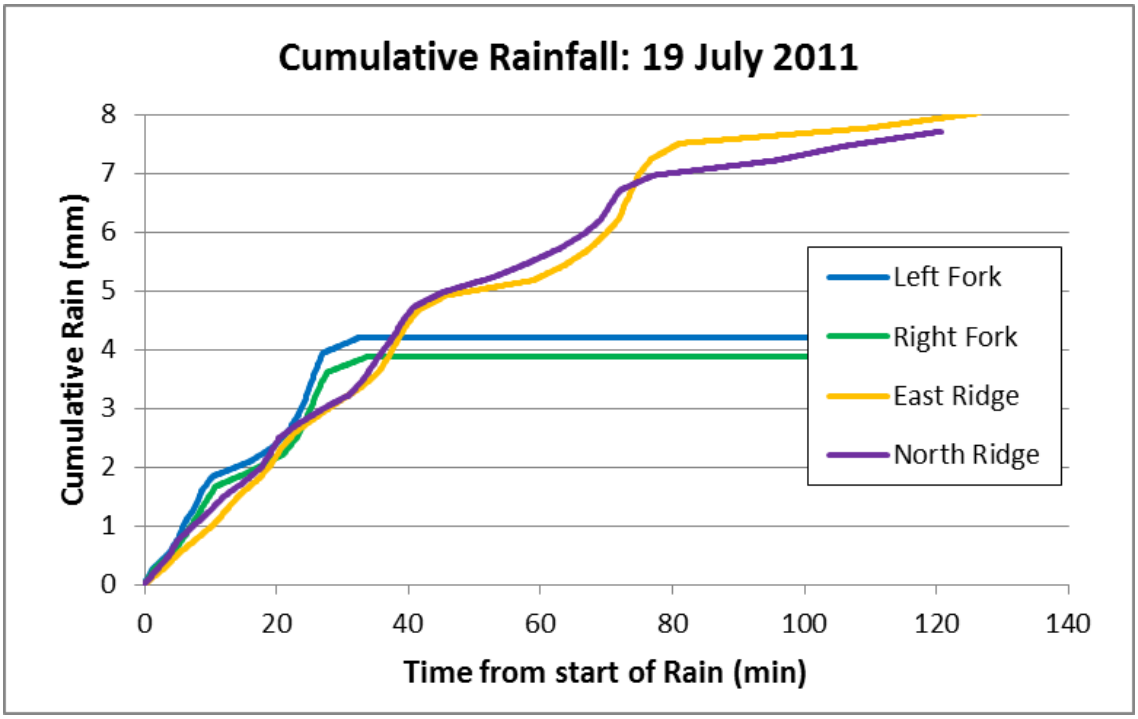
Cumulative Rainfall: 19 July 2011
Cumulative Rain (mm)
0
1
2
3
4
5
6
7
8
0
20
40
60
80
100
120
140
Time from start of Rain (min)
Left Fork
Right Fork
East Ridge
North Ridge

APPENDIX B- SPATIAL DISTRIBUTION OF RAINFALL

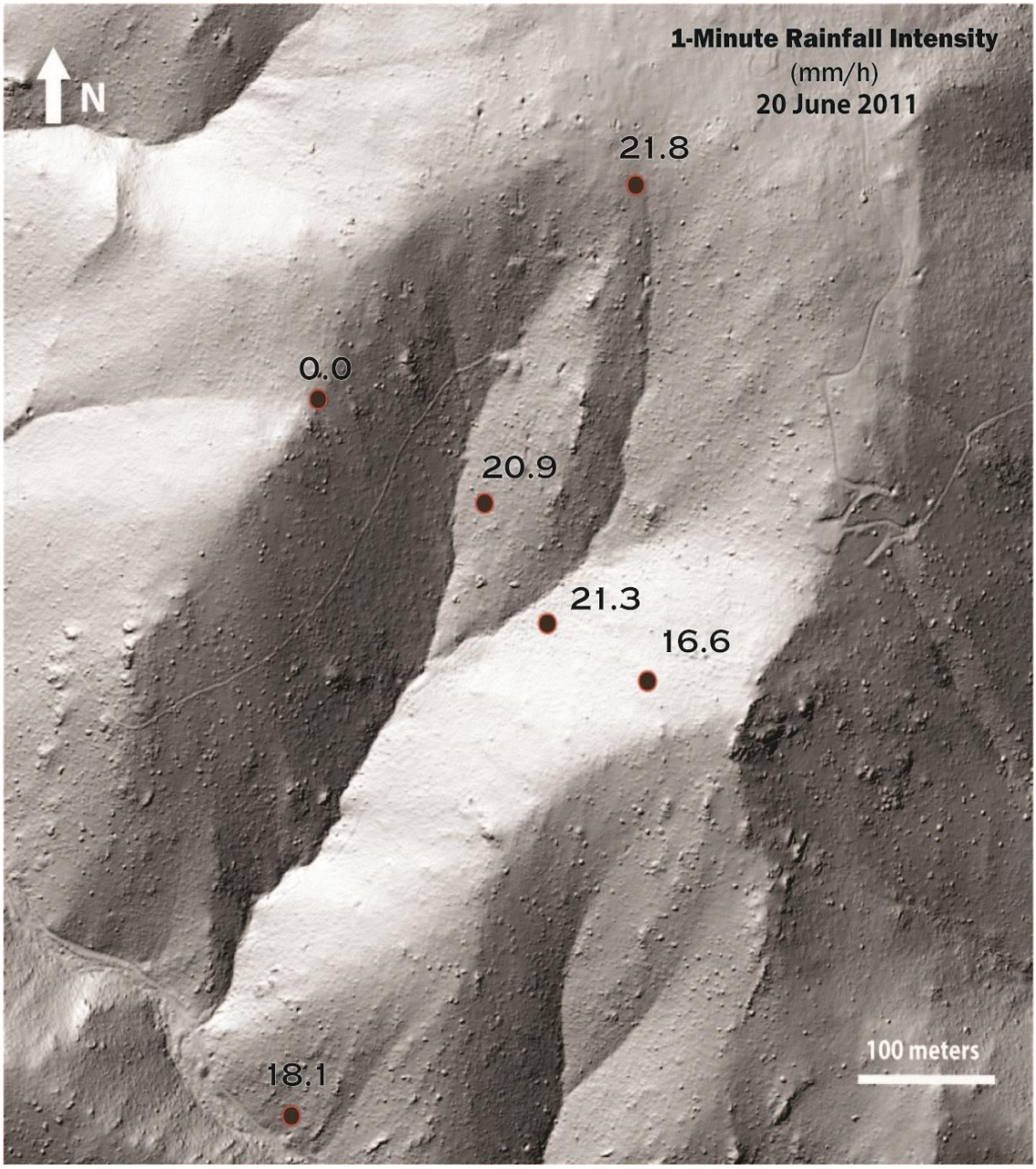

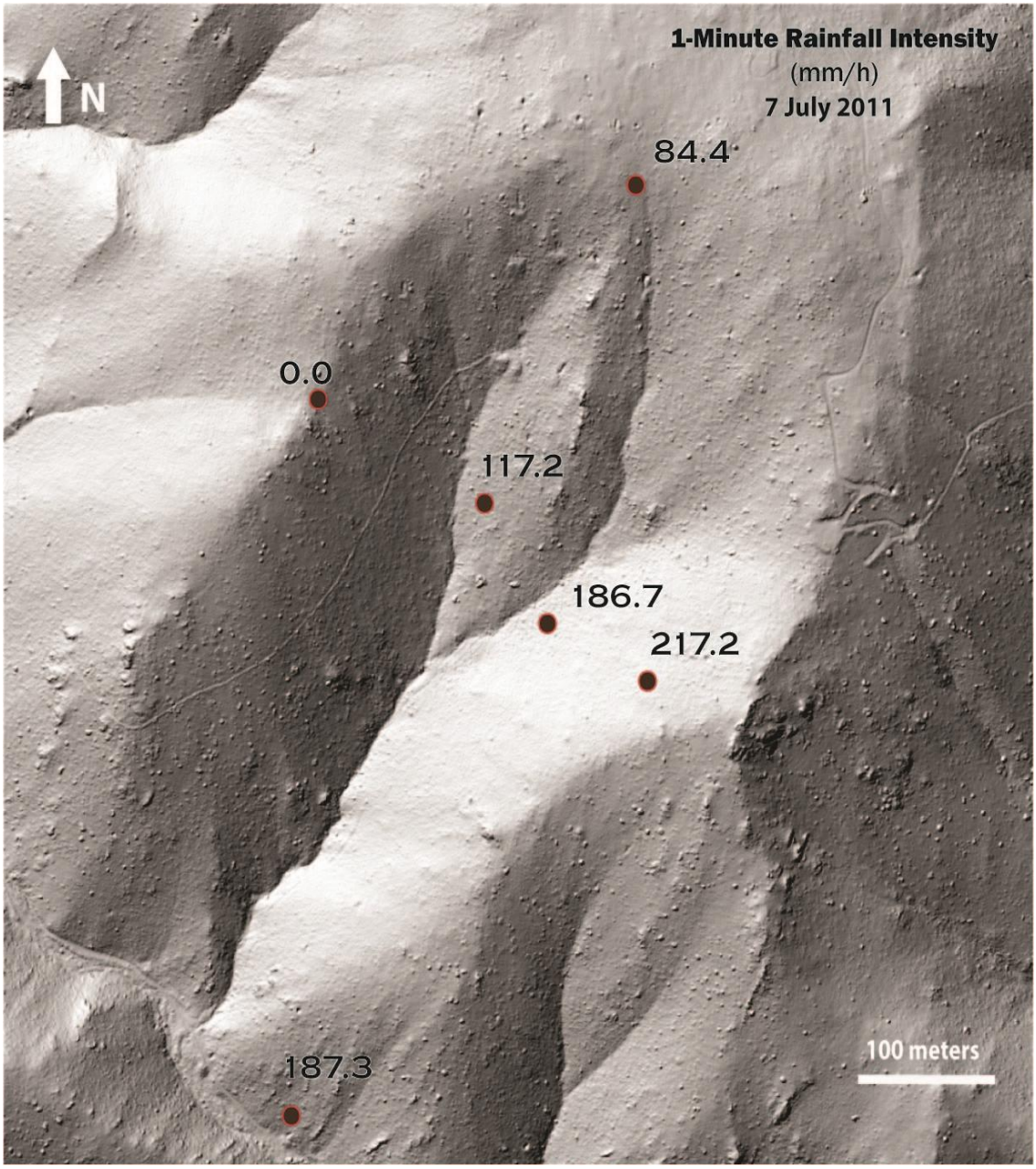
1-Minute Rainfall Intensity
(mm/h)
7 July 2011
N
84.4
0.0
117.2
186.7
217.2
187.3
100 meters

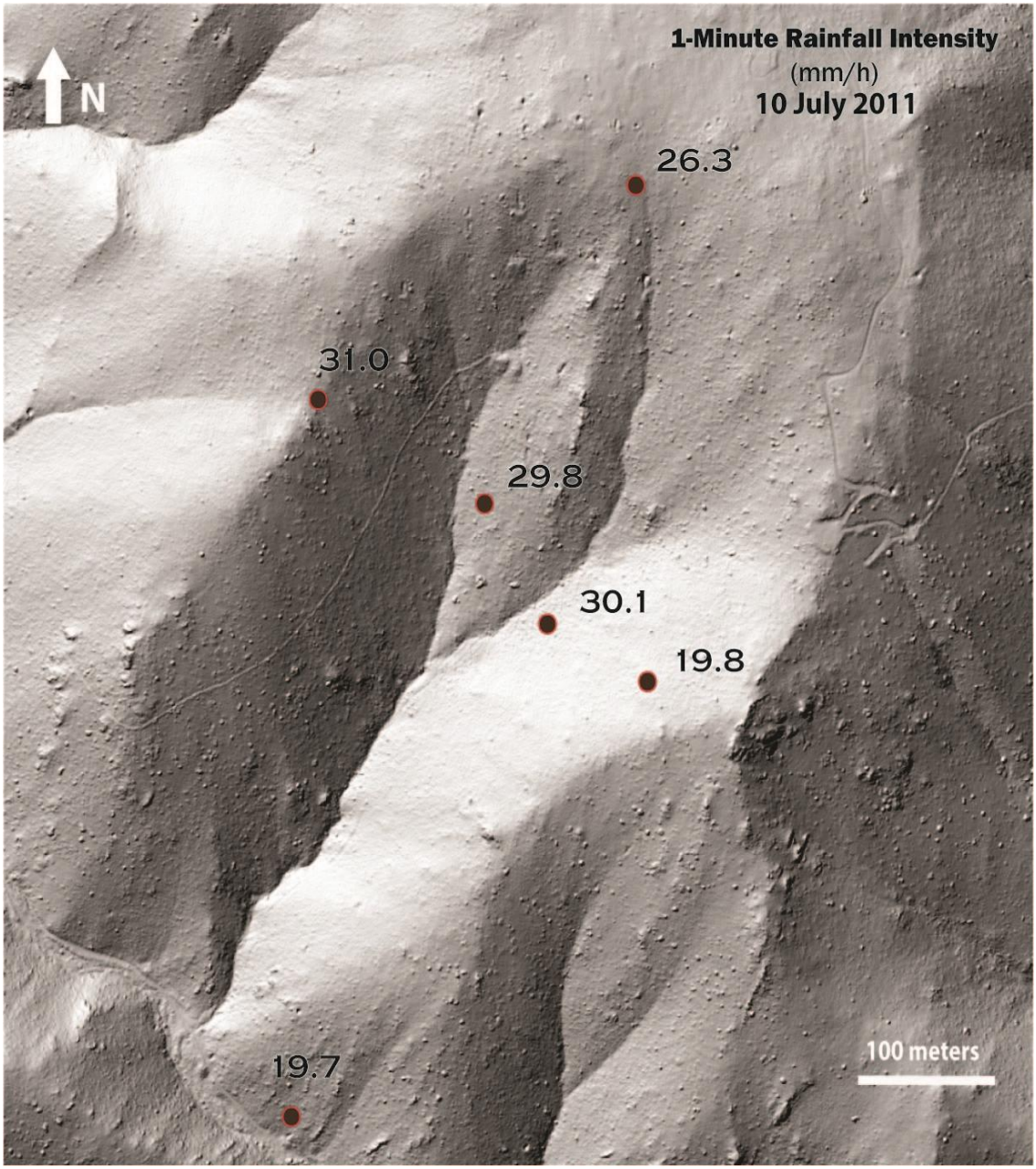
1-Minute Rainfall Intensity
(mm/h)
10 July 2011
N
26.3
31.0
29.8
30.1
19.8
19.7
100 meters

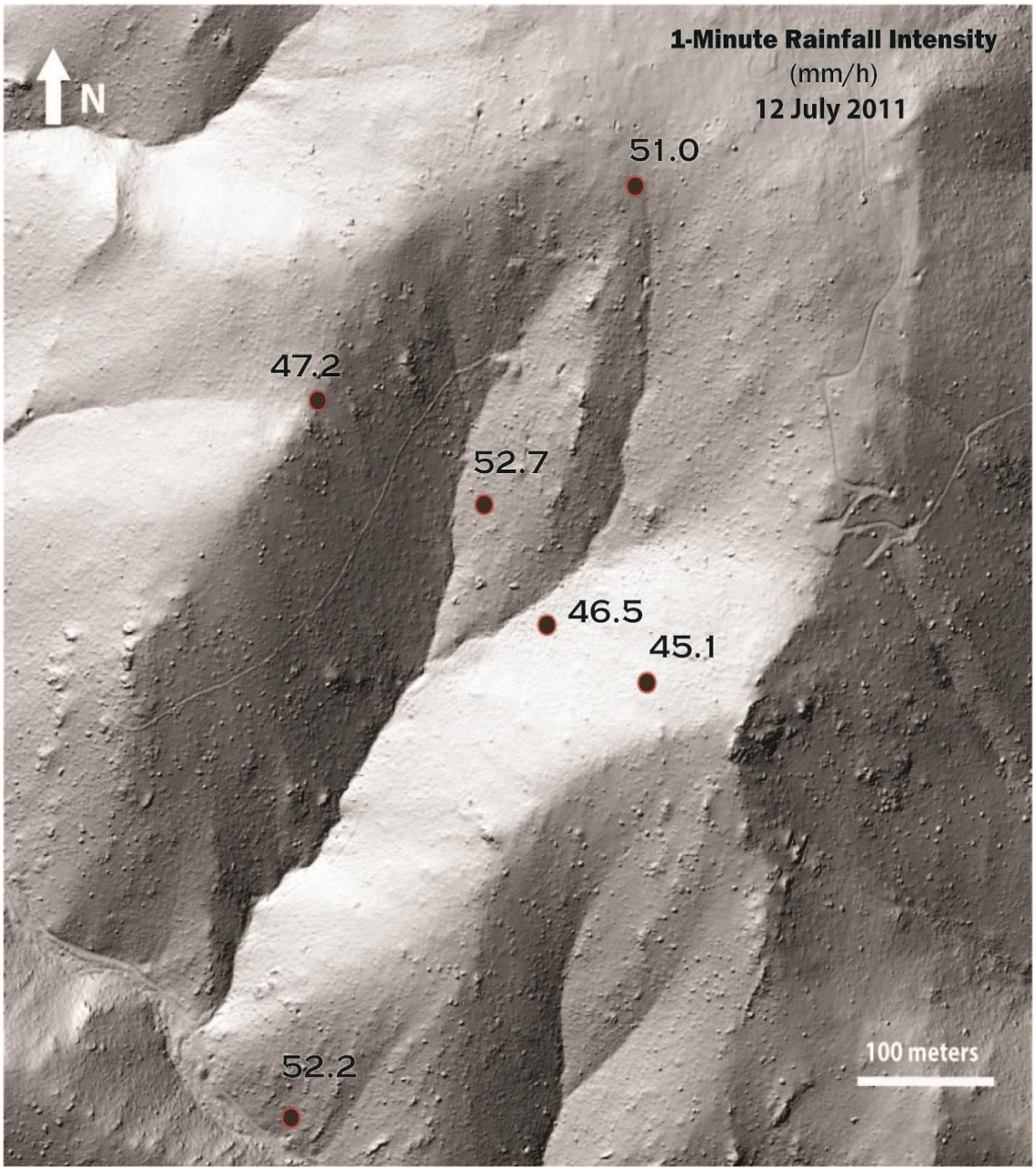
1-Minute Rainfall Intensity
(mm/h)
12 July 2011
N
51.0
47.2
52.7
46.5
45.1
52.2
100 meters

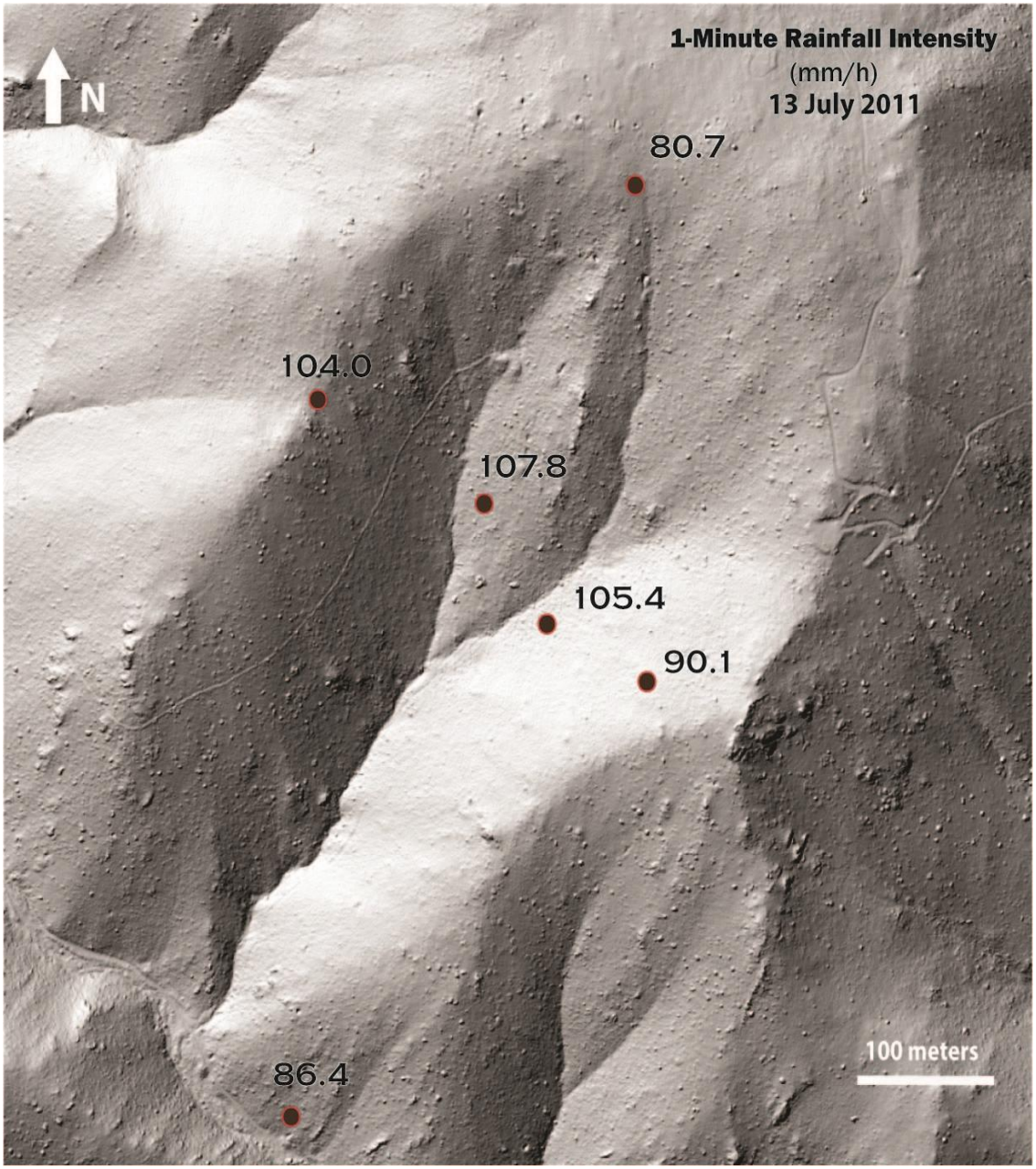
1-Minute Rainfall Intensity
(mm/h)
13 July 2011
N
80.7
104.0
107.8
105.4
90.1
86.4
100 meters

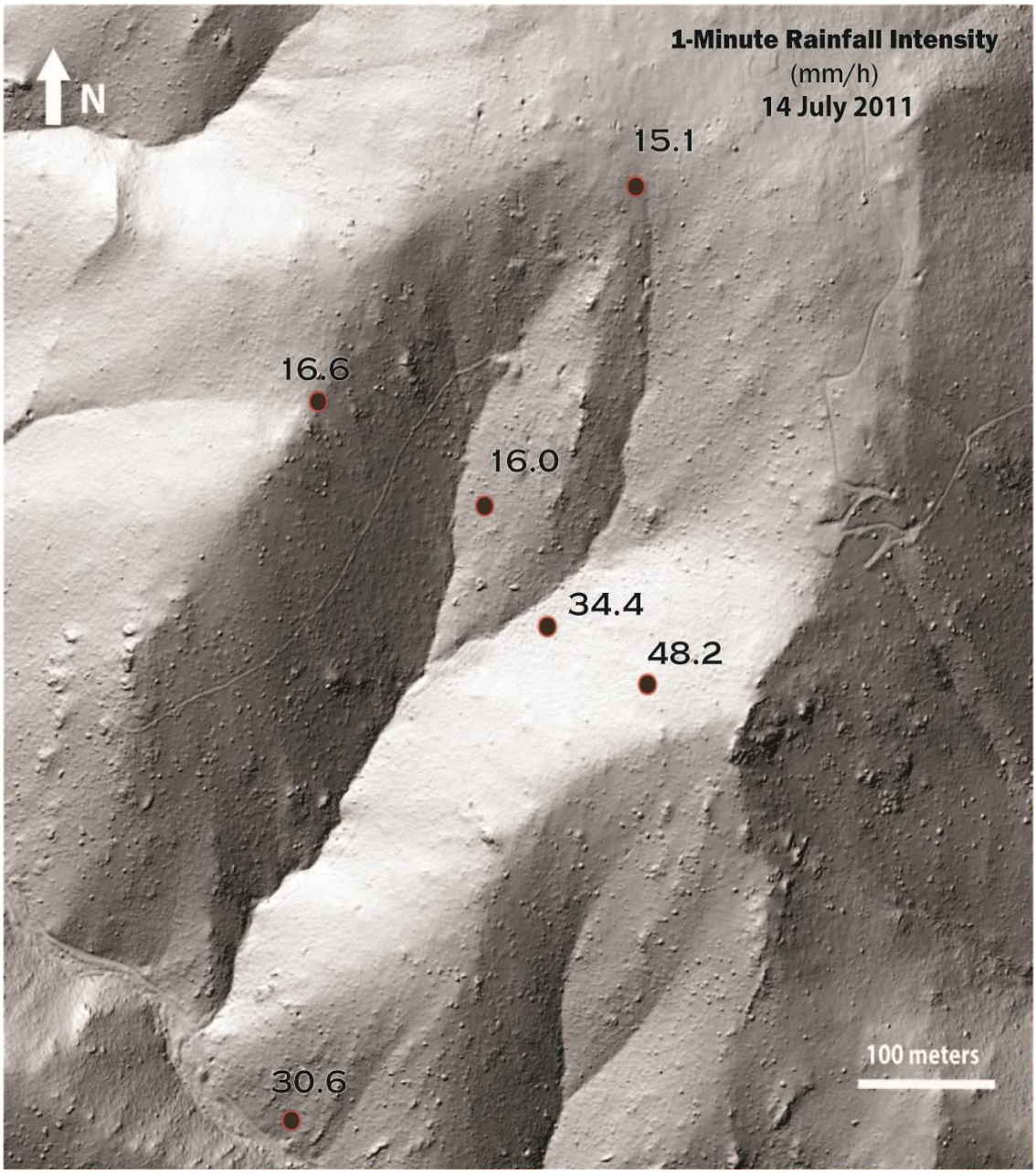
1-Minute Rainfall Intensity
(mm/h)
14 July 2011
N
15.1
16.6
16.0
34.4
48.2
30.6
100 meters

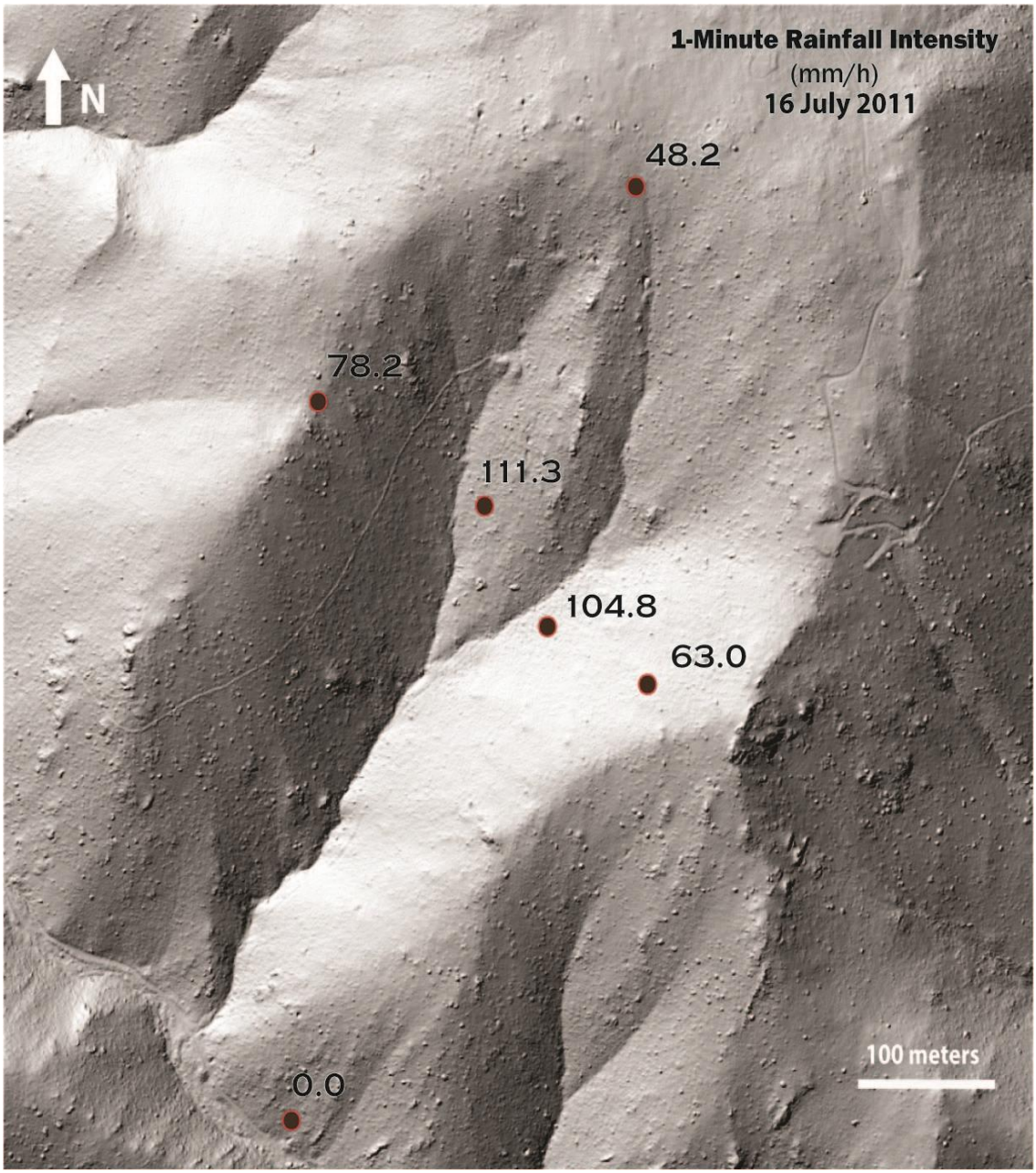
1-Minute Rainfall Intensity
(mm/h)
16 July 2011
N
48.2
78.2
111.3
104.8
63.0
0.0
100 meters

APPENDIX C- RAINFALL INTENSITY

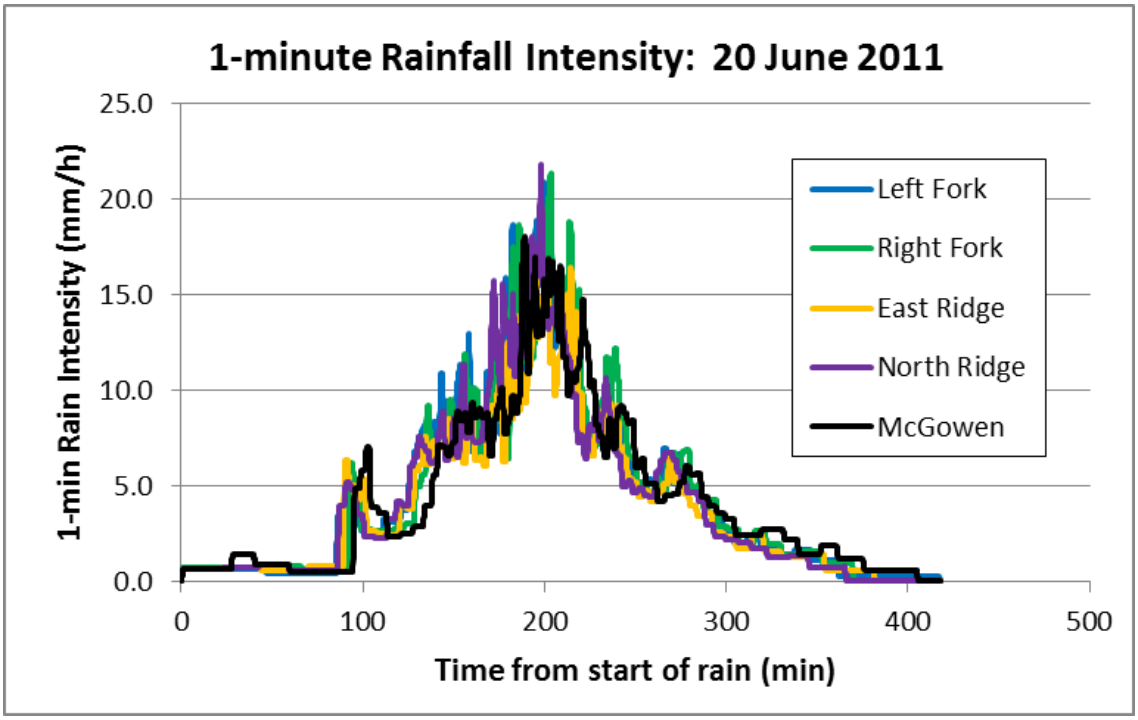

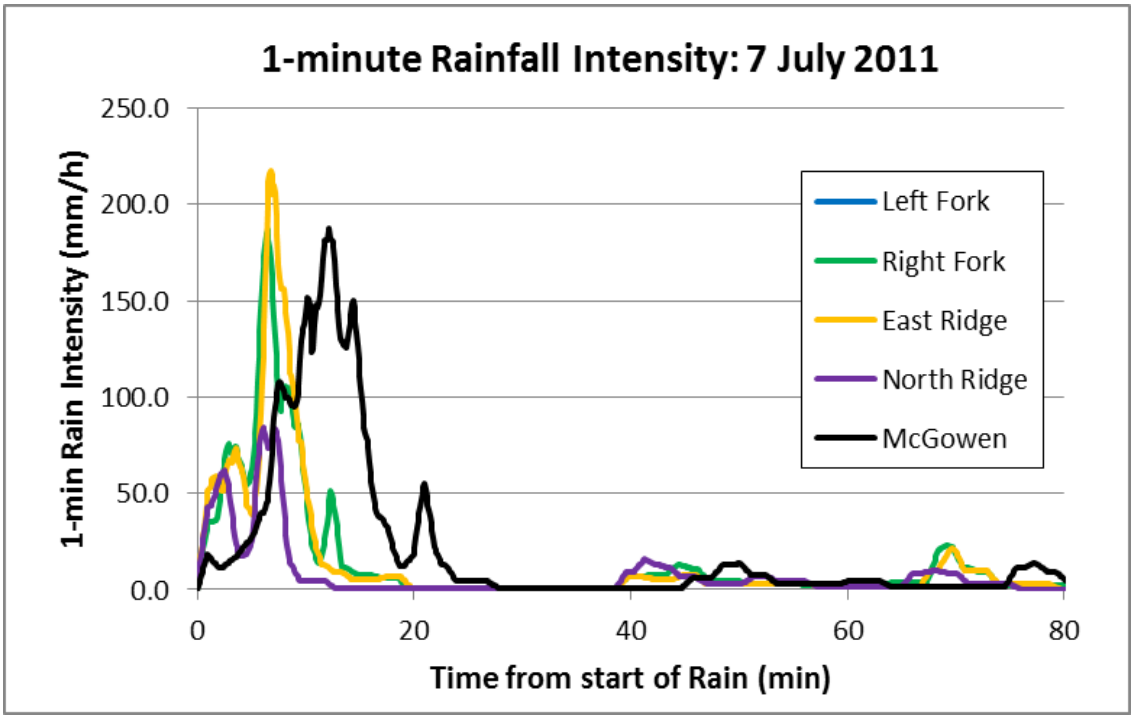

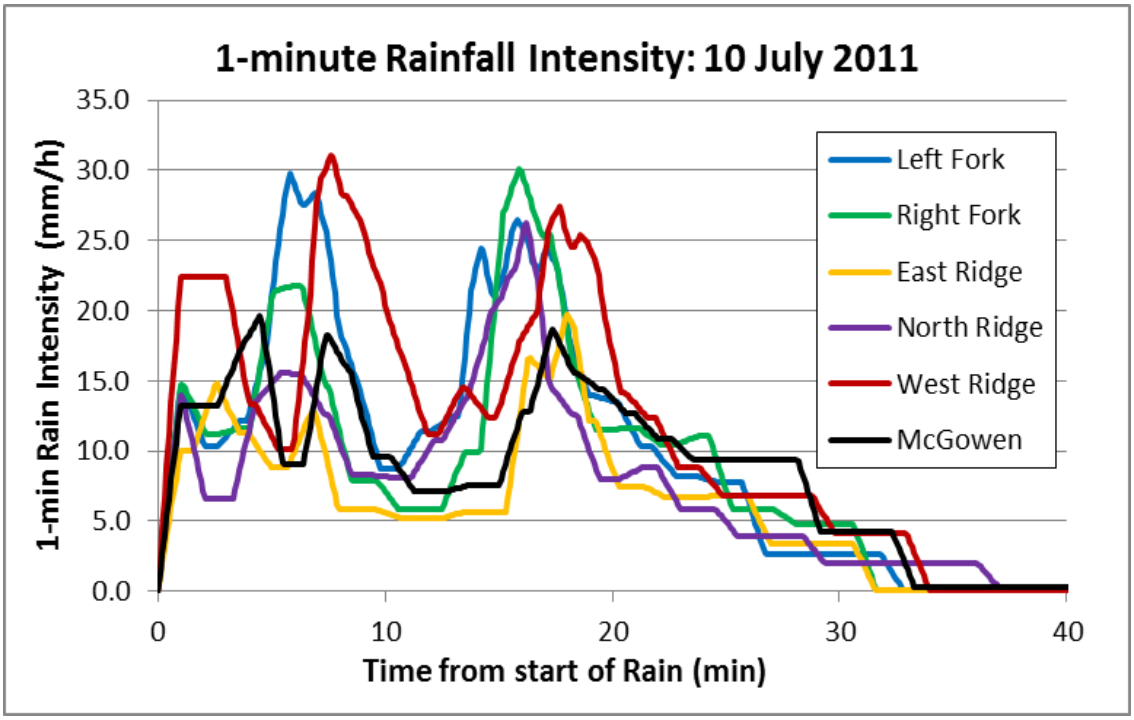
1-minute Rainfall Intensity: 10 July 2011
1-min Rain Intensity (mm/h)
35.0
30.0
25.0
20.0
15.0
10.0
5.0
0.0
0
10
20
30
40
Time from start of Rain (min)
Left Fork
Right Fork
East Ridge
North Ridge
West Ridge
McGowen

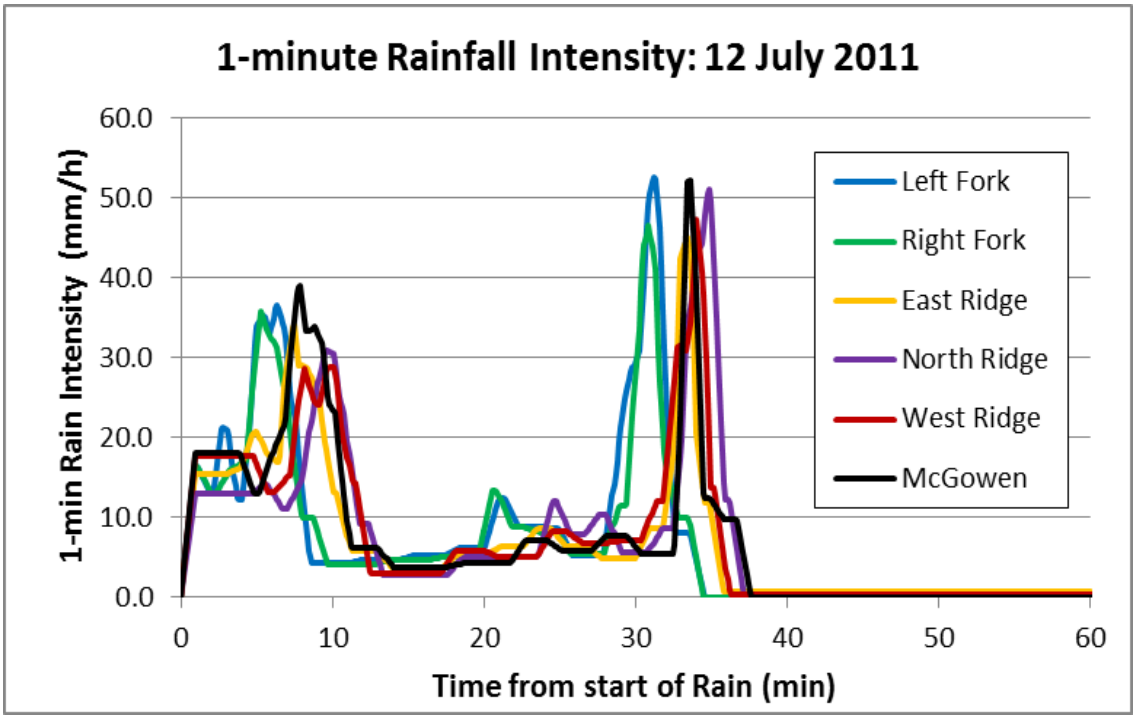
1-minute Rainfall Intensity: 12 July 2011
1-min Rain Intensity (mm/h)
60.0
50.0
40.0
30.0
20.0
10.0
0.0
0
10
20
30
40
50
60
Time from start of Rain (min)
Left Fork
Right Fork
East Ridge
North Ridge
West Ridge
McGowen

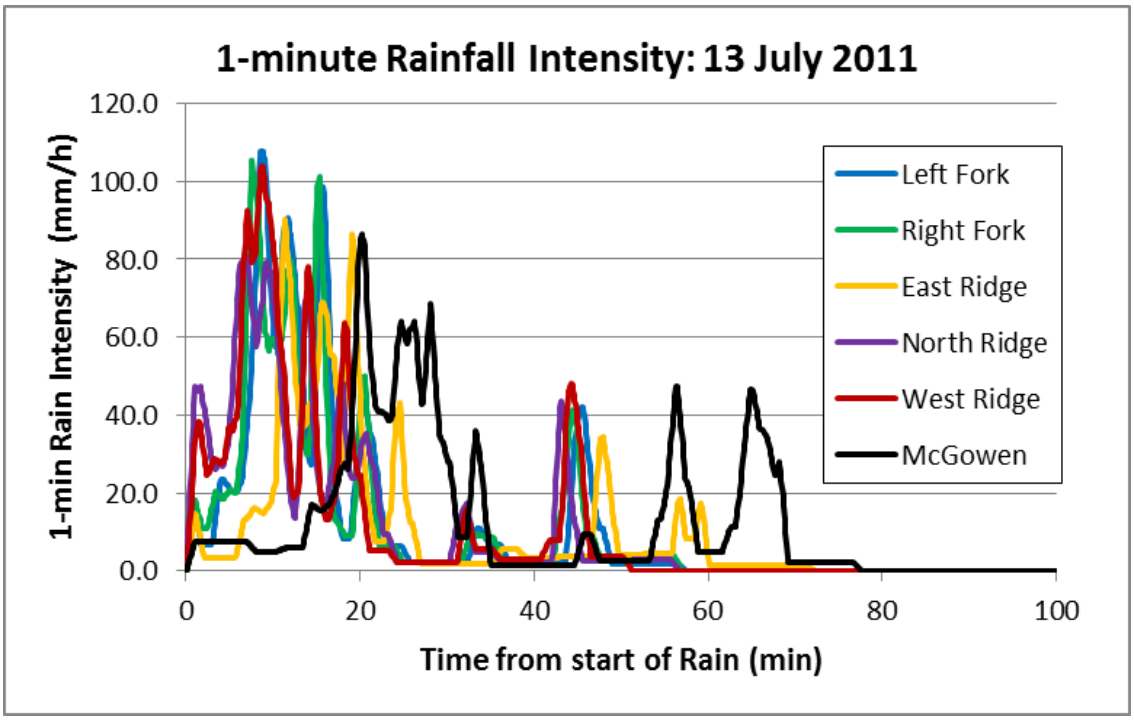
1-minute Rainfall Intensity: 13 July 2011
1-min Rain Intensity (mm/h)
120.0
100.0
80.0
60.0
40.0
20.0
0.0
0
20
40
60
80
100
Time from start of Rain (min)
Left Fork
Right Fork
East Ridge
North Ridge
West Ridge
McGowen

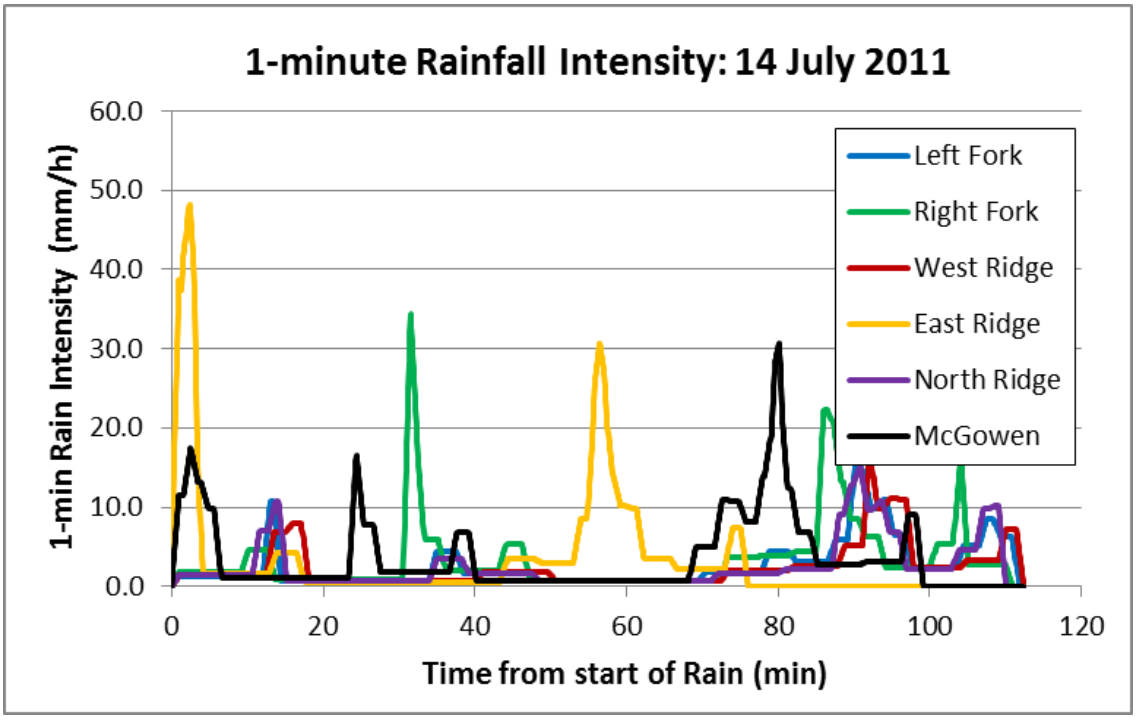
1-minute Rainfall Intensity: 14 July 2011
1-min Rain Intensity (mm/h)
60.0
50.0
40.0
30.0
20.0
10.0
0.0
0
20
40
60
80
100
120
Time from start of Rain (min)
Left Fork
Right Fork
West Ridge
East Ridge
North Ridge
McGowen

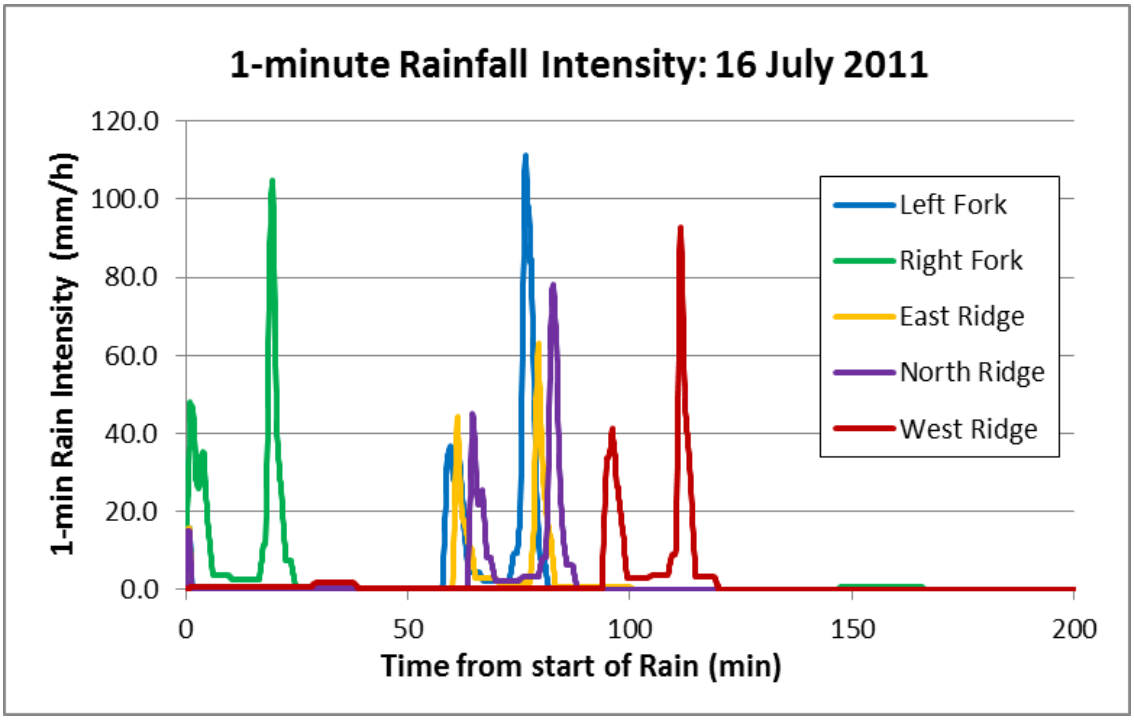
1-minute Rainfall Intensity: 16 July 2011
1-min Rain Intensity (mm/h)
120.0
100.0
80.0
60.0
40.0
20.0
0.0
0
50
100
150
200
Time from start of Rain (min)
Left Fork
Right Fork
East Ridge
North Ridge
West Ridge

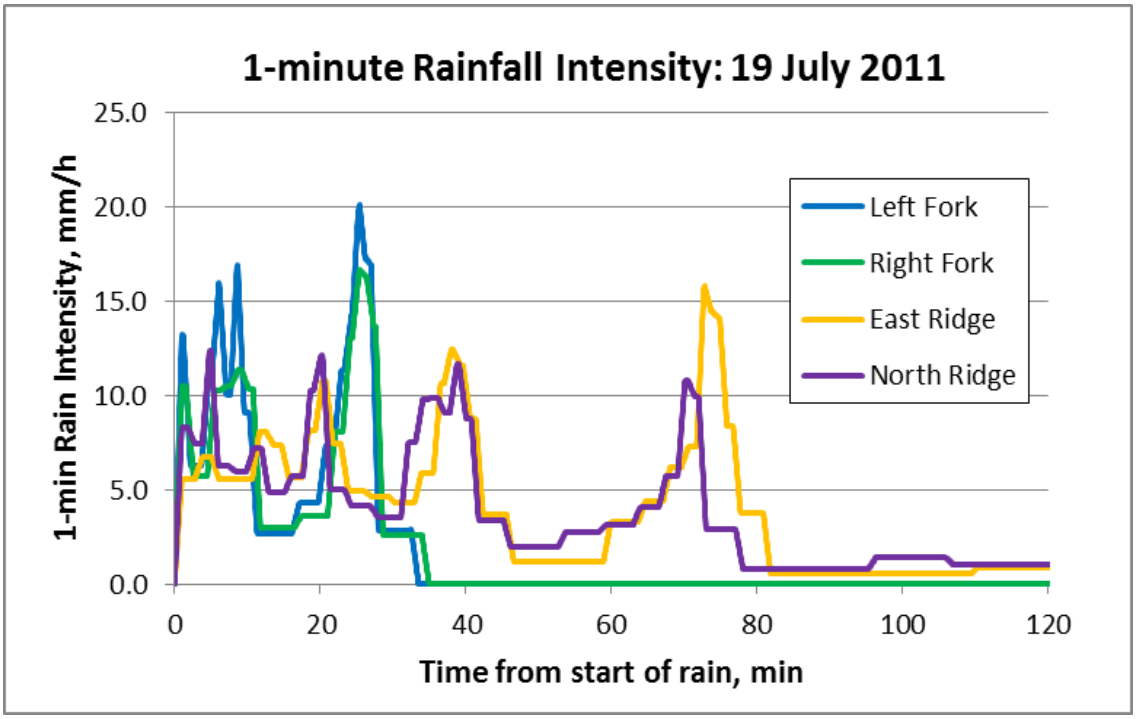
1-minute Rainfall Intensity: 19 July 2011
1-min Rain Intensity, mm/h
25.0
20.0
15.0
10.0
5.0
0.0
0
20
40
60
80
100
120
Time from start of rain, min
Left Fork
Right Fork
East Ridge
North Ridge

APPENDIX D- FLUME-MEASURED DISCHARGE

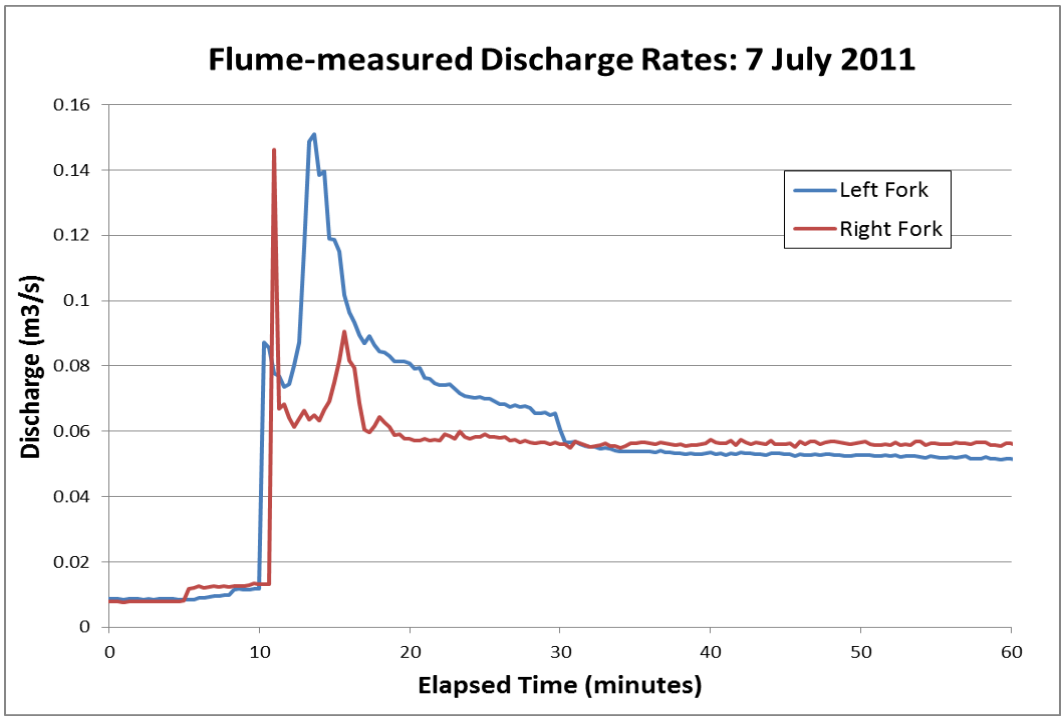

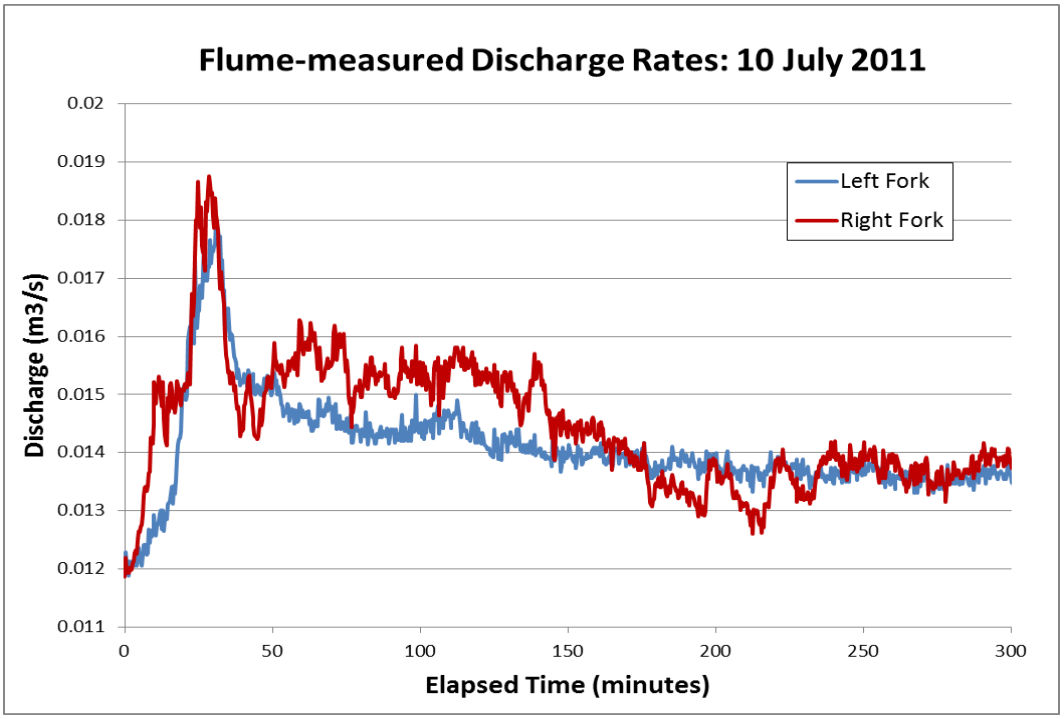

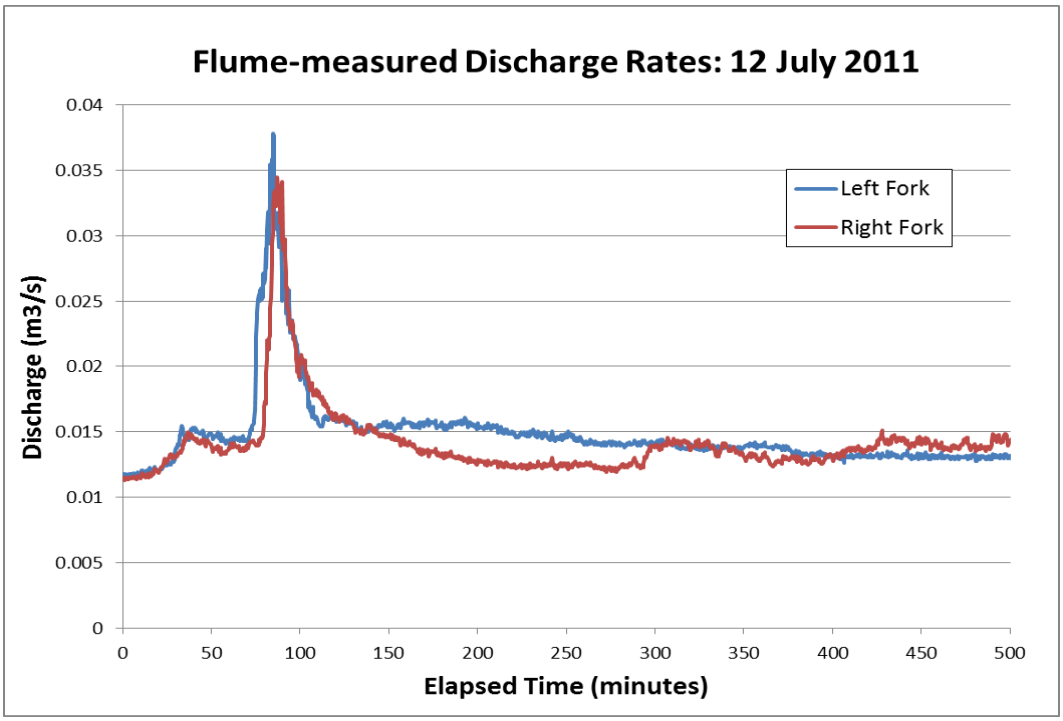
Flume-measured Discharge Rates: 12 July 2011
Discharge (m3/s)
0.04
0.035
0.03
0.025
0.02
0.015
0.01
0.005
0
0
50
100
150
200
250
300
350
400
450
500
Elapsed Time (minutes)
Left Fork
Right Fork

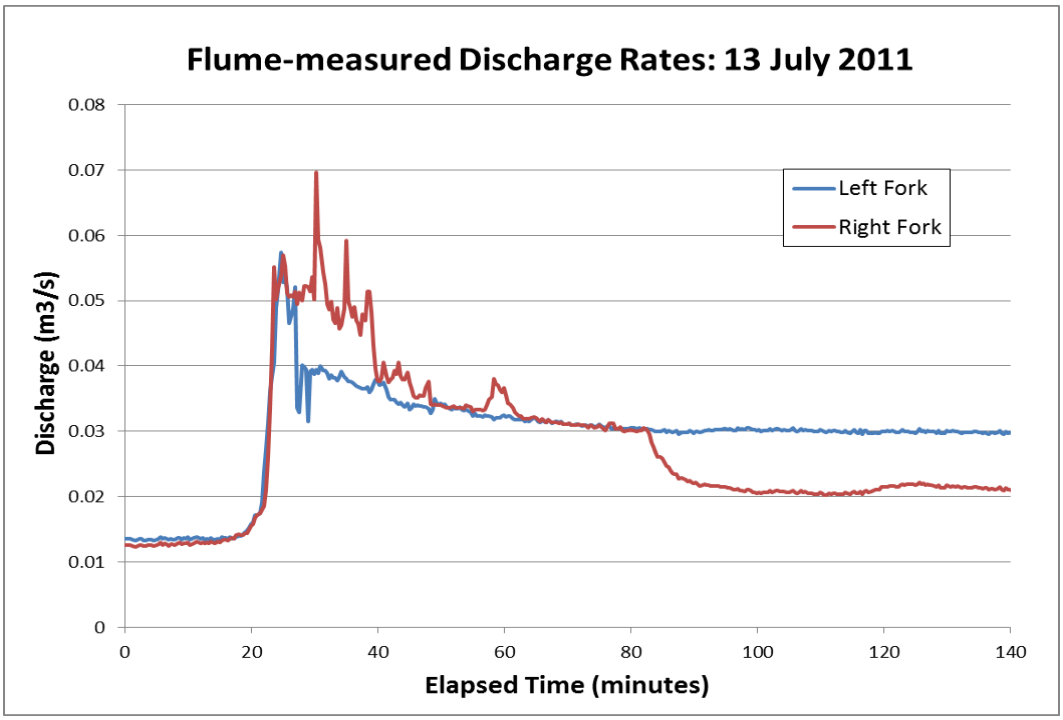
Flume-measured Discharge Rates: 13 July 2011
Discharge (m3/s)
0.08
0.07
0.06
0.05
0.04
0.03
0.02
0.01
0
0
20
40
60
80
100
120
140
Elapsed Time (minutes)
Left Fork
Right Fork

APPENDIX E- INFILTRATION

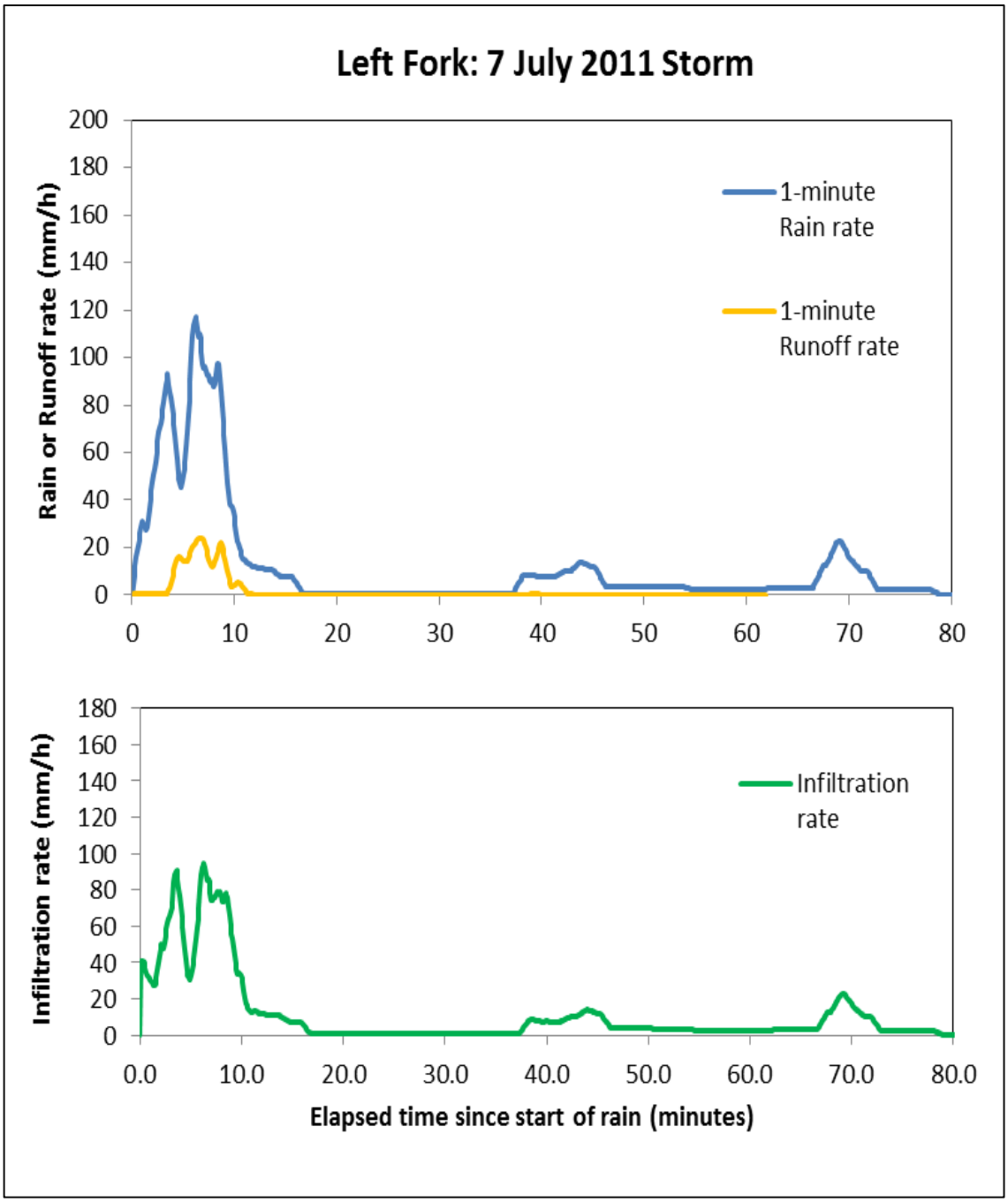

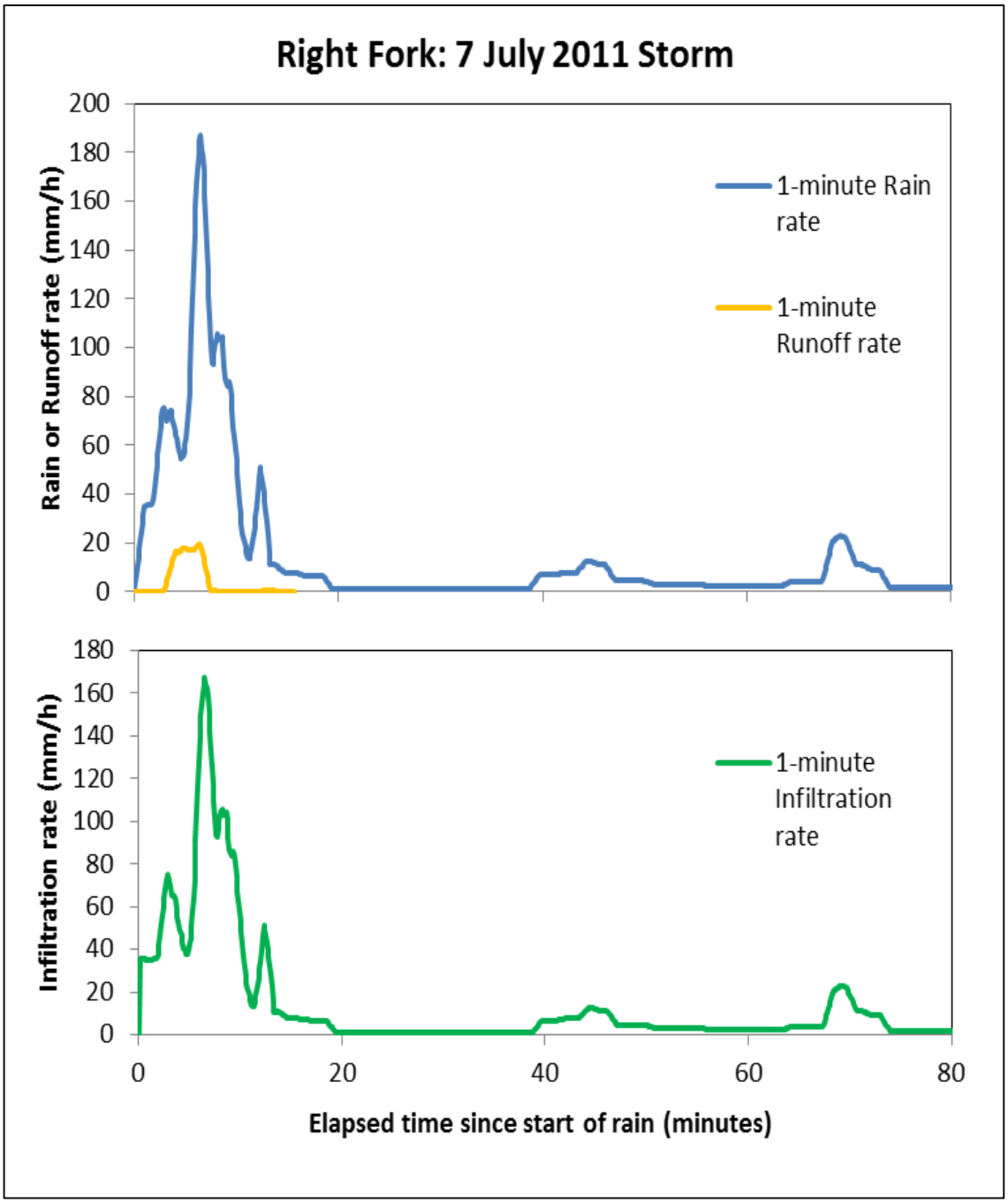
Right Fork: 7 July 2011 Storm
Rain or Runoff rate (mm/h)
200
180
160
140
120
100
80
60
40
20
0
1-minute Rain rate
1-minute Runoff rate
Infiltration rate (mm/h)
180
160
140
120
100
80
60
40
20
0
1-minute Infiltration rate
0
20
40
60
80
Elapsed time since start of rain (minutes)

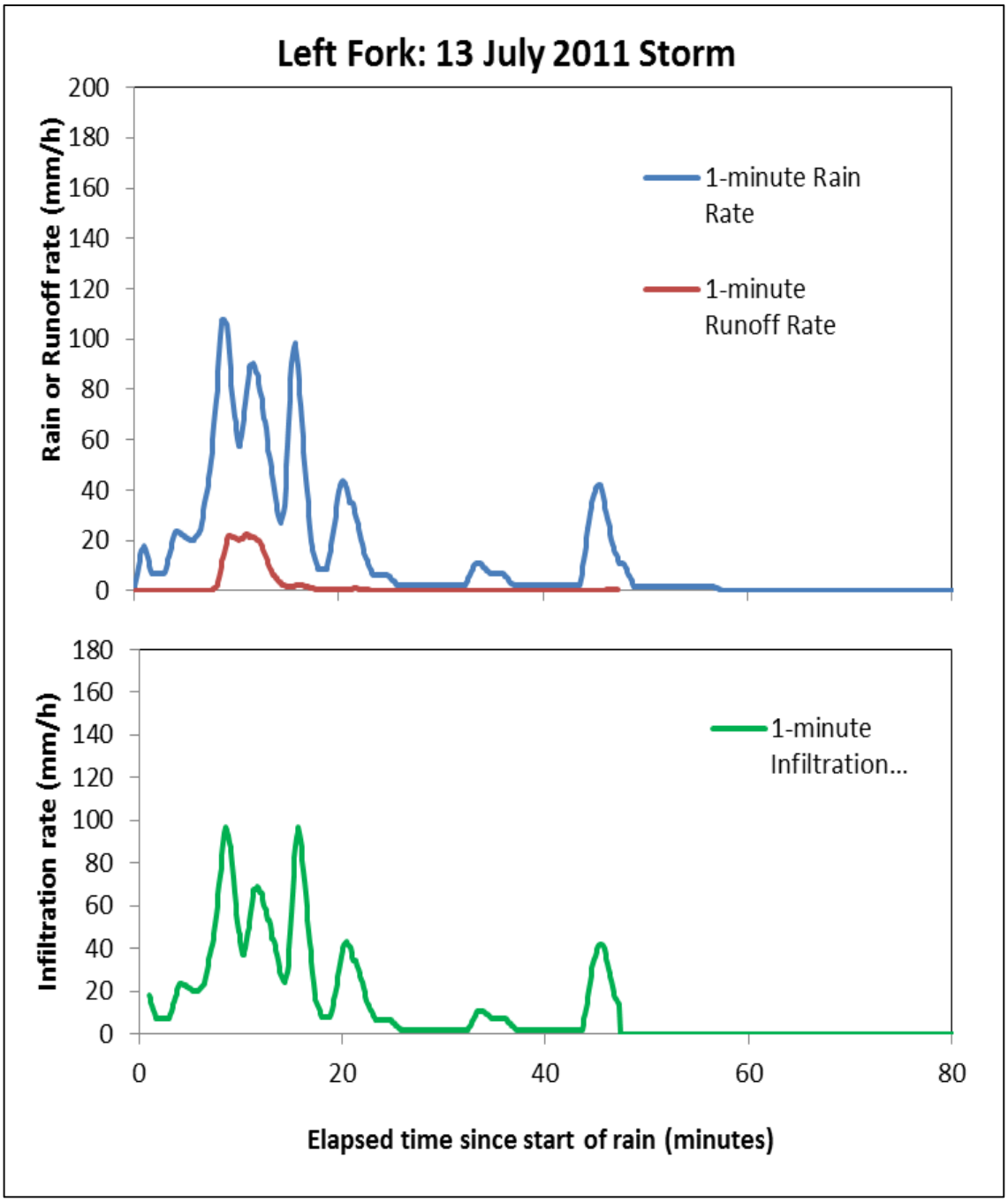
Left Fork: 13 July 2011 Storm
Rain or Runoff rate (mm/h)
200
180
160
140
120
100
80
60
40
20
0
1-minute Rain Rate
1-minute Runoff Rate
Infiltration rate (mm/h)
180
160
140
120
100
80
60
40
20
0
1-minute Infiltration...
0
20
40
60
80
Elapsed time since start of rain (minutes)

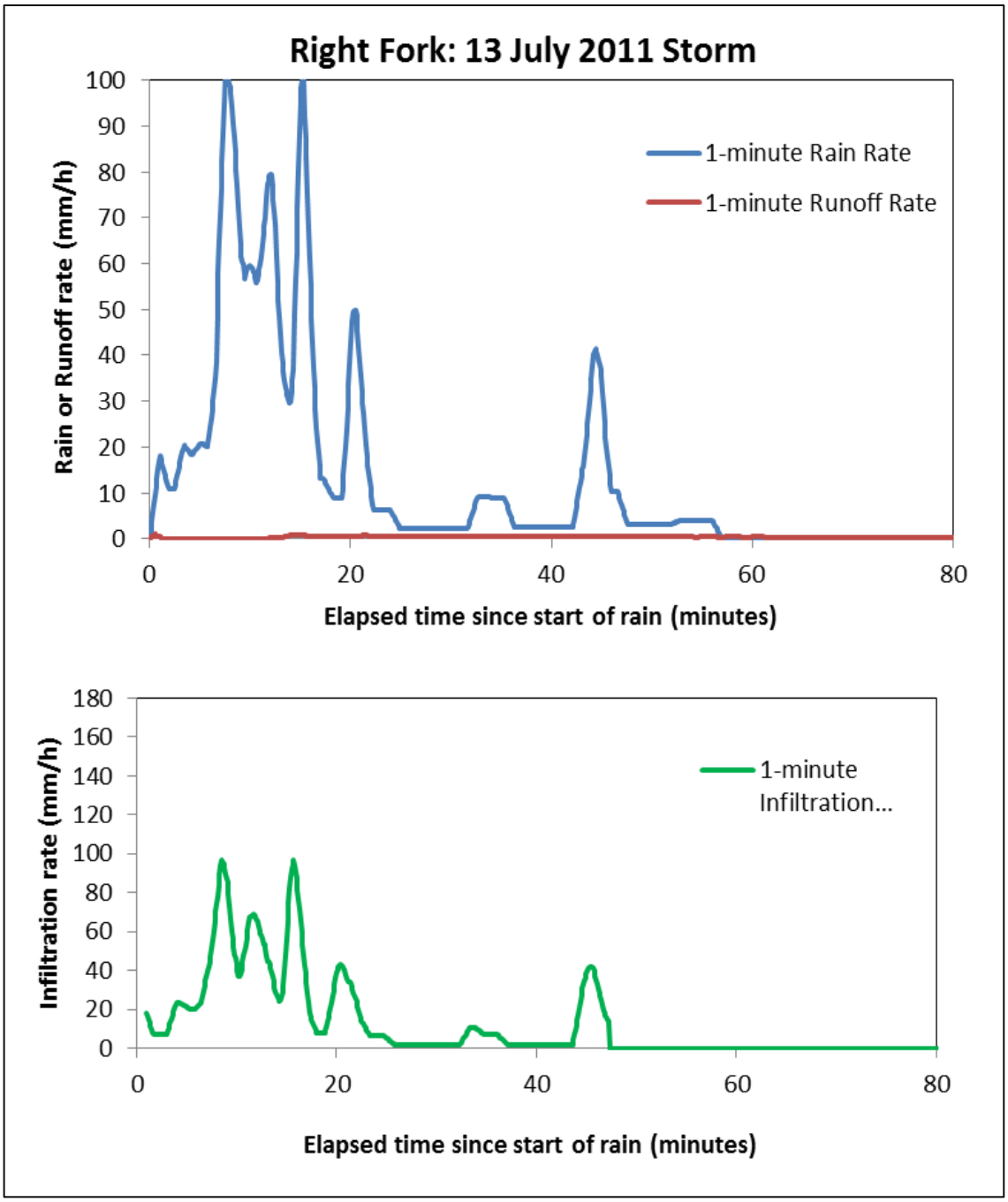
Right Fork: 13 July 2011 Storm
Rain or Runoff rate (mm/h)
100
90
80
70
60
50
40
30
20
10
0
0
20
40
60
80
Elapsed time since start of rain (minutes)
1-minute Rain Rate
1-minute Runoff Rate
Infiltration rate (mm/h)
180
160
140
120
100
80
60
40
20
0
0
20
40
60
80
Elapsed time since start of rain (minutes)
1-minute Infiltration...

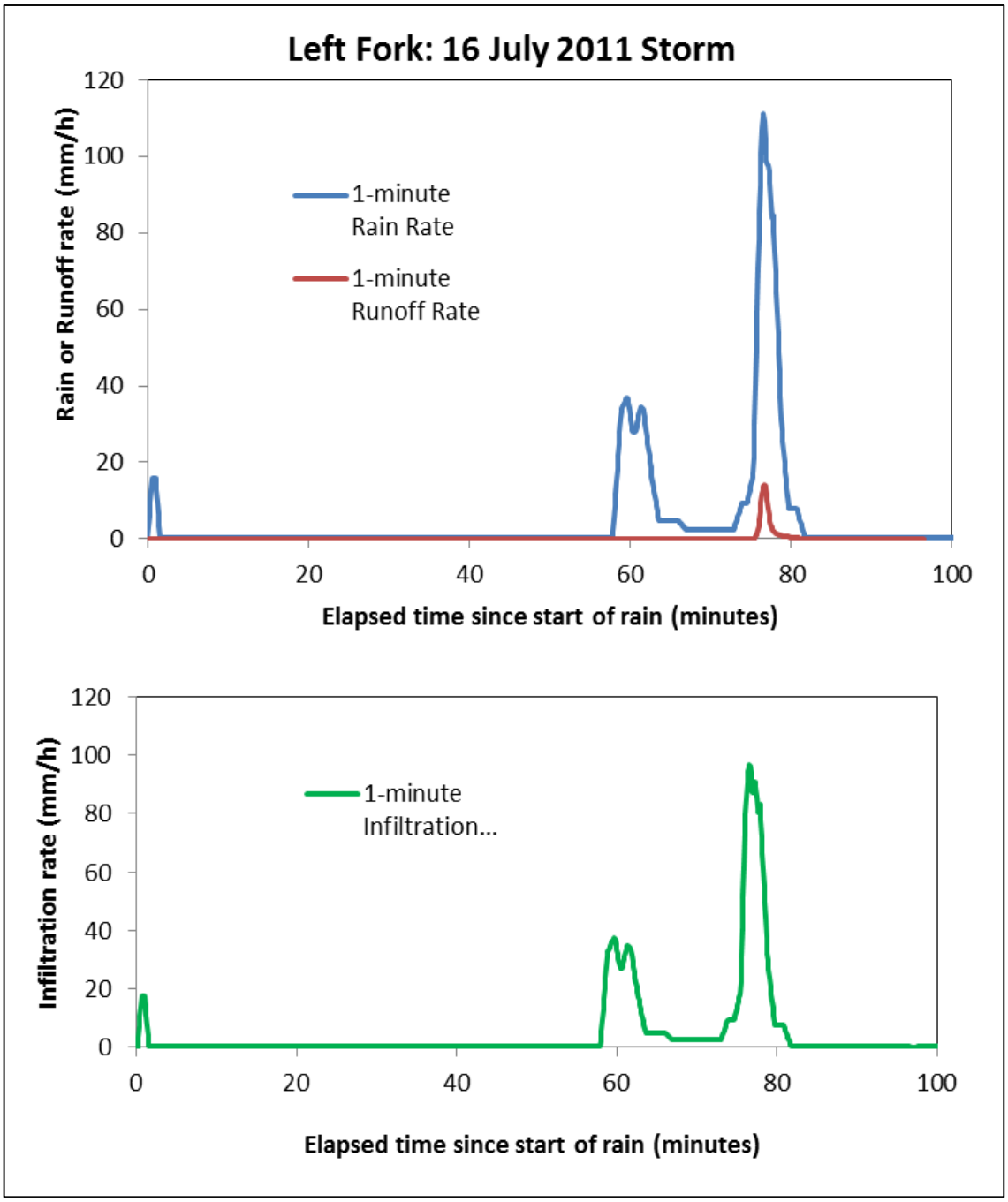
Left Fork: 16 July 2011 Storm
Rain or Runoff rate (mm/h)
120
100
80
60
40
20
0
1-minute Rain Rate
1-minute Runoff Rate
0
20
40
60
80
100
Elapsed time since start of rain (minutes)
Infiltration rate (mm/h)
120
100
80
60
40
20
0
1-minute Infiltration...
0
20
40
60
80
100
Elapsed time since start of rain (minutes)

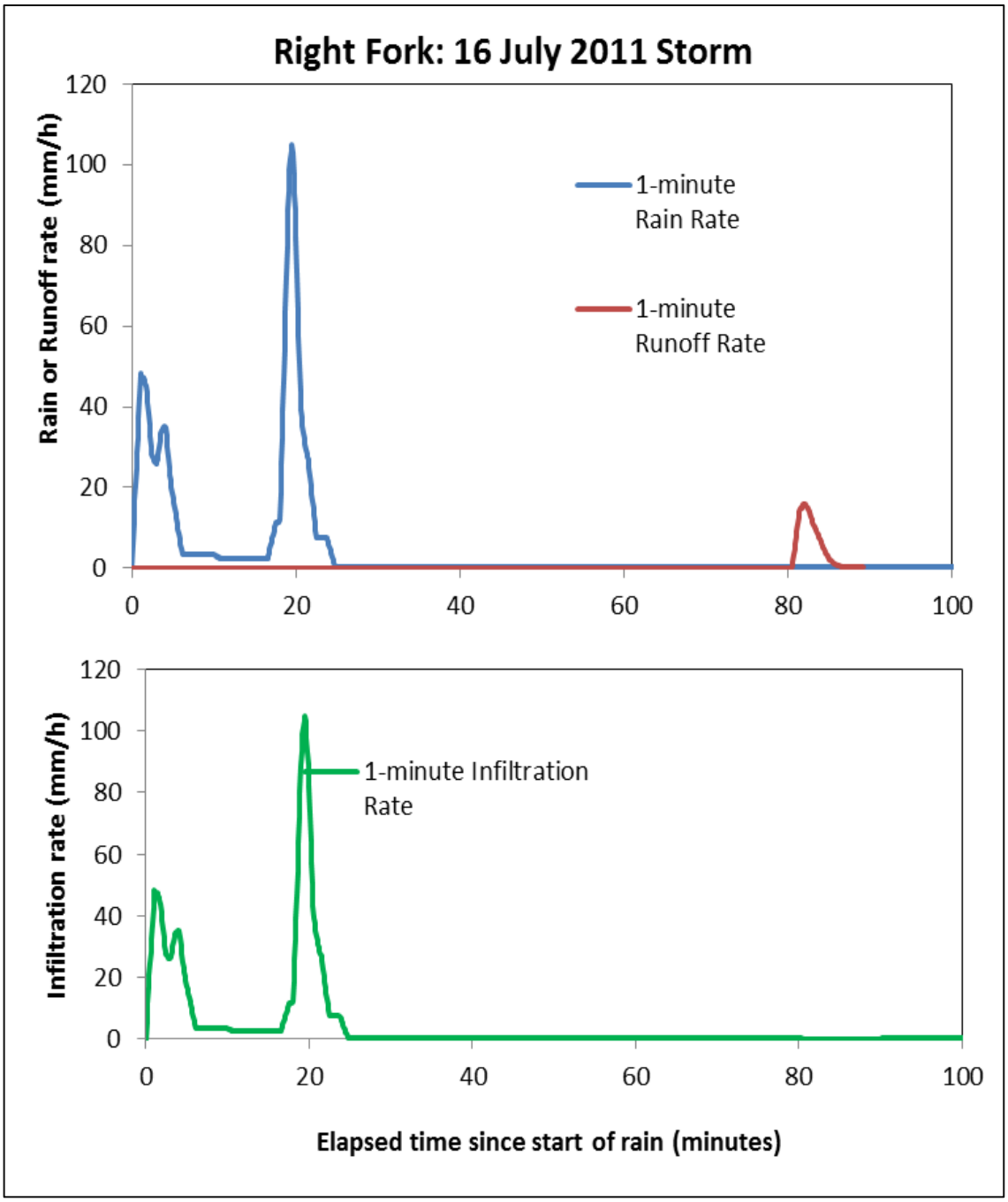
Right Fork: 16 July 2011 Storm
Rain or Runoff rate (mm/h)
120
100
80
60
40
20
0
0
20
40
60
80
100
1-minute Rain Rate
1-minute Runoff Rate
Infiltration rate (mm/h)
120
100
80
60
40
20
0
0
20
40
60
80
100
1-minute Infiltration Rate
Elapsed time since start of rain (minutes)

APPENDIX F- SWAT PARAMETERS

Parameter	Lower Bound	Upper Bound	Calibration result	
			SWAT 99.2	SWAT -G
Snow melt rate (mm/d/°C)	1.00	3.00	1.05	1.00
Surface runoff lag time (d)	1.00	5.00	1.43	1.00
Curve number for coniferous forest	5030	60.0	52.4	51.0
Maximum potential interception for coniferous forest (mm)	3.00	6.00	3.11	2.58
Manning's "n" value for overland flow ($m^{/1/3}s$)	0.20	0.50	0.47	0.50
Groundwater recession coefficient (d^{-1})	0.030	0.060	0.054	0.031
Delay of the groundwater recharge (d)	1.00	20.00	4.12	19.65
Deep aquifer percolation fraction	0.00	0.80	0.77	0.05
Thickness of the rocky base of soil no. 202[a] (mm)	1000	5000	1060	1870
Thickness of the rocky base of soil no. 2458[b] (mm)	3000	10000	9620	3990
Density, soil no. 2458[b], third layer (g/cm^3)	1.50	1.60	1.56	1.60
Density of the bedrock (g/cm^3)	2.51	2.64	2.52	2.64
Available water capacity soil no. 2458[b], first layer (mm/mm)	0.16	0.20	0.16	0.19
Saturated conductivity, soil no. 202[a], third layer (mm/h)	1.0	45.0	39.3	44.8
Saturated conductivity, soil no. 2458[b], third layer (mm/h)	10.0	85.0	53.9	84.8
Anisotropy factor[c], soil no. 2458[b], third layer	2.00	8.00	-	8.00
Maximum leaf area index for coniferous forest	4.00	14.00	5.80	5.95
Maximum lead area index for pasture	1.50	5.50	1.69	2.31

[a]Shallow cambisol on the lower slope
[b]Shallow cambisol on the upper slope
[c]Only available in SWAT-G

(table modified from Eckhardt et al., 2001)

APPENDIX G- SMITH PARLANGE EQUATIONS

$F_c = K_s + \gamma^*(K_s - K_i) / [\exp(\gamma^* F/J)-1]$ = infiltrability [m/sec] (max infiltration rate)

$J = G * (\Theta_s - \Theta_i)$ = a quantity used in previous equation (meters)

$V_0 = \min[(P + M) f_c]$ = infiltration rate at surface (mm/sec)(K_s<(P+M))

$= (P + M)$ = infiltration rate at surface (mm/sec)(K_s<(P+M))

$F = \int v_0 (t)\, dt$, (from times 0 to t) = cumulative infiltration depth (meters)

where:

K_s = saturated hydraulic conductivity (m/s)

K_i = initial hydraulic conductivity (m/s) (typically much less than K_s)

Θ_s = soil water content at $\psi = 0$ (unitless) (typically set to the porosity, φ)

Θ_i = initial soil water content (unitless)

G = capillary length scale (meters)

= integral over all ψ of $K(\psi)/K_s$

= (almost always between ψ_B and $2^* \psi_B$)

P = precipitation rate (mm/sec)

M = snowmelt rate (mm/sec)

γ = Smith-Parlange method parameter (between 0 and 1, near 0.8)